Università degli Studi di Torino

Scuola di Dottorato in Scienze della Natura e Tecnologie Innovative

Dottorato in Scienze Farmaceutiche e Biomolecolari

(XXXII ciclo)

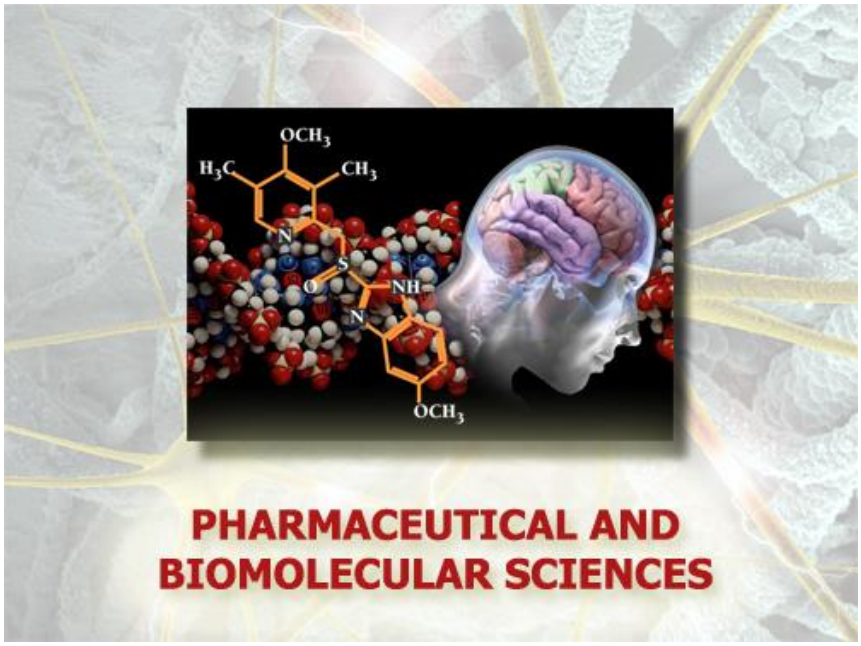

DESIGN AND DEVELOPMENT OF NOVEL NANOFORMULATION-BASED DELIVERY SYSTEMS FOR THE PREVENTION AND TREATMENT OF CHALLENGING PATHOLOGICAL CONDITIONS

Candidata: Dr. Federica Bessone **Supervisor: Prof.ssa Roberta Cavalli**

List of contents

Abstract

In the last decades, nanoformulation-based tools started to draw attention as novel entities in diagnostic and therapeutic fields. Nanomedicine has become an important key to overcome and solve intricate medical limitations. The challenge to design and develop new nanodelivery systems was faced in this doctoral project. In particular, two main topics were investigated: tissue hypoxia and drug resistance. The first topic aimed to develop nanoformulations suitable for the delivery of oxygen in a controlled manner. Notably, hypoxic tumors are more resistant to chemotherapy and radiation. In particular, the pancreatic tumor is an aggressive type of cancer in which the microenvironment is extremely hypoxic and the cells become easily resistant to drugs. For this purpose, core-shell nanodroplets were purposely designed for the supply of oxygen, drugs and adjuvant agents to the tumor site. Novel nanodroplet formulations were developed to combine Oxygen, Gemcitabine as chemotherapeutic and Curcumin as a modulator of overexpressed efflux pump proteins (P-glycoprotein) in resistant cancer cells. The synergistic effect of Oxygen-loaded nanodroplets carrying Gemcitabine and Curcumin may represent an interesting triple-delivery nanoplatform to overcome current drawbacks with the present treatment of pancreatic cancer. Moreover, nanodroplets can be ultrasound-activated, thus enabling an “on-demand” release of their cargo at specific tumor sites.

Another delivery strategy was investigated for preventing metastatic spreading in prostate cancer cells. For this purpose, Curcuminoid-loaded in dextran-shelled nanodroplets were prepared as adjuvant theranostic tools. Indeed, Curcuminoids were released with a prolonged *in vitro* kinetics and the nanodroplets prevented their degradation. Additionally, nanodroplet echogenic properties allow their visualization by ultrasound imaging.

In addition, hypoxia-sensitive liposomes were studied for co-delivery of siRNA and Paclitaxel specifically targeting hypoxic areas. The synergic effect of the silencing of P-glycoproteins with the siRNA and chemotherapy could potentially offer a novel and effective treatment for patients who have established multidrug resistance.

Summing up, resistance to chemotherapy is a major problem that limits the effectiveness of successful treatment of cancer. Albumin-based Doxorubicin-loaded nanoparticles were prepared to provide controlled release of the drug, to reduce the toxicity due to side effects and to overcome the resistance. They showed significant viability and proliferation inhibition on cancer cell lines resistant for Doxorubicin, representing a promising nanoplatform for increasing the efficacy of chemotherapy.

In conclusion, during my PhD the study of several nanoplatforms was conducted with the aim to overcome therapeutic limitations and enhancing the success of the treatment of different tumor pathological conditions.

Introduction

Cancer is one of the most deadly diseases in the developed world and definitive resolution strategies for its treatment are not yet discovered. Nevertheless, many approaches have been studied to try to fight cancer from different points of view. Notably, there are many difficulties for the diagnosis of this malignancy, and if it occurs at late stages, the possibilities for positive outcomes of the therapies are weak. Moreover, cancer can develop metastasis, drug resistance, hypoxia at the tumor site, thus reducing the efficacy of the conventional chemotherapeutic drugs [1].
In my PhD thesis, my research was focused on the development of two approaches to overcome the present drawbacks in the chemotherapy outcomes, that are following described: drug resistance and hypoxia.

Drug resistance

The development of drug resistance, due to intrinsic or acquired mechanisms [BOX 1], is a key problem in the treatment of cancer. In particular, resistance to chemotherapy can cause relapses, which represent one of the major reasons for death during the effort to fight cancer. In the beginning, this phenomenon was compared to the resistance developed for antimicrobial therapy, and at first was observed in the use of the early chemotherapeutics, such as the alkylating agents [2]. Nowadays, drug resistance remains the principal limiting factor for the achievement of cures in patients and is one of the biggest challenges in the treatment of cancer [3]. Certainly, there is a huge heterogeneity among patients and type of tumors, and many factors have to be considered to increase the positive results of the treatment. Initially, many tumors respond to chemotherapy, but after a while they become tolerant to one or more drugs, developing a multidrug resistance (MDR) [4,5].

Mechanism of drug resistance

The principles underlying the development of anticancer drug resistance are multiple and most of the time they occur together.

Overexpression of drug efflux

One of the major causes of chemotherapy resistance is an increased efflux of anticancer drugs from the cells, leading to a consequent reduction of intracellular drug accumulation [6,7]. The prevalent mechanism of cancer resistance is the overexpression of drug efflux pumps, in particular of a class of energy-dependent efflux pumps called ATP-binding cassette (ABC) transporter superfamily. Among the ABC protein members, three transporters have been more characterized: MDR-protein 1 (MDR1 in short, also called ABCB1 or P-glycoprotein), MDR-associated protein 1 (MRP1 or ABCC1), and breast cancer resistance protein (BCRP or ABCG2) [8,9]. Notably, MDR1 is extremely involved in the acquisition of resistance. This membrane protein is composed of two transmembrane domains (TMD), that form a channel for the substrates, and two nucleotide-binding domains (NBD) for ATP. The conformational modification in the transporter, due to the binding and the hydrolysis of ATP, leads to the elimination of the substrates from the cells (Figure 1). Mutations and upregulation of

ABC transporter proteins affect the sensitivity of the tumor and the chemotherapy efficacy. Indeed, the transporter ejects drugs from the cell faster than their uptake, rendering the cell resistant.

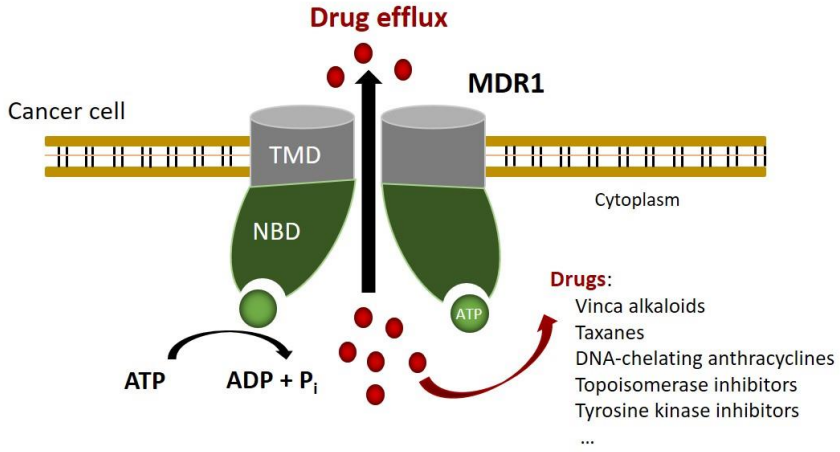

Figure 1. Schematic representation of the mechanism of drug efflux by MDR1 transporter. Abbreviation: TMD = transmembrane domains; NBD = nucleotide-binding domains.

BOX 1 - INTRINSIC AND ACQUIRED DRUG RESISTANCE

Intrinsic resistance is innate, meaning that exists in cancer cells prior to drug administration. It can be caused by: a) inherent genetic mutations; b) heterogeneity of tumors; c) activation of intrinsic pathways used as defense. Intrinsic drug resistance could be due to the genetic mutations of genes involved in cancer cell growth and/or apoptosis.

Acquired resistance corresponds to the gradual decrease of chemotherapeutic efficacy of a drug after the administration. Initially, tumor cells are drug-sensitive, but later these cells are selectively removed, and resistant cells come to dominate the cancer cell population. Acquired resistance can be a result of: a) mutations or altered expression levels of drug targets; b) modification in tumor microenvironment after treatment.

Alteration of drug targets

Resistance can also be related to alterations in the expression of target proteins involved in tumor development. Targeted therapy is considered a new strategy for the targeting of specific molecular pathways, thus being more selective and effective to cancer cells [10]. A clear example of this mechanism is the downregulation of target gene expression.

Activation of detoxification mechanisms

Altered drug metabolism and detoxification represent crucial resistance mechanisms for different types of cancers. Modification in the two pathways for the metabolism of drugs, phase I (oxidation, reduction, hydrolysis) and phase II reactions (acetylation, glucuronidation, glutathionylation, methylation and sulfonation), can decrease the chemotherapeutic efficacy [6].

Enhanced DNA damage repair

The administration of chemotherapeutic drugs or the exposure to radiation promotes considerable DNA damage, leading to cell death. Nevertheless, the affected cells to anticancer drugs trigger the activation of DNA lesion repairs, reducing dramatically the therapeutic efficacy [11]. In cancer cells, the DNA repair pathways are frequently up-regulated, causing resistance to chemotherapeutics.

Microenvironment

Tumors are heterogeneous entities, characterized by different types of cells and extracellular matrix (ECM) that contribute to identifying the tumor microenvironment (TME). TME may play an important role in the development of intrinsic resistance to chemotherapies. In tumors, it is easy to find acidic regions due to the increase of proton pumps that reduce the extracellular pH. This altered homeostasis influences the anticancer drug efficacy since weakly basic chemotherapeutics (such as doxorubicin, vinblastine and vincristine) are ionized at acidic pH, hampering passive cellular uptake [12,13]. On the other hand, the uptake of weakly acidic drugs is improved at acidic extracellular pH [14]. Moreover, hypoxia is also a typical factor of TME due to variation and disruption of vasculature inside tumors. Hypoxia contributes to the progression of more malignant and resistant tumor cells, being also responsible for increasing MDR acquisition. This altered condition can lead to the generation of oxidative stress, responsible for DNA damages in tumor cells and consequently genetic instability with the accumulation of additional mutations. In addition, hypoxia is mainly induced by hypoxia-inducible factor 1α (HIF-1α), which regulates the expression of several target genes involved in the treatment outcome [15,16].

Strategies for fighting drug resistance

Tumors present high heterogeneity and complexity in terms of different population of cells, gene mutations, and altered microenvironment. Moreover, there is high variability among patients, and each one responds to chemotherapy in different ways. This multifactoriality makes even harder the fight against cancer. Certainly, tumors have to be faced from several angles, in order to find the best strategy to defeat them. Without any doubt, drug resistance remains a major obstacle to the complete recovery of patients. The constant monitoring of patients, the development of personalized and combinational therapies are required to overcome drug resistance. For this reason, the administration of cocktails of anticancer drugs is preferred. Chemotherapeutics/target drugs with different molecular targets represent a promising approach to enhance anticancer efficiency and thus combating drug resistance [17,18]. In tumors, the presence of subclonal populations of cells resistant to chemotherapy is the cause of the development of resistance. Using single-target drugs, after the first cycle of treatment, the sensitive cancer cells are killed while the resistant ones are able to survive and proliferate. The use of multi-targeting drugs may contrast this pathological mechanism. Multi-targeting anticancer drugs can act in producing an additive or synergistic effect due to the administration of several drugs with different targets. An example of these combinational therapies is the regimen of adriamycin and cyclophosphamide and sometimes docetaxel in the treatment of breast cancer [19]. Another method is to design single agents that can act on multiple targets simultaneously. For example, levatinib is an inhibitor of tyrosine kinase that inhibits VEGFR1, VEGFR2 and VEGFR3 receptors [20]. However, the results of chemotherapies on patient survival depend on the distinctive resistance profile of tumor cells and the toxicity tolerance of patients.

An alternative approach to overcome drug resistance consists of the use of drug delivery systems to circumvent the different mechanisms of multidrug resistance. Nanoparticles can be exploited based on their intrinsic characteristics. Indeed, they can be preferentially accumulated at the tumor site through the enhanced permeability and retention (EPR) effect and can be modified for favorite an active targeting, thus reducing systemic toxicity and side effects. Moreover, nanoparticles can escape the efflux mediated by MDR pumps and increase the intracellular concentration of chemotherapeutics. Besides, the nanoparticles can represent suitable platforms for the co-administration of multiple drugs. The co-loading of anticancer drugs in specific formulations can be useful for the precise control of drug ratio and delivery.

An example of a synergistic effect due to the co-delivery of a chemotherapeutic (novantrone) and a drug efflux inhibitor (verapamil) is described in the work of Dong *et al.* [21]. They enhanced the efficiency of the anticancer drug inside sensitive and resistant breast cancer cells exploiting the inhibition of MDR pumps. Moreover, the formulation that they developed was decorated with an antibody, able to actively direct the co-delivery nanoparticles to the tumor site. Recently, Zhao *et al.* [22] described the synergistic effect of curcumin and paclitaxel on ovarian cancer cells. They reversed the cell resistance and improved the drug efficacy with the co-delivery in polymeric nanoparticles. Furthermore, Zhang *et al.* [23] demonstrated that nanocarriers loaded with celecoxib, a cyclooxygenase 2 (COX-2) inhibitor, and the chemotherapeutic doxorubicin improved the chemosensitivity of cancer breast cells that presented an up-regulation of MDR1 proteins. Indeed, COX-2 is involved in cancer progression and proliferation and has also a role in the overexpression of MDR1. The synergistic effect of celecoxib and doxorubicin increased the amount of drug accumulated inside the cells and cytotoxicity efficiency.

Hypoxia

Tumor microenvironment (TME) is mainly composed of blood vessels, lymphatic vessels, fibroblasts, immune cells and extracellular matrix (ECM). These elements interact with cancer cells and are responsible for the evolution of the malignancy. In the mechanism of tumor development and progression, cancer and stromal cells often present restricted access to nutrients and oxygen. Indeed, most solid tumors have regions permanently or transiently subjected to limited availability of oxygen and poor blood supply. Hypoxia is a hallmark of TME, and contributes to aberrant proliferation, vascularization, metastasis, and drug resistance [24,25]. The oxygen deficiency in tumor tissues derives from an imbalance between increased oxygen consumption and inadequate oxygen supply. In this condition, cancer cells usually induce the formation of new blood capillaries, but the mechanism of angiogenesis drives to irregular and disrupted vasculature organization and consequently persistent hypoxia. Over time, in an attempt to adapt to hypoxia, tumor cells become more aggressive and therapeutically resistant.

In tumor tissues, the cells are subjected to an oxygen gradient (Figure 2). The cells situated next to functional blood vessels are considered normoxic and are usually viable and proliferative. Then, there is a hypoxic region, where cells are exposed to less oxygen concentration. In normal conditions, cells die if the oxygen levels are too low. But in tumors, hypoxia can induce metabolic mutations that permit cells to survive even in a hostile milieu. Finally, if the distance between blood vessels and the cells is higher than 100-150 µm, the cells become necrotic [26].

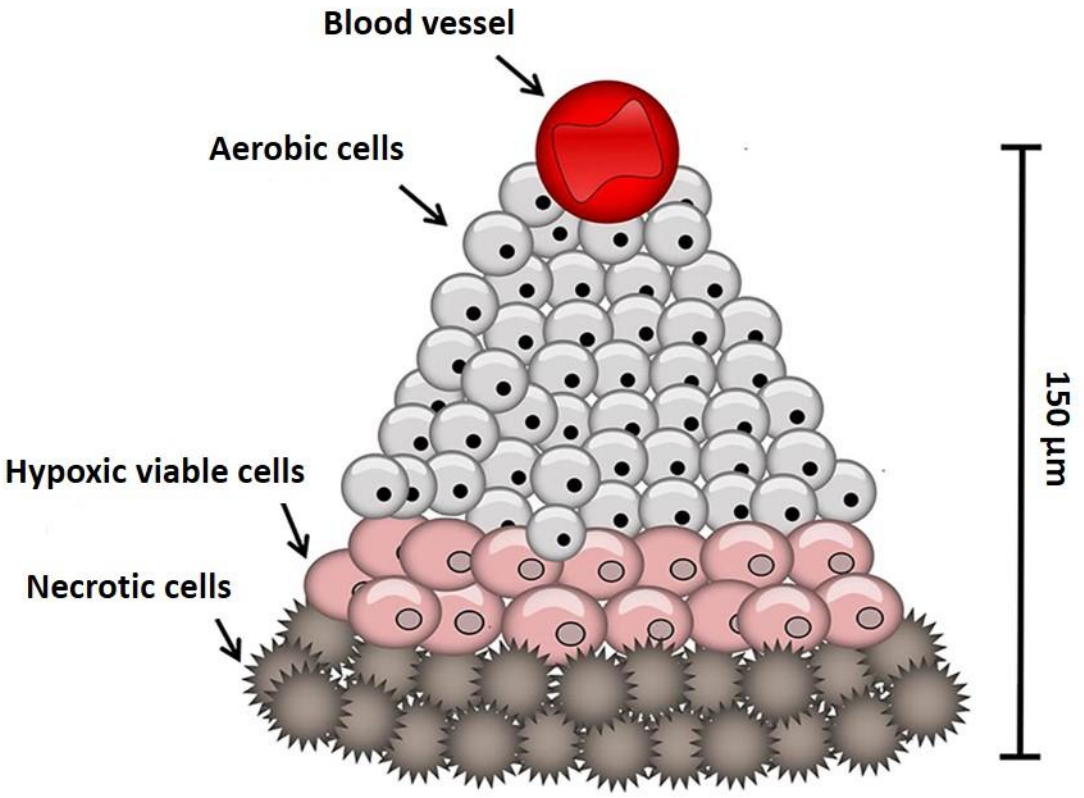

Figure 2. Solid tumors present increasingly hypoxic regions when the cells increase the distance from blood capillaries. Modified from Al Tameemi *et al.* [26].

The hypoxic response is mostly ascribed to the expression of hypoxia-inducible factors (HIFs). Indeed, HIFs play an important role in promoting the adaptation and progression of tumor cells. The HIF isoforms are three: HIF-1, HIF-2 and HIF-3 [27]. These transcription factors present an oxygen-sensitive α-subunit and a β-subunit. The most implicated in the hypoxia process and the most expressed in cancer cells is HIF-1. Under oxygen stress, HIF-1α is accumulated and associated to HIF-1β. Then, the heterodimer binds to the hypoxia response element of target genes; conversely, in normoxia HIF-1α is quickly degraded.
The active form HIF-1α regulates, directly and indirectly, several genes (reported in Table 1), implicated in the progression of cancer. For example, HIF-1α is involved in the promotion of angiogenesis, erythropoiesis, cell growth and proliferation, invasion, metastasis and metabolic adaptation [28,29].

Table 1. HIF-1α target genes expressed in the case of cancer progression [30].

HIF-1α-mediated cancer progression	**HIF-1α target genes**
Increased cell proliferation and survival	Transforming growth factor-a (TGFA) Insulin-like growth factor-2 (IGF2) Vascular endothelial growth factor (VEGF) Endothelin 1 (EDN1) Erythropoietin (EPO)
Metabolic reprogramming	Glucose transporters (GLUT 1 and 3) Glycolytic enzymes Pyruvate dehydrogenase kinase 1 (PDK1)
Angiogenesis	Vascular endothelial growth factor (VEGF) Stromal-derived factor 1 (SDF1) Platelet derived growth factor B (PDGFB) Angiopoietin (ANGPT) 1 and 2
Epithelial–mesenchymal transition	Inhibitor of differentiation 2 (ID2) Snail 1 and 2 (SNAI1, SNAI2) Transcription factor 3 (TCF3) and TGFA Vimentin (VIM) Zinc finger E-box-binding homeobox (ZEB1, ZEB2)
Invasion and metastasis	Autocrine motility factor (AMF) Angiopoietin-like 4 (ANGPTL4) L1 cell adhesion molecule (L1CAM) Met proto-oncogene/hepatocyte growth factor receptor (MET) Matrix metalloproteinases (MMP2, MMP9, MMP14) Urokinase plasminogen activator receptor (PLAUR)

Strategies for fighting hypoxia

Several clinical applications (i.e. radio- and chemotherapies) required the presence of oxygen next to the tumor site to achieve better outcomes with the treatments. Oxygen, indeed, represents the key to reduce the malignancy. Without any doubt, an approach to reduce the hypoxic stress in tumor cells is to deliver oxygen to optimize the oxygenation [31].

HIF-1α–targeted therapy

Different drugs have been studied to block the activity of HIF-1α in order to decrease the response to hypoxia in tumor cells. These HIF-1α–targeted drugs can act through different molecular mechanisms, and they include inhibitors of the HIF-1α signaling pathway (RAF kinase, mTOR, and EGFR) and inhibitors of HIF-1α activation (topoisomerase I and HSP90) [32]. These drugs can be administrated alone or conjugated in nanoparticles.
In addition, HIF-1α inhibition into hypoxic tumors by miRNA or siRNA may efficiently mediate recovery from hypoxia. Indeed, the silencing of HIF-1α expression can inhibit the cascade of pathways that are regulated from this protein, thus circumventing hypoxia. Different nanoparticles have been designed for the delivery of siRNA targeting HIF-1α [33–35].

Oxygen vehicles

Hyperbaric Oxygenation

Oxygen administration by hyperbaric oxygenation (HBO) can enhance the amount of dissolved oxygen in the plasma. In this way, HBO improves tumor perfusion and cell sensitivity to chemotherapy, helping to impair the drug resistance [36]. Hyperbaric oxygen can be a chemotherapy adjuvant, but it also plays an important role in improving radiotherapy outcomes. Indeed, HBO and radiotherapy combination reduce the neoplastic progression and increase the survival rate [37].

Red blood cell-based oxygen carriers

Red blood cells (RBCs) can be used as endogenous carriers for active compounds because of their biocompatibility, long circulation time and high loading capacity. In particular, they can be exploited for the delivery of oxygen. RBC–nanoparticle conjugates have been studied for the delivery of oxygen in order to improve the efficiency of radiotherapy by Gao *et al.* [38]. These nanoparticles can deliver oxygen in tumor tissues and then relieve tumor hypoxia.

Perfluorocarbons as oxygen carriers

Currently, perfluorocarbons (PFCs) are employed as alternative oxygen carriers for fighting hypoxia. Perfluorocarbons are organofluorine compounds able to dissolve respiratory gases, CO_2 and N_2 with a high rate capacity because of their weak intermolecular interactions. Perfluorocarbons are hydrophobic, biocompatible and extreme inert compounds, and once administrated they can be excreted by exhalation from lungs or skin pores [39,40]. PFCs have been largely used in the clinic for several functions, such as ultrasound imaging contrast, organ transplantation, and prevention of

ischemia/reperfusion injury of tissue and organs. They are considered a promising artificial blood substitutes [41].

Different nanoplatforms based on perfluorocarbons for sustained oxygen release have been developed. For example, Bi_2Se_3 nanoparticles with a hollow structure to load PFC were designed by Song *et al.* for a rapid O_2 release under NIR irradiation for increasing the tumor oxygenation [42]. Sheng *et al.* [43] developed a nanoliposome formulation carrying perfluorooctyl bromide in the core with a bilipidic shell. They observed a sustained release of O_2 from the nanoparticles by diffusion for at least 24 hours.

Besides the nanoparticles, another approach for O_2 delivery consists of the use of micro-/nanobubbles to bring oxygen to the hypoxic tumor tissues [44]. In these nanoplatforms, the shell usually consists of a mono-/bilayer biomaterial (lipids, proteins, polymers) that encapsulates the PFC gas core. Moreover, Ultrasound (US) combined with O_2 carriers can be used to enhance cell permeability for a higher uptake of the bioactive molecules to distribute oxygen to hypoxic regions [45]. Cavalli *et al.* [46,47] developed novel biocompatible nanobubble formulations with polymeric shells for the delivery of oxygen in hypoxic conditions. More recently, Song *et al.* [48] designed oxygen nanobubbles shelled with acetylated dextran polymer for natural oxygenation in response to the acidic pH in the tumor microenvironment. The polymeric shell acts as a barrier against gas dispersion in the circulating blood, and its pH-responsive property targets the tumor microenvironment and avoids an unexpected burst release of oxygen.

Nanoplatform as oxygen carriers

Other systems were taken into consideration for the storage and the delivery of oxygen. In particular, Cyclodextrin-based polymers and nanosponges were investigated by Cavalli *et al.* for their ability to store and release oxygen for a prolonged period [49]. Moreover, different types of α-Cyclodextrin-based polymers were studied as suitable systems for oxygen transport. These nanoplatforms showed to have the capability to limit hypoxia/reoxygenation injury in a cardiac cell model [50]. Finally, PLGA microsphere demonstrated to be capable to increase cell viability under hypoxic conditions [51].

In order to counteract drug resistance and hypoxia, many approaches have been studied. In my PhD thesis, the approach that I investigated was nanomedicine.

Nanomedicine approach

In the last decades, a strong interest in applying nanotechnology to medicine was growing to revolutionize drug delivery, diagnosis, imaging, and immunization. Nanotechnology is defined as the science involved in the design, synthesis, characterization, and application of materials and devices at the nanoscale. In particular, nanomedicine incorporates appealing features needed to develop better solutions for medical problems, exploiting materials with nanoscale dimensions for acting as delivery vehicles for imaging or therapeutic approaches [52]. Nanomedicine offers a versatile platform of biocompatible and biodegradable systems able to carry drugs, increasing their bioavailability and concentration at the target tissues, and improving their efficacy and safety. Moreover, these nanosystems can be useful to overcome critical side effects caused by conventional therapies. The current attention in nanomedicine is also focused on the development of individualized therapies for patients with different pathological conditions: cancer, genetic diseases, inflammatory diseases, etc. In particular, anticancer therapy is one of the hottest subjects in nanomedicine investigation and includes a wide range of branches [53].
Nanoparticles represent precise nanocarriers able to address diseases in a smart, personalized and safe manner. Nanoparticles are nanosize systems (1–1,000 nm) with peculiar physico-chemical properties because of their size and high surface-to-volume ratio. The use of nanodelivery systems can be advantageous to increase the pharmacological features of existing drugs and generate new therapies with sophisticated targeting strategies and multi-functionality [54]. Nanoparticles can load active compounds increasing their solubility by different means: chemically (conjugation), physically (encapsulation), or via adsorption. The employment of nanotechnology in medicine allows an increment of the bioavailability of the drugs by improving their internalization, decreasing their degradation/clearance, and providing a slow-release mechanism. Moreover, the circulation time of the nanoparticles can be managed by modulating their surface charge and characteristics, according to their precise target. For instance, the positive charges encourage the uptake of the nanoparticles inside the cells, while the negative charges prolong the circulation in the bloodstream. Additionally, the nanoparticles can modify the pharmacokinetics of the loaded drugs, decreasing the side effects and reducing the required doses [55].

Principle keys of nanomedicine in cancer

The major advantages and rationale for the development of nanoparticle-based drug delivery systems for cancer therapy are listed as follows (Figure 3) [56].

a) The nanoparticles can contribute to enhancing the physico-chemical properties of conventional drugs, overcoming problems of solubility and chemical stability. Indeed, poor water solubility could limit the bioavailability of a compound. The employment of hydrophilic nanocarriers can be useful for increasing the delivery, and thus the chemical stability of a drug.
b) The nanocarriers improve the pharmacokinetic and pharmacodynamics profiles of conventional drugs, optimizing the efficacy of existing therapies. Moreover, they protect anticancer drugs from biodegradation by enzymes or early excretion.

c) The nanoparticles can improve the biodistribution of the chemotherapeutics and enhance their penetration into cancer tissues. They can redirect the drugs directly to the tumor site, both with passive and active targeting strategies. In this way, nonspecific toxicity and side effects are reduced.
d) The nanodelivery systems can be designed to release their cargo upon physical, chemical, or biological triggers, resulting in stimuli-sensitive nanomedicine therapeutics [57].
e) The nanoparticles can co-delivery multiple drugs to improve therapeutic efficacy and overcome drug resistance. Moreover, it is possible to combine therapeutic agents with imaging modalities, resulting in hybrid formulations in the field of nanotheranostics.

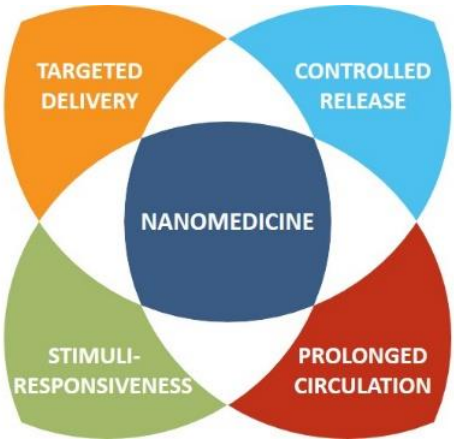

Figure 3. Design of nanomedicine for enhanced therapy.

Smart nanodelivery systems

Concerning the treatment of clinical diseases such as cancer, the use of "smart" drug delivery systems is essential to increase the drug concentration directly to the tumor site, minimizing potential side effects. For this reason, smart nanoparticles are the tools to improve precision in the target shooting of anticancer therapies [58]. Smart nanoparticles (SNPs) are nanosized active delivery systems that evolve their physico-chemical proprieties in response to the microenvironment, such as pH, enzyme concentration or redox gradients associated with different pathological conditions. These types of vehicle promote the release of their cargo to the specific biological target thanks to many features such as the degradability or the rapid conformational changes in response to mild physical/chemical conditions. Concerning this point, SNPs can deliver drugs to the target sites with reduced dosage frequency, improved drugability and in a spatially controlled manner [59]. The *in vivo* stimuli that can lead the response of SNPs are generally classified into chemical-biochemical (environmental or internal) stimuli and physical (external) stimuli [60].

Environmental stimuli

The chemical and biochemical stimuli include, among others, cellular pH-shift, redox and ionic microenvironment of specific tissues, and enzyme overexpression in certain pathological states [61]. Some examples are listed below.

pH-responsive SNPs

The acidic milieu of the tumor microenvironment allows the employment of pH-sensitive nanodelivery systems to target cancer cells and release drugs around the tumor tissues. An example is represented by the pH-sensitive poly(N,N-dimethylaminoethyl methacrylate/2-hydroxyethyl methacrylate) nanoparticles, which can be effectively triggered by mild physiological changes in pH within values between 0.2 and 0.6 [58]. Moreover, micelles based on a co-polymer stearoyl–PEG–poly-sulfadimethoxine methacrylate were proposed by Ravazzolo *et al.* as pH-sensitive vesicular systems for tumor targeting [62].

Redox-responsive SNPs

Redox-responsive nanoparticles (NPs), in particular glutathione (GSH)-responsive NPs, are very appealing for targeted intracellular drug delivery because the major redox couple in animal cells is GSH/glutathione disulfide (GSSG) that determines the anti-oxidative capacity of cells. GSH-sensitive NPs carry amphiphilic copolymers with disulfide bonds in their hydrophobic segments that allow drug release concomitantly in response to elevated GSH concentrations at the tumor site [63]. One interesting redox-responsive NPs were prepared by Daga *et al.* with GSH-nanosponges loaded with doxorubicin. This smart delivery system was able to increase the doxorubicin toxicity in cells with high GSH content [64].

Hypoxia-responsive SNPs

Since hypoxia is involved in many aspects of the biology of many diseases, including cancer, it can be significantly considered as an internal target for the delivery of nanocarriers. Nowadays, hypoxia is emerging as a primary target in the development of diagnostic and therapeutic agents. The characteristic reductive environment of hypoxia affects many therapeutic responses. For example, doxorubicin-loaded nanoparticles derived with 2-nitroimidazole under hypoxic conditions converted the hypoxia-responsive portion to the hydrophilic 2-aminoimidazoles, thus enhancing the drug released [65].

Enzyme-responsive SNPs

Enzymes promote physiological function and exhibit dysregulation in many disease-associated microenvironments. Exploiting altered enzyme activity and expression, the design of targeted delivery systems is currently promising [66]. Naz *et al.* designed an enzyme-responsive drug delivery system able to targeting both cell and organelle levels based on mesoporous silica nanoparticles, which have both CD44-targeting and mitochondrial-targeting properties.

External stimuli

Additionally, physical stimuli can be applied externally to bring a triggered release of drugs, involving among others temperature, light, mechanical pressure, magnetic or electrical fields. Some examples are here reported.

Thermo-responsive SNPs

Thermally responsive polypeptides and polymers provide an interesting example of thermo-responsive materials that can be used in nanocarrier. To have a consistent accumulation of the thermo-responsive nanodelivery systems is required a level of heating found in mild clinical hyperthermia. Temperature-responsive macromolecules exhibiting a lower critical solution temperature transition are soluble below their transition temperature and undergo aggregation into insoluble polymer coacervates above it. So the use of biopolymers such as elastin-like polypeptides can be exploited to improve the delivery of attached therapeutics to tumors that are subjected to mild hyperthermia [67,68]. Moreover, much research has been done on Pluronic F-127, a thermo-responsive polymer that undergoes a sol–gel transition at body temperature. Almeida *et al.* studied eyedrops based on the combination of nanostructured lipid carriers and Pluronic F-127 for controlled delivery of ibuprofen [69].

Magnetic-responsive SNPs

Thanks to the real-time response and a brief triggering impulse, magnetic NPs can be functionalized and studied as useful vehicles in drug delivery and biomedical targeting. These systems, combined with a high frequency alternating magnetic field (AMF), induce heat generation and enhance the release of the drug, such as doxorubicin in specific tumor sites [70].

Electrical-responsive SNPs

Electrically triggered smart nanocarriers can be exploited for sustained, pulsed, or on-demand drug release via the application of external electric fields. The develop of electro-responsive hydrogel NPs for targeted delivery of an antiepileptic drug (phenytoin sodium) is an example of these physical responsive stimuli [71].

Light-responsive SNPs

Light irradiation can be used as a stimulus to trigger the drug release. Carbon dots with strong fluorescent emission, polymeric hydrogels exhibiting a hydration/dehydration transition mechanism, gold NPs for photogenerated localized heating and core-shell particles are all examples of these physical stimuli responsive nanodelivery systems with a drug-release especially toward tumor cells [72,73].

Mechanical-responsive SNPs

Cyclodextrin inclusion complexes are considered mechano-responsive nanostructures. They can be affected by pressure and the destabilization of the inclusion complex in cyclodextrin–alginate hydrogels by mechanical compression was reported for the purpose of the patient-controlled release of ondansetron [74].

Ultrasound-responsive SNPs

One of the most common external stimulus applied to smart nanocarriers for chemotherapy is Ultrasound (US). Ultrasound covers great importance in modern medicine and plays a role in many medical applications such as diagnosis or treatment (i.e. for the removal of masses such as tumors). This type of physical stimulus is commonly used for its safety, non-invasiveness and its great spatiotemporal control [75]. US can induce thermal and mechanical effects, radiation force, pressure variation, acoustic fluid streaming, cavitation and local hyperthermia, and all these effects can be exploited for different medical applications. Indeed, these proprieties could make this application the future of on-demand drug release [76].
As an example, with a US-induced temperature increase, mesoporous silica nanoparticles grafted with PEG are able to disengage the PEG chains from the surface displaying the positive charges of the particles, for an improved cancer cell uptake [77]. Other examples of nanoparticles associated with US are PLGA NPs. They were used to induce US responsive vibrations, which destabilized the membrane of liposomes enclosing PLGA NPs. In this way, mitoxantrone-loaded US-sensitive liposomes showed enhanced drug release in the presence of US (~90%) as compared to that without US stimulus (~50%) after 10 hours [78]. But not only polymeric nanoparticles or liposomes can be used in association with Ultrasound. Microbubbles (MBs) are commonly used as ultrasound contrast agents with micrometer size for non-invasive real-time molecular imaging techniques and as drug and oxygen carriers [78,79]. Notably, the association of a drug with microbubble structures allows controlled drug release and deposition. Polymer-shelled microbubbles have been developed to improve system stability [80], but because of their microsize these systems can not extravasate, thus decreasing the delivery of their cargo at the target site. Besides, several perfluorocarbon-based nanodroplet formulations have been developed for US-controlled drug delivery and gene delivery [79,80]. Exploiting their nanosize, these nanorfulations can reach the tumor via passive or active targeting. Once there, the application of US promote a phase-shift from their vapor to gas form. This phenomenon, called acoustic droplet vaporization (ADV), favor the release of their drug cargo that can be also followed through real-time imaging [81]. Indeed, the newly formed microbubbles present enhanced contrast properties. These nanodroplets represent an effective promising nanotheranostic tool.

Aim of the work

The aim of my PhD work was to address two aspects that make the fight against cancer tough: drug resistance and hypoxia. For this purpose, nanomedicine-based platforms were elected for studying innovative approaches for the treatment of this deathly malignancy. Several nanodelivery systems were designed and developed to overcome either the resistance that arises in the cancer cells after chemotherapeutic treatment or the hypoxia that occurs in the tumor microenvironment rendering cancer more aggressive. Different nanostructures have been considered to optimally perform these tasks, and the most suitable ones have been selected. Notably, nanodroplets with their echogenic and multifunctional properties, liposomes with their versatility and albumin-based nanoparticles with their high biocompatibility were studied as suitable nanotools. The results of these works are reported in four chapters of this PhD thesis.

1) OXYGEN-CURCUMIN-GEMCITABINE LOADED NANODROPLETS: A TRIPLE COMBINATION THERAPY TO HAMPER HYPOXIC PANCREATIC CANCER

   Oxygen-Curcumin-Gemcitabine loaded nanodroplets were designed to hinder the mechanisms related to hypoxia in pancreatic cancer and to reduce the resistance developed after treatment with Gemcitabine exploiting the effect of Curcumin. Of note, nanodroplets possess echogenic properties that can be exploited for a theranostic approach. This triple-combinational nanoformulation may represent a novel nanoplatform for the treatment of pancreatic cancer.

2) LOW-DOSE CURCUMINOID-LOADED IN DEXTRAN-BASED NANODROPLETS CAN PREVENT METASTATIC SPREADING IN PROSTATE CANCER CELLS

   Curcumin derivatives, Curcuminoids, were loaded in dextran sulfate coated nanodroplets for their adjuvant involvement in preventing the metastatic spreading in the prostate cancer cells. The echogenic properties of the nanodroplets may render them a promising theranostic nanotool with the simultaneous delivery of active compounds and imaging.

3) HYPOXIA-SENSITIVE LIPOSOMES FOR CO-DELIVERY OF siRNA AND PACLITAXEL

   Another approach to overcome drug resistance was to develop environmentally sensitive liposomes. Exploiting a polymeric conjugate sensitive to the hypoxia typical of the tumor microenvironment, a liposomal formulation for the co-delivery of small interfering RNA (siRNA) against for the overexpressed P-glycoprotein, responsible for inducing chemoresistance, and paclitaxel was designed and tested.

4) ALBUMIN-BASED NANOPARTICLES FOR IMPROVING INTRACELLULAR DELIVERY OF DOXORUBICIN IN RESISTANT CANCER CELL LINES

   Albumin-based Doxorubicin-loaded nanoparticle formulations were designed for overcoming *per se* the resistance of ovarian and breast cancer cells. Uncoated and coated with glycol chitosan formulations were prepared and the cytotoxicity was *in vitro* assessed.

References

[1] S. Chakraborty, T. Rahman, The difficulties in cancer treatment., Ecancermedicalscience. 6 (2012) ed16. doi:10.3332/ecancer.2012.ed16.

[2] W. Hospital, disease , verified pathologically by biopsy , were treated, (1946) 409–415.

[3] N. Vasan, J. Baselga, D.M. Hyman, A view on drug resistance in cancer, Nature. 575 (2019) 299–309. doi:10.1038/s41586-019-1730-1.

[4] I.A. Cree, P. Charlton, Molecular chess ? Hallmarks of anti-cancer drug resistance, BMC Cancer. (2017) 1–8. doi:10.1186/s12885-016-2999-1.

[5] D. Waghray, Q. Zhang, Q. Zhang, Inhibit or Evade Multidrug Resistance P-Glycoprotein in Cancer Treatment, (2018). doi:10.1021/acs.jmedchem.7b01457.

[6] R.K. Vadlapatla, A.D. Vadlapudi, D. Pal, A.K. Mitra, Mechanisms of Drug Resistance in Cancer Chemotherapy : Coordinated Role and Regulation of Efflux Transporters and Metabolizing Enzymes, (2013) 7126–7140.

[7] Q. Wu, Z. Yang, Y. Nie, Y. Shi, D. Fan, Multi-drug resistance in cancer chemotherapeutics : Mechanisms and lab approaches, Cancer Lett. 347 (2014) 159–166. doi:10.1016/j.canlet.2014.03.013.

[8] M. Sciences, A multidrug resistance transporter from human MCF-7 breast cancer cells, 95 (1998) 15665–15670.

[9] S.P.C. Coie, G. Bhardwaj, J.H. Gerlach, J.E. Mackie, C.E. Grant, K.C. Almquist, A.J. Stewart, E.U. Kurz, A.M. V Duncan, R.G. Deeley, Overexpression of a Transporter Gene in a Multidrug-Resistant Human Lung Cancer Cell Line, 258 (1992).

[10] N. Chatterjee, T.G. Bivona, Polytherapy and Targeted Cancer Drug Resistance, TRENDS in CANCER. 5 (n.d.) 170–182. doi:10.1016/j.trecan.2019.02.003.

[11] D. Version, University of Birmingham DNA repair pathways as targets for cancer therapy, (2020). doi:10.1038/nrc2342.

[12] I. Kolosenko, S. Avnet, N. Baldini, J. Viklund, A. De Milito, Seminars in Cancer Biology Therapeutic implications of tumor interstitial acidification, Semin. Cancer Biol. 43 (2017) 119–133. doi:10.1016/j.semcancer.2017.01.008.

[13] M.R. Asgharzadeh, J. Barar, M.M. Pourseif, M. Eskandani, M.J. Niya, Molecular machineries of pH dysregulation in tumor microenvironment : potential targets for cancer therapy, Tabriz Univ. Med. Sci. 7 (2017) 115–133. doi:10.15171/bi.2017.15.

[14] L.E. Gerweck, S. Vijayappa, Tumor pH controls the in vivo efficacy of weak acid and base chemotherapeutics, 5 (2006) 1275–1280. doi:10.1158/1535-7163.MCT-06-0024.

[15] A.A. Tirpe, D. Gulei, S.M. Ciortea, C. Crivii, Hypoxia : Overview on Hypoxia-Mediated Mechanisms with a Focus on the Role of HIF Genes, (2019) 1–20. doi:10.3390/ijms20246140.

[16] X. Jing, F. Yang, C. Shao, K. Wei, M. Xie, H. Shen, Y. Shu, Role of hypoxia in cancer therapy by regulating the tumor microenvironment, (2019) 1–15.

[17] B. Kumar, S. Singh, I. Skvortsova, V. Kumar, Promising Targets in Anti-cancer Drug Development: Recent Updates, Curr. Med. Chem. 24 (2017). doi:10.2174/0929867324666170331123648.

[18] N.M. Raghavendra, D. Pingili, S. Kadasi, A. Mettu, S.V.U.M. Prasad, Dual or multi-targeting inhibitors: The next generation anticancer agents, Eur. J. Med. Chem. 143 (2018) 1277–1300. doi:10.1016/j.ejmech.2017.10.021.

[19] G. von Minckwitz, Docetaxel/anthracycline combinations for breast cancer treatment, Expert Opin. Pharmacother. 8 (2007) 485–495. doi:10.1517/14656566.8.4.485.

[20] L. Tao, F. Zhu, F. Xu, Z. Chen, Y.Y. Jiang, Y.Z. Chen, Co-targeting cancer drug escape pathways confers clinical advantage for multi-target anticancer drugs, Pharmacol. Res. 102 (2015) 123–131. doi:10.1016/j.phrs.2015.09.019.

[21] Y. Dong, H. Liao, J. Yu, H. Fu, D. Zhao, K. Gong, Q. Wang, Y. Duan, Incorporation of drug efflux inhibitor and chemotherapeutic agent into an inorganic/organic platform for the effective treatment of multidrug resistant breast cancer, J. Nanobiotechnology. 17 (2019) 1–15. doi:10.1186/s12951-019-0559-y.

[22] M.D. Zhao, J.Q. Li, F.Y. Chen, W. Dong, L.J. Wen, W.D. Fei, X. Zhang, P.L. Yang, X.M. Zhang, C.H. Zheng, Co-delivery of curcumin and paclitaxel by “core-shell” targeting amphiphilic copolymer to reverse resistance in the treatment of ovarian cancer, Int. J. Nanomedicine. 14 (2019) 9453–9467. doi:10.2147/IJN.S224579.

[23] S. Zhang, N. Guo, G. Wan, T. Zhang, C. Li, Y. Wang, Y. Wang, Y. Liu, PH and redox dual-responsive nanoparticles based on disulfide-containing poly(β-amino ester) for combining chemotherapy and COX-2 inhibitor to overcome drug resistance in breast cancer, J. Nanobiotechnology. 17 (2019) 1–17. doi:10.1186/s12951-019-0540-9.

[24] C. Macedo-Silva, V. Miranda-Gonçalves, R. Henrique, C. Jerónimo, I. Bravo, The critical role of hypoxic microenvironment and epigenetic deregulation in esophageal cancer radioresistance, Genes (Basel). 10 (2019). doi:10.3390/genes10110927.

[25] X. Jing, F. Yang, C. Shao, K. Wei, M. Xie, H. Shen, Y. Shu, Role of hypoxia in cancer therapy by regulating the tumor microenvironment, Mol. Cancer. 18 (2019) 1–15. doi:10.1186/s12943-019-1089-9.

[26] W. Al Tameemi, T.P. Dale, R.M.K. Al-Jumaily, N.R. Forsyth, Hypoxia-Modified Cancer Cell Metabolism, Front. Cell Dev. Biol. 7 (2019) 1–15. doi:10.3389/fcell.2019.00004.

[27] A.A. Tirpe, D. Gulei, S.M. Ciortea, C. Crivii, I. Berindan-Neagoe, Hypoxia: Overview on Hypoxia-Mediated Mechanisms with a Focus on the Role of HIF Genes, Int. J. Mol. Sci. 20 (2019) 1–20. doi:10.3390/ijms20246140.

[28] G.L. Semenza, Hypoxia-inducible factors in physiology and medicine, Cell. 148 (2012) 399–408. doi:10.1016/j.cell.2012.01.021.

[29] N. Goda, M. Kanai, Hypoxia-inducible factors and their roles in energy metabolism, Int. J. Hematol. 95 (2012) 457–463. doi:10.1007/s12185-012-1069-y.

[30] M.A. Akanji, D. Rotimi, O.S. Adeyemi, Hypoxia-inducible factors as an alternative source of treatment strategy for cancer, Oxid. Med. Cell. Longev. 2019 (2019). doi:10.1155/2019/8547846.

[31] L. Larue, B. Myrzakhmetov, A. Ben-Mihoub, A. Moussaron, N. Thomas, P. Arnoux, F. Baros, R. Vanderesse, S. Acherar, C. Frochot, Fighting hypoxia to improve PDT, Pharmaceuticals. 12 (2019). doi:10.3390/ph12040163.

[32] E. Paolicchi, F. Gemignani, M. Krstic-Demonacos, S. Dedhar, L. Mutti, S. Landi, Targeting hypoxic response for cancer therapy, Oncotarget. 7 (2016) 13464–13478.

doi:10.18632/oncotarget.7229.

[33] W.H. Chen, R.L.G. Lecaros, Y.C. Tseng, L. Huang, Y.C. Hsu, Nanoparticle delivery of HIF1α siRNA combined with photodynamic therapy as a potential treatment strategy for head-and-neck cancer, Cancer Lett. 359 (2015) 65–74. doi:10.1016/j.canlet.2014.12.052.

[34] X. Zhao, F. Li, Y. Li, H. Wang, H. Ren, J. Chen, G. Nie, J. Hao, Co-delivery of HIF1α siRNA and gemcitabine via biocompatible lipid-polymer hybrid nanoparticles for effective treatment of pancreatic cancer, Biomaterials. 46 (2015) 13–25. doi:10.1016/j.biomaterials.2014.12.028.

[35] Y. Yong, C. Zhang, Z. Gu, J. Du, Z. Guo, X. Dong, J. Xie, G. Zhang, X. Liu, Y. Zhao, Polyoxometalate-Based Radiosensitization Platform for Treating Hypoxic Tumors by Attenuating Radioresistance and Enhancing Radiation Response, ACS Nano. 11 (2017) 7164–7176. doi:10.1021/acsnano.7b03037.

[36] I. Moen, L.E.B. Stuhr, Hyperbaric oxygen therapy and cancer - A review, Target. Oncol. 7 (2012) 233–242. doi:10.1007/s11523-012-0233-x.

[37] K. Stępień, R.P. Ostrowski, E. Matyja, Hyperbaric oxygen as an adjunctive therapy in treatment of malignancies, including brain tumours, Med. Oncol. 33 (2016) 1–9. doi:10.1007/s12032-016-0814-0.

[38] M. Gao, C. Liang, X. Song, Q. Chen, Q. Jin, C. Wang, Z. Liu, Erythrocyte-membrane-enveloped perfluorocarbon as nanoscale artificial red blood cells to relieve tumor hypoxia and enhance cancer radiotherapy, Adv. Mater. 29 (2017) 1–7. doi:10.1002/adma.201701429.

[39] J.G. Riess, Understanding the fundamentals of perfluorocarbons and perfluorocarbon emulsions relevant to in vivo oxygen delivery, Artif. Cells. Blood Substit. Immobil. Biotechnol. 33 (2005) 47–63. doi:10.1081/BIO-200046659.

[40] K.B. Ferenz, A.U. Steinbicker, Artificial oxygen carriers—past, present, and future—a review of the most innovative and clinically relevant concepts, J. Pharmacol. Exp. Ther. 369 (2019) 300–310. doi:10.1124/jpet.118.254664.

[41] C.I. Castro, J.C. Briceno, Perfluorocarbon-based oxygen carriers: Review of products and trials, Artif. Organs. 34 (2010) 622–634. doi:10.1111/j.1525-1594.2009.00944.x.

[42] G. Song, C. Liang, X. Yi, Q. Zhao, L. Cheng, K. Yang, Z. Liu, Perfluorocarbon-Loaded Hollow Bi2Se3 Nanoparticles for Timely Supply of Oxygen under Near-Infrared Light to Enhance the Radiotherapy of Cancer, Adv. Mater. 28 (2016) 2716–2723. doi:10.1002/adma.201504617.

[43] D. Sheng, T. Liu, L. Deng, L. Zhang, X. Li, J. Xu, L. Hao, P. Li, H. Ran, H. Chen, Z. Wang, Perfluorooctyl bromide & indocyanine green co-loaded nanoliposomes for enhanced multimodal imaging-guided phototherapy, Biomaterials. 165 (2018) 1–13. doi:10.1016/j.biomaterials.2018.02.041.

[44] M.S. Khan, J. Hwang, K. Lee, Y. Choi, K. Kim, H.J. Koo, J.W. Hong, J. Choi, Oxygen-carrying micro/nanobubbles: Composition, synthesis techniques and potential prospects in photo-triggered theranostics, Molecules. 23 (2018) 1–19. doi:10.3390/molecules23092210.

[45] C. Greve, L. Jorgensen, Therapeutic Delivery, Ther. Deliv. 7 (2016) 117–138. doi:10.4155/tde.15.92.

[46] R. Cavalli, A. Bisazza, A. Rolfo, S. Balbis, D. Madonnaripa, I. Caniggia, C. Guiot, Ultrasound-mediated oxygen delivery from chitosan nanobubbles, Int. J. Pharm. 378 (2009) 215–217. doi:10.1016/j.ijpharm.2009.05.058.

[47] R. Cavalli, A. Bisazza, P. Giustetto, A. Civra, D. Lembo, G. Trotta, C. Guiot, M. Trotta, Preparation and characterization of dextran nanobubbles for oxygen delivery, Int. J. Pharm. 381 (2009) 160–165. doi:10.1016/j.ijpharm.2009.07.010.

[48] R. Song, S. Peng, Q. Lin, M. Luo, H.Y. Chung, Y. Zhang, S. Yao, PH-Responsive Oxygen Nanobubbles for Spontaneous Oxygen Delivery in Hypoxic Tumors, Langmuir. 35 (2019) 10166–10172. doi:10.1021/acs.langmuir.8b03650.

[49] R. Cavalli, A.K. Akhter, A. Bisazza, P. Giustetto, F. Trotta, P. Vavia, Nanosponge formulations as oxygen delivery systems, Int. J. Pharm. 402 (2010) 254–257. doi:10.1016/j.ijpharm.2010.09.025.

[50] S. Femminò, C. Penna, F. Bessone, F. Caldera, N. Dhakar, D. Cau, P. Pagliaro, R. Cavalli, F. Trotta, α-cyclodextrin and α-cyclodextrin polymers as oxygen nanocarriers to limit hypoxia/reoxygenation injury: Implications from an in vitro model, Polymers (Basel). 10 (2018). doi:10.3390/polym10020211.

[51] S.I.H. Abdi, J.Y. Choi, H.C. Lau, J.O. Lim, Controlled release of oxygen from PLGA-alginate layered matrix and its in vitro characterization on the viability of muscle cells under hypoxic environment, Tissue Eng. Regen. Med. 10 (2013) 131–138. doi:10.1007/s13770-013-0391-7.

[52] C. Pucci, C. Martinelli, G. Ciofani, Innovative approaches for cancer treatment: current perspectives and new challenges, Ecancermedicalscience. 13 (2019). doi:10.3332/ecancer.2019.961.

[53] J. Wang, Y. Li, G. Nie, Y. Zhao, Precise design of nanomedicines: perspectives for cancer treatment, Natl. Sci. Rev. (2019) 1–4. doi:10.1093/nsr/nwz012.

[54] A. Wicki, D. Witzigmann, V. Balasubramanian, J. Huwyler, Nanomedicine in cancer therapy: Challenges, opportunities, and clinical applications, J. Control. Release. 200 (2015) 138–157. doi:10.1016/j.jconrel.2014.12.030.

[55] J. Shi, P.W. Kantoff, R. Wooster, O.C. Farokhzad, Cancer nanomedicine: Progress, challenges and opportunities, Nat. Rev. Cancer. 17 (2017) 20–37. doi:10.1038/nrc.2016.108.

[56] R. Wang, P.S. Billone, W.M. Mullett, An overview of Cancer Nanomedicine on the Market and in Clinical Trials, J. Coast. Life Med. 3 (2015). doi:10.12980/JCLM.3.2015JCLM-2015-0018.

[57] J.L. Paris, A. Baeza, M. Vallet-Regí, Overcoming the stability, toxicity, and biodegradation challenges of tumor stimuli-responsive inorganic nanoparticles for delivery of cancer therapeutics, Expert Opin. Drug Deliv. 16 (2019) 1095–1112. doi:10.1080/17425247.2019.1662786.

[58] Z. Fang, L.Y. Wan, L.Y. Chu, Y.Q. Zhang, J.F. Wu, Smart nanoparticles as drug delivery systems for applications in tumor therapy, Expert Opin. Drug Deliv. 12 (2015) 1943–1953. doi:10.1517/17425247.2015.1071352.

[59] S. Hossen, M.K. Hossain, M.K. Basher, M.N.H. Mia, M.T. Rahman, M.J. Uddin, Smart nanocarrier-based drug delivery systems for cancer therapy and toxicity studies: A review, J. Adv. Res. 15 (2019) 1–18. doi:10.1016/j.jare.2018.06.005.

[60] S. Fajardo, García-Galvan, F. R., V. Barranco, J.C. Galvan, S.F. Batlle, We are IntechOpen , the world ' s leading publisher of Open Access books Built by scientists , for scientists TOP 1 %, Intech. i (2016) 13. doi:http://dx.doi.org/10.5772/57353.

[61] E. Fleige, M.A. Quadir, R. Haag, Stimuli-responsive polymeric nanocarriers for the controlled transport of active compounds: Concepts and applications, Adv. Drug Deliv. Rev. 64 (2012)

866–884. doi:10.1016/j.addr.2012.01.020.

[62] E. Ravazzolo, S. Salmaso, F. Mastrotto, S. Bersani, E. Gallon, P. Caliceti, PH-responsive lipid core micelles for tumour targeting, Eur. J. Pharm. Biopharm. 83 (2013) 346–357. doi:10.1016/j.ejpb.2012.11.002.

[63] R. Cheng, F. Feng, F. Meng, C. Deng, J. Feijen, Z. Zhong, Glutathione-responsive nano-vehicles as a promising platform for targeted intracellular drug and gene delivery, J. Control. Release. 152 (2011) 2–12. doi:10.1016/j.jconrel.2011.01.030.

[64] M. Daga, C. Ulllio, M. Argenziano, C. Dianzani, R. Cavalli, F. Trotta, C. Ferretti, G.P. Zara, C.L. Gigliotti, E.S. Ciamporcero, P. Pettazzoni, D. Corti, S. Pizzimenti, G. Barrera, GSH-targeted nanosponges increase doxorubicin-induced toxicity “in vitro” and “in vivo” in cancer cells with high antioxidant defenses, Free Radic. Biol. Med. 97 (2016) 24–37. doi:10.1016/j.freeradbiomed.2016.05.009.

[65] T. Thambi, V.G. Deepagan, H.Y. Yoon, H.S. Han, S.H. Kim, S. Son, D.G. Jo, C.H. Ahn, Y.D. Suh, K. Kim, I. Chan Kwon, D.S. Lee, J.H. Park, Hypoxia-responsive polymeric nanoparticles for tumor-targeted drug delivery, Biomaterials. 35 (2014) 1735–1743. doi:10.1016/j.biomaterials.2013.11.022.

[66] P. Daniel Harris, BA, Lynn McNicoll, MD, Gary Epstein-Lubow, MD, and Kali S. Thomas, 乳鼠心肌提取 HHS Public Access, Physiol. Behav. 176 (2017) 139–148. doi:10.1016/j.physbeh.2017.03.040.

[67] N. Vijayakameswara Rao, H. Ko, J. Lee, J.H. Park, Recent progress and advances in stimuli-responsive polymers for cancer therapy, Front. Bioeng. Biotechnol. 6 (2018). doi:10.3389/fbioe.2018.00110.

[68] S.R. MacEwan, D.J. Callahan, A. Chilkoti, Stimulus-responsive macromolecules and nanoparticles for cancer drug delivery, Nanomedicine. 5 (2010) 793–806. doi:10.2217/nnm.10.50.

[69] H. Almeida, P. Lobão, C. Frigerio, J. Fonseca, R. Silva, J.M. Sousa Lobo, M.H. Amaral, Preparation, characterization and biocompatibility studies of thermoresponsive eyedrops based on the combination of nanostructured lipid carriers (NLC) and the polymer Pluronic F-127 for controlled delivery of ibuprofen, Pharm. Dev. Technol. 22 (2017) 336–349. doi:10.3109/10837450.2015.1125922.

[70] E.C.D.S. Santos, A. Watanabe, M.D. Vargas, M.N. Tanaka, F. Garcia, C.M. Ronconi, AMF-responsive doxorubicin loaded β-cyclodextrin-decorated superparamagnetic nanoparticles, New J. Chem. 42 (2018) 671–680. doi:10.1039/c7nj02860a.

[71] H. Jiang, L. Fan, S. Yan, F. Li, H. Li, J. Tang, Tough and electro-responsive hydrogel actuators with bidirectional bending behavior, Nanoscale. 11 (2019) 2231–2237. doi:10.1039/c8nr07863g.

[72] A. Raza, U. Hayat, T. Rasheed, M. Bilal, H.M.N. Iqbal, “smart” materials-based near-infrared light-responsive drug delivery systems for cancer treatment: A review, J. Mater. Res. Technol. 8 (2019) 1497–1509. doi:10.1016/j.jmrt.2018.03.007.

[73] Y. Wang, Y. Deng, H. Luo, A. Zhu, H. Ke, H. Yang, H. Chen, Light-Responsive Nanoparticles for Highly Efficient Cytoplasmic Delivery of Anticancer Agents, ACS Nano. 11 (2017) 12134–12144. doi:10.1021/acsnano.7b05214.

[74] H.K. and T.J. Das C, Lucia MS, 乳鼠心肌提取 HHS Public Access, Physiol. Behav. 176 (2017)

139–148. doi:10.1016/j.physbeh.2017.03.040.

[75] A. Raza, T. Rasheed, F. Nabeel, U. Hayat, M. Bilal, H.M.N. Iqbal, Endogenous and exogenous stimuli-responsive drug delivery systems for programmed site-specific release, Molecules. 24 (2019) 1–21. doi:10.3390/molecules24061117.

[76] Z. Luo, K. Jin, Q. Pang, S. Shen, Z. Yan, T. Jiang, X. Zhu, L. Yu, Z. Pang, X. Jiang, On-Demand Drug Release from Dual-Targeting Small Nanoparticles Triggered by High-Intensity Focused Ultrasound Enhanced Glioblastoma-Targeting Therapy, ACS Appl. Mater. Interfaces. 9 (2017) 31612–31625. doi:10.1021/acsami.7b10866.

[77] J.L. Paris, M. Manzano, M.V. Cabañas, M. Vallet-Regí, Mesoporous silica nanoparticles engineered for ultrasound-induced uptake by cancer cells, Nanoscale. 10 (2018) 6402–6408. doi:10.1039/c8nr00693h.

[78] Y. Xin, Q. Qi, Z. Mao, X. Zhan, PLGA nanoparticles introduction into mitoxantrone-loaded ultrasound-responsive liposomes: In vitro and in vivo investigations, Int. J. Pharm. 528 (2017) 47–54. doi:10.1016/j.ijpharm.2017.05.059.

[79] R. Cavalli, A. Bisazza, M. Trotta, M. Argenziano, A. Civra, M. Donalisio, D. Lembo, New chitosan nanobubbles for ultrasound-mediated gene delivery: Preparation and in vitro characterization, Int. J. Nanomedicine. 7 (2012) 3309–3318. doi:10.2147/IJN.S30912.

[80] S. Zullino, M. Argenziano, I. Stura, C. Guiot, R. Cavalli, From Micro- to Nano-Multifunctional Theranostic Platform: Effective Ultrasound Imaging Is Not Just a Matter of Scale, Mol. Imaging. 17 (2018). doi:10.1177/1536012118778216.

[81] A.L.Y. Kee, B.M. Teo, Biomedical applications of acoustically responsive phase shift nanodroplets: Current status and future directions, Ultrason. Sonochem. 56 (2019) 37–45. doi:10.1016/j.ultsonch.2019.03.024.

CHAPTER 1

OXYGEN-CURCUMIN-GEMCITABINE LOADED NANODROPLETS: A TRIPLE COMBINATION THERAPY TO HAMPER HYPOXIC PANCREATIC CANCER

Introduction

Pancreatic cancer is one of the most aggressive types of cancer, and ductal adenocarcinoma (PDAC) is the malignancy most commonly diffused. It is usually diagnosed at advanced stages because it is often related to nonspecific or lack of symptoms. The curative resection and chemotherapy is the standard of care for PDAC patients, but frequently it only provides a short-term survival benefit. Indeed, pancreatic cancer is characterized by a significant resistance to most conventional treatments, such as chemotherapy, radiotherapy and molecularly targeted therapy [1]. The tumor microenvironment (TME) of pancreatic cancer consists of different cell types and extracellular matrix. The TME is characterized by fibrosis separating tumor cells from blood vessels, extensive desmoplasia (abundant and dense collagenous stroma) and hypoxia. Pancreatic cancer is indeed significantly more hypoxic than other solid tumors (Table 1) [2]. Hypoxia in pancreatic cancer tissue is developed through an intricate relationship between pancreatic cancer cells and the stromal cells. The crosstalk between these two kinds of cells initiates a cascade of events that causes the deposition of a dense extracellular matrix, that compromises capillary function [3]. In response to decreased oxygen levels, due to the low perfusion caused by aberrant vasculatures and the adaptation within the tumor microenvironment, pancreatic cancer cells activate hypoxia-inducible factors (HIFs) [4]. Among others, HIF-1α induces the expression of different factors involved in cancer progression, including extracellular matrix remodeling, angiogenesis, cell migration, metastasis, and drug resistance [5]. Insufficient oxygenation has opposing effects on cancer biology: it limits tumor cell division, but it also selects for more malignant cells inducing multiple cellular adaptations that sustain and foster cancer progression and invasion [6]. Moreover, hypoxia has been associated with resistance to chemotherapy and radiotherapy because it slows down the cell cycle and thereby limits the number of cells that these treatment modalities can target, as their mechanism of toxicity depends on DNA synthesis and proliferation.
Since hypoxia is a hallmark of solid tumors, a possible strategy to reduce the malignancy could be to supply oxygen near the tumor regions. Besides treatments with hyperbaric oxygenation or systemic erythropoietin [7], the nanomedicine approach has been largely explored exploiting the capability of the nanodelivery systems to extravasate from the bloodstream via leaky vasculature into the tumor and to accumulate [8].

Table 1. Comparison of the oxygenation in organs and respective tumors. Modified from Muz et al. [2].

Tissue/organ	Physoxia (mean % O_2)	Cancer	Hypoxia (mean % O_2)
Brain	4.6	Brain tumor	1.7
Breast	8.5	Breast cancer	1.5
Cervix	5.5	Cervical cancer	1.2
Kidney cortex	9.5	Renal cancer	1.3
Liver	4.0-7.3	Liver cancer	0.8
Lung	5.6	Non-small-cell lung cancer	2.2
Pancreas	7.5	**Pancreatic tumor**	**0.3**
Rectal mucosa	3.9	Rectal carcinoma	1.8

Among others, several nanoplatforms based on perfluorocarbons (PFCs) for sustained oxygen release have been studied, in particular core-shell nanostructured [9–11]. Indeed, perfluorocarbons exhibit high oxygen dissolving capacity and can be employed as alternative oxygen carriers. Previously, we have prepared oxygen-loaded nanobubbles, nanoformulations composed of a core mostly of PFCs (such as perfluoropentane or 2H,3H-decafluoropentane), and a shell of phospholipids and polymers (polysaccharides) [12,13]. These systems have been called nanobubbles, but for the sake of brevity here we name them nanodroplets (NDs).

The nanodroplets represent a versatile nanoplatform for the delivery of gases, drugs and genetic materials. Depending on the compound to be delivered, different nanodroplet formulations can be customized for a sustained and prolonged release of their cargo. The nanosize of the nanodroplets guarantees the possibility of their extravasation from the bloodstream into the cancer tissue and their accumulation in tumors via the enhanced permeability and retention (EPR) effect [14]. Besides, NDs are responsive to external physical stimuli, such as Ultrasound (US). NDs have a perfluorocarbon liquid core and can change phase from liquid to vapor when exposed to US in a physical process called acoustic droplet vaporization (ADV) [15]. During the phase shift, the mechanical and heating effect and the pressure waves of US induce the conversion from liquid nanodroplets to gas microbubbles, expanding their diameter approximately 3–6 times. Moreover, once these droplets are converted to gas bubbles, their echogenic properties increase, being more effective as contrast enhancers [16,17]. In addition, the acoustic cavitation activity permeabilizes cell membranes inducing transient pores (sonoporation), thus improving the intracellular uptake of the active compounds. Thanks to this echogenic feature, NDs can be considered a theranostic nanotool [18]. Currently, the image-guided drug delivery systems are under the magnifying glass because of their strong potential to improve the diagnosis and treatment of cancer. The use of real-time noninvasive imaging assessment offers the possibility to quantify the nanocarriers directly at the target sites and guarantees an adequate treatment and diagnosis in a shorter period [19,20].

The gold standard for the treatment of pancreatic cancer is the first-line single drug Gemcitabine (GEM). This chemotherapeutic is a prodrug, which is administered in an inactive form and phosphorylated into its clinically active form gemcitabine triphosphate within cells after its cellular uptake. Gemcitabine has poor membrane permeability and needs nucleoside transporters to be internalized inside the cells. The active metabolite of Gemcitabine acts as a competitive substrate of deoxycytidine triphosphate and is incorporated into DNA locking DNA polymerase, thus causing DNA chain termination which is required for DNA synthesis [21]. Notably, Gemcitabine is metabolically unstable and possesses a low therapeutic efficacy, particularly it is rapidly cleared in the bloodstream. Usually, to compensate for this limitation, Gemcitabine is administered at high doses, which turns in the generation of severe side effects and contributes to the development of chemoresistance. Indeed, within weeks from the initiation of the treatment with Gemcitabine, the cancer cells become less sensitive to the chemotherapeutic [22]. To circumvent these drawbacks, a possible therapeutic approach could be incorporate the drug in a nanodelivery system, thus overcoming various pathological and pharmacological barriers and thereby attenuate chemoresistance in pancreatic cancer [23].

Curcumin (Cur), a polyphenol derivate from the turmeric *Curcuma longa* L. plant, has shown to inhibit several resistance-related pathways in cancer cells. Curcumin can inhibit overexpressed P-glycoproteins (P-gp), responsible for drug resistance, through NF-κB pathway downregulation, and also exhibits adjuvant antioxidant, antiinflammatory, antimetastatic, antiproliferative and pro-apoptotic properties [24]. Despite these favorable features, the limit for the Curcumin clinical use is

its poor physicochemical properties, such as light- and heat-sensitivities and very low water solubility. To overcome these limitations, Curcumin has been formulated in many nanotechnology-based drug carriers [25,26].

Aim of the project

Currently, the clinical practice for treating cancer is to administer chemotherapeutics with different mechanisms of action to fight cancer from multiple sides. Pancreatic cancer is one of the most hypoxic types of cancer in which the development of drug resistance is highly common. Indeed, the depleted levels of oxygen at the tumor site activate a cascade of events that make cancer more aggressive. Moreover, the gold standard for the treatment, represented by gemcitabine, commonly develops chemoresistance in cancer cells.

In this PhD project, we focused on the design and development of novel nanodroplet formulations for hampering pancreatic cancer exploiting an innovative triple co-delivery approach. A stable nanodroplet formulation was developed for the simultaneous delivery of Oxygen, Gemcitabine and Curcumin. The nanoplatform based on the 2H,3H-decafluoropentane core enables the storage and the prolonged release of oxygen, with the aim to revert hypoxia. Then, the encapsulation of gemcitabine allows the delivery directly at the tumor site of the drug, exploiting the mechanism of passive targeting of the nanodroplets. In this way, the side effects may be reduced and the accumulation of the drug inside the cancer cells increased. With this strategy, the onset of the chemorosistance is postponed. Moreover, the co-delivery of curcumin, a natural anticancer adjuvant, may contribute to inhibit different resistance-related pathways, thus making the cancer cells more sensitive to chemotherapy. Lastly, the nanodroplet formulations can work as a theranostic tool, thereby present the capability to be visualized by echographic imaging.

Materials and Methods

Materials

Dextran sulfate (Mw = 100,000 Da), palmitic acid, Ethanol 960, 2H,3H-decafluoropentane, Curcumin from *Curcuma longa* L. (Turmeric) powder, PBS (pH 7.4), ammonium sulfate, chloroform were purchased from Sigma-Aldrich (St Louis, MO, US). Gemcitabine (40 mg/mL) concentrate for solution for infusion was from Sandoz S.p.A, Italy. Epikuron® 200 (soya phosphatidylcholine 95%) was gifted by Cargill (Wayzata, MI, US). Tween® 80 was from Fluka (Buchs, CH). Ultrapure water was purified using a 1-800 Millipore system (Molsheim, France). Tubular semi-permeable cellulose membrane with a cut-off of 14kDa was from Carl Roth (Karlsruhe, Germany). Oxygen was from SIAD, Italy. All cell culture reagents were of analytical grade and obtained from Gibco/Invitrogen (Life Technologies, Paisley, UK).

Methods

Preparation of Nanodroplet formulations

Unloaded Nanodroplets

The nanodroplets (NDs) were prepared by a tuned method, as previously described [13]. Briefly, dextran sulfate solution (Mw= 100,000 Da) was used for the shell and 2H,3H-decafluoropentane for the inner core. An ethanolic solution of Epikuron® 200 (2.5% w/v) and palmitic acid (0.5 % w/v) was added to 2H,3H-decafluoropentane to form a pre-emulsion. Then, ultrapure water was added and homogenized using an Ultra-Turrax® (IKA, Konigswinter, Germany) until the nanoemulsion was formed. After that, the sample was heated for 15 minutes at 37 °C and an aqueous solution of the dextran sulfate (2% w/v) was added dropwise under mild magnetic stirring for 15 minutes. Polymeric-shelled unloaded nanodroplets (blank NDs) were obtained.

Oxygen loaded Nanodroplets

The nanodroplets were prepared as previously described with slight modifications. Indeed, oxygen was purged during all the steps of the preparation, obtaining dextran sulfate coated oxygen loaded nanodroplets (Oxy-NDs).

Gemcitabine loaded Nanodroplets

The formulation was prepared as described for the Unloaded Nanodroplets, with purposely tailored modifications. Briefly, after the deposition of the polymer, 200 µL of Gemcitabine hydrochloride solution (2 mg/mL) were added dropwise. The nanosuspension was left under magnetic stirring for 1 hour when the drug was homogeneously loaded for electrostatic interaction with the polymeric shell. Gemcitabine loaded nanodroplets (GEM-NDs) were obtained.

Oxygen-Gemcitabine loaded Nanodroplets

The formulation was prepared as described for the Oxygen loaded Nanodroplets, with some modifications to load Gemcitabine. Briefly, oxygen was purged during all the steps of the preparation. After the deposition of the polymeric shell, a Gemcitabine hydrochloride solution (2

mg/mL) was added dropwise under magnetic stirring for 1 hour. Oxygen-Gemcitabine loaded nanodroplets (Oxy-GEM-NDs) were then obtained.

Curcumin loaded Nanodroplets

Curcumin was dissolved in 2H,3H-decafluoropentane and sonicated for 15 minutes. A Tween 80 solution (2% w/v) was added to increase its solubility. To this mixture, a solution of Epikuron® 200 (2.5% w/v) and palmitic acid (0.5% w/v) was added. To complete the formulation, ultrapure water was added. Then, the sample was homogenized for 2 minutes with Ultra-Turrax® and Cur-NDs were obtained after the addition drop by drop of a solution of dextran sulfate polymer.

Oxygen-Curcumin-Gemcitabine loaded Nanodroplets

To obtain a triple co-loaded nanodelivery system, Oxygen-loaded NDs were prepared including at first Curcumin in the preparation. Then, after the deposition of the polymer-shell, Gemcitabine hydrochloride solution (2 mg/mL) was added as described above. In this way, a nanodroplet formulation containing Oxygen and Curcumin in the core and Gemcitabine in the shell (Oxy-Cur-GEM-NDs).

Physico-chemical characterization of Nanodroplet formulations

The nanodroplet formulations were physico-chemically characterized measuring average size diameter, dispersity (Đ), and zeta potential. Before the measurement, the different nanoformulations were previously diluted with deionized filtered water in an electrophoretic cell. Then, the average diameters and dispersity of the samples were measured by photocorrelation spectroscopy using a 90 Plus instrument (Brookhaven, New York City, NY, US) with a scattering angle of 90° at 25 °C. The zeta potential was measured with the same instrument.
The samples were placed in an electrophoretic cell and then subjected to an electric field of around 15 V cm^{-1}. The analyses were done in triplicate of three different batches.

Echogenic Properties of Nanodroplet formulations

Echogenic images were visualized using MyLab 25Gold (Esaote, Genova, Italy) instrument. The frequency was 12 MHz, and the Mechanical Index was 1.1; contrast Res modality. For this purpose, all the NDs formulations were evaluated at 37 °C.

Quantitative determination method of Gemcitabine by Spectrophotometer

The Gemcitabine hydrochloride concentration was determined using an ultraviolet-visible spectrophotometer (DU 730, Beckman Coulter, Fullerton, CA). The wavelength for Gemcitabine was set at 267 nm. A linear calibration curve was set in the concentration range between 1.0 µg/mL and 40 µg/mL (R^2 >0.998), starting from a stock standard solution prepared in filtrated water.

Encapsulation efficiency and loading capacity of Gemcitabine in nanodroplets

The encapsulation efficiency of GEM-NDs and Oxy-GEM-NDs was determined as follows. Briefly, a part of the different ND nanosuspensions was placed in a centrifugal filter device (Amicon® Ultra-0.5) and centrifuged for 15 minutes at 15000 rpm with a Beckman Coulter 64R Centrifuge. Then, the

filtered solution containing free Gemcitabine was analyzed at the spectrophotometer as previously described. The encapsulation efficiency of Gemcitabine was quantified by Equation 1.

Encapsulation Efficiency (EE):

$$EE = \frac{Total_{GEM} - Free_{GEM}}{Total_{GEM}} \times 100$$

(Equation 1)

The loading capacity of GEM-NDs and GEM-Oxy-NDs was determined as follows. The different nanodroplet formulations were freeze-dried overnight. Then, a weighted amount of the samples was suspended in 1 mL of filtered water. After that, the samples were sonicated for 15 minutes and then centrifuged for 5 minutes at 15000 rpm with a Beckman Coulter 64R Centrifuge. The supernatant of each sample was analyzed in the spectrophotometer as previously described. The loading capacity of Gemcitabine was calculated by Equation 2.

Loading Capacity (LC):

$$LC = \frac{Total_{GEM}}{ND\ weight} \times 100$$

(Equation 2)

In vitro release study of Gemcitabine

The *In vitro* release study of Gemcitabine from GEM-NDs and Oxy-GEM-NDs was investigated using a multi-compartment rotating cell at room temperature. GEM-NDs, Oxy-GEM-NDs and a free drug solution as control were placed in the donor chambers. The donor and the receiving chambers were separated by a semipermeable cellulose membrane (cut-off 14 kDa). The receiving phase for all the samples was phosphate-buffered saline (PBS) at pH 7.4. At fixed times, the samples were collected and the receiving phase was replaced with fresh PBS. The withdrawn samples were analyzed at the spectrophotometer as previously described.

In vitro release study of Gemcitabine in presence of Ultrasound

The *in vitro* release kinetics of Gemcitabine from the GEM-NDs was determined also in the presence of Ultrasound (US) using the dialysis bag technique [27] at room temperature. Briefly, after US application (frequency 2.5 ± 0.1 MHz, insonation time = 1 min), three mL of the nanodroplet suspensions were put in a dialysis bag (cellulose dialysis membrane Spectrapore, cut-off 12–14 kDa) as donor phase. PBS at pH 7.4 was used as the receiving phase. Gemcitabine release was followed up to 8 hours. At fixed times, 1 mL of the receiving phase was withdrawn and replaced with 1 mL of fresh PBS. All the withdrawn samples were analyzed spectrophotometrically to evaluate the drug concentration, as described above.

In vitro release study of Oxygen

The *in vitro* oxygen release was determined by HACH HQ30D Portable Dissolved Oxygen Meter with an Intellical TM LDO101 probe. The release kinetics was monitored at 37 °C. Oxy-NDs, Oxy-GEM-NDs and Oxy-Curc-GEM-NDs were respectively placed in a hermetically sealed semipermeable cellulose membrane (cut-off 14 kDa), forming a dialysis bag as donor chamber. Nitrogen was purged in the receiving phase, 50 mL of NaCl (0.9% w/v) saline solution, to mimic hypoxic conditions. The oxygen release was measured for 24 hours continuously. The oximeter was calibrated previously to check the temperature of the study.

Hemolytic assay

In order to determine the biocompatibility of nanodroplet formulations, an *ex vivo* hemolytic assay was performed. Blank NDs were tested at increasing dilution (1:10 – 1:400 v/v) with saline solution. 100 µL of each diluted sample were incubated at 37 °C for 90 minutes with rat blood previously diluted 1:4 v/v with freshly prepared PBS. After that, the samples were centrifuged at 2000 rpm for 5 minutes and the amount of hemoglobin released due to hemolysis was determined in the supernatants. The samples were measured at λ = 543 nm with the spectrophotometer. As controls, the diluted blood cells were incubated with 0.1% Triton X-100 solution (positive control) and 0.9% w/v NaCl (negative control), in order to determine the theoretical 100% and 0% lysis, respectively. The percentage of hemolysis was calculated based on the following equation (Equation 3).

$$Hemolysis\ (\%) = \frac{Abs_{sample} - Abs_{negative\ control}}{Abs_{positive\ control} - Abs_{negative\ control}} \times 100$$

(Equation 3)

Cell culture

Murine pancreatic cancer cell (mPDAC), were isolated from tumor-bearing *p48^{cre}*, *Kras^{LSL_G12D}*, *p53$^{R172H/+}$*, *Ink4a/Ar $^{flox/+}$* mice in 2012, as described in [28]. The cells were cultured in Dulbecco's Modified Eagle's Medium (DMEM) supplemented with 10% fetal bovine serum (FBS), 2 mM L-Glutamine, and 1% Penicillin-Streptomycin solution in a humidified 5% CO_2/air incubator at 37°C. The cell line was kindly provided by Prof. Doug Hanahan (École Polytechnique Fédérale De Lausanne, CH).

Cell viability assay

For this purpose, 2x10^3 PDAC cells were suspended in complete medium (DMEM, 10% FBS) and seeded into 96-well plates. The day after, the cells were treated in triplicate at increasing concentrations of Gemcitabine solution and GEM-NDs, corresponding to 1.95, 3.90, 7.80, 15.60, 31.25, 62.50 nM of the drug. Blank NDs were also tested, and the control consisted of only cell medium. The cells were incubated for 48 hours, and then the viability was evaluated by CellTiter-Glo® Luminescent Cell Viability Assay (Promega, WI, US). Firstly, the plate and the CellTiter-Glo® reagent were equilibrated at room temperature for approximately 30 minutes. Then, CellTiter-Glo®

reagent was added equally to the volume of cell culture medium present in each well. The plate, protected from light, was gently mixed with a plate shaker at 150 rpm for 15 minutes at room temperature. After that, an equal amount of the samples was transferred from 96-well plates to an opaque-walled 96-plate reader. The viable cells were measured based on the quantitation of the ATP present, an indicator of metabolically active cells. The luminescence was recorded at λ = 560 nm with a VICTOR X Multilabel Plate Readers (Perkin Elmer, MA, US). Values were normalized on controls and the percentage of cell viability/controls was determined.

Cell invasion

PDAC cells ($2x10^4$) were seeded in the upper chamber of polyethylene terephthalate Transwell membrane with 8.0 µm pores. For the invasion assay, the inserts were precoated with Corning® Matrigel® Matrix, previously diluted to 1 µg/mL with PBS. The matrigel was allowed to solidify in the cell incubator at 37 °C for 2 hours and the excess was then washed with PBS. After that, PDAC cells were trypsinized, resuspended in 1% FBS DMEM, and seeded in the upper chamber in the presence of Gemcitabine solution, GEM-NDs or only medium as control. The cells were allowed to invade through the membrane for 48 hours. Then, the Transwell membranes were washed twice with PBS, fixed in 2.5% glutaraldehyde and stained with 0.1% crystal violet for 15 minutes, respectively. The Traswells were washed with filtered water and left to dry. Pictures of the stained cells on the bottom side of the membrane were taken under an Olympus BX60F-3 microscope, using a 2.5X original magnification. The quantification was done using ImageJ2 software [29]. The relative invasion of the cells was represented as the percentage of average invaded cell numbers in the control group.

3D PDAC cell experiment

Three-dimensional PDAC spheroids were prepared following the hanging drop method. This technique relies on the formation of spheroids in small drops of culture medium, which are suspended on a glass coverslip [30]. Each drop contained $5x10^4$ PDAC cells. The cells were cultured for 4 days. After that, the formed spheroids were collected and seeded with complete medium in Falcon® 8-chambered cell culture slides (BD Falcon, Corning, NY, US) previously coated with matrigel. The day after the seeding, the spheroids were treated with Gemcitabine solution, GEM-NDs, Oxy-GEM-NDs, and only medium as control. The concentration of Gemcitabine for the different preparations was 25 nM. The size changes of the spheroids were photographed by Leica DM1400B microscope (Leica Microsystems) using a 5X magnification and quantified by means of ImageJ2 software [29].

Evaluation of the oxygen contribution in hypoxic condition

PDAC cells ($8x10^4$) were seeded in 6-wells plate. The experiments were carried out in normoxic or hypoxic conditions (Table 2). The day after the seeding, the cells were incubated for 1, 3, 6, 12, 24 and 48 hours with different concentrations of Oxy-NDs (1:100 and 1:200 v/v dilutions with cell medium) and only DMEM as control. In the case of hypoxia, the cells were incubated in hypoxic conditions for three hours previous the treatment with Oxy-NDs.

Table 2. The gas composition of cell incubator in normoxic and hypoxic environment.

	CO_2	O_2	N_2
Normoxic condition	5%	20%	---
Hypoxic condition	5%	1%	To maintain the balance

RNA isolation and reverse transcription

For RNA extraction, the cells were lysed with 0.5 mL of QIAzol (Qiagen; Hilden, Germany) each well, and incubated for 5 minutes in tubes. After that, 100 µL of chloroform were added to each tube, mixed vigorously and left to rest for 2 minutes at room temperature. Then, the samples were centrifuged for 15 minutes at 12000 g at 4°C and the supernatants, containing the RNAs, were transferred to new tubes. 250 µL of isopropanol were added to precipitate the RNAs and left to incubate 10 minutes at room temperature. Finally, the samples were centrifuged 10 minutes at 12000 g at 4°C and the supernatants were eliminated. The obtained pellets were washed with 75% EtOH, mixed by vortexing and centrifuged at 7500 g for 5 minutes at 4°C. Then, the RNA precipitated were resuspended in sterile nuclease-free water (Thermo Fisher Scientific; Waltham, MA, US). The RNA concentration was quantified through a NanoDrop 1000 Spectrophotometer (Thermo Fisher Scientific). cDNAs were generated from 2 µg of total RNA using the High Capacity cDNA Reverse Transcription Kit (Applied Biosystems; Foster City, CA, US). As reported in Table 3, 2X Reverse Transcription master mix was prepared using the kit components and supplemented with 10 µL of template RNA.

Table 3. Reverse Transcription mix preparation.

Component	Volume / Reaction (µl)
2X Reverse transcription master mix	
10X RT Buffer	2
25X dNTP mix (100 mM)	0.8
10X RT Random Primers	2
MultiScribe® Reverse Transcriptase	1
Nuclease-free water	4.2
Template RNA	
2 µg RNA diluted with nuclease-free water	10
Total volume/well	10

The thermal cycle settings were: primer annealing at 25°C for 25 minutes (step 1), reverse transcription at 37°C for 120 minutes (step 2), and denaturation of the enzyme at 85°C for 5 minutes to stop the reaction (step 3). The final cDNAs were stored at -20°C.

TaqMan real-time RT-PCR assay

mRNA expression of several genes and an endogenous control gene (glyceraldehyde 3-phosphate dehydrogenase (GAPDH)) (Table 4) was measured in the samples by real-time RT-PCR using TaqMan Gene Expression Assays run on an ABI PRISM 7900HT Fast Real-Time PCR System (Applied Biosystems). Three replicates were run for each gene for each sample in a 384-well format plate (cDNA concentration 40 ng/well), according to the scheme reported in Table 5. The real-time RT-PCR data were quantified by calculating the gene expression values, using the formula $2^{-\Delta\Delta Ct}$ to calculate the expression of target genes normalized to a calibrator. mRNA was normalized to the housekeeping gene.

Table 4. TaqMan probes (Life Technologies).

Target genes		**Housekeeping gene**	
Name	**Abbreviation**	**Name**	**Abbreviation**
Carbonic anhydrase 9	CA9	Glyceraldehyde 3-phosphate dehydrogenase	GAPDH
Glucose transporter 1	GLUT-1		
Mesenchymal–epithelial transition factor	c-MET		

Table 5. RT-PCR reaction mix.

Component	**Volume / Reaction (µL)**
2x TaqMan Master Mix	10
Taqman probes	1
cDNA (100 ng/µL)	1
Nuclease-free water	8
Total volume/well	20

Reactive Oxygen Species detection

The reactive oxygen species (ROS) detection was determined as described in Daga *et al.* [31] following a fluorimetric method. Briefly, PDAC cells ($8x10^4$) were seeded in a 6-well plate. The cells were treated in hypoxic conditions with Oxy-NDs and Oxy-GEM-NDs at different dilutions for 3 and 24 hours. After the incubation time, the cells were harvested, centrifuged, suspend in 100 µL of PBS and sonicated for lysis. Then, 25 µL of 5 µM 2', 7' dichlorofluorescein diacetate (DCFH-DA) were added and the samples were incubated for 20 minutes at 37 °C. The reaction was quenched by adding PBS/0.1% Triton X-100. In the presence of ROS, DCFH-DA was oxidized to 2',7'-dichlorofluorescein (DCF), detected by fluorimeter (λ_{ex} = 488, λ_{em} = 525). The results are expressed as fold change relative to untreated cells (control).

Statistical analysis

Data are presented as mean ± standard deviation (SD). Statistical analysis was performed by GraphPad Prism program (version 6; GraphPad Software). A 2-tailed Student's t-test was performed to analyze the statistical significance between two groups.

Results and discussion

For the purpose to hamper the hypoxic pancreatic cancer, a novel theranostic nanodroplet (ND) formulation aimed at the triple co-delivery of Oxygen (Oxy), Curcumin (Cur) and Gemcitabine (GEM) was obtained. In order to evaluate the contribution of the single active components, different nanodroplet formulations were prepared, including blank NDs, Oxygen loaded NDs (Oxy-NDs), Gemcitabine loaded NDs (GEM-NDs), Oxygen-Gemcitabine loaded NDs (Oxy-GEM-NDs) and Curcumin-loaded NDs (Cur-NDs).

Physico-chemical characterization of Nanodroplet formulations

The average diameter, dispersity (Đ) and zeta potential (Z-potential) of the nanodroplet formulations are reported in Table 6. The average diameter of all the NDs was less than 250 nm. The loading of the oxygen in the inner core increased slightly the size. The Z-potential values of the NDs no loaded with Gemcitabine were around - 60 mV, while after the addition of the drug the ND surface charge increased of about 40%. This behavior proved the electrostatic interaction between the drug and the polymeric shell composed of dextran sulfate.
All the ND nanosuspensions presented a pH in the physiological range of 5.50-6.80. Moreover, the formulations showed to be stable over time. After 2 months from the preparation, no significant increase of the size ranges was observed, and in all the cases the size was less than 300 nm. Zeta potential and dispersity remained very similar to the ones measured directly after the preparation.

Table 6. Physico-chemical characteristics of nanodroplet formulations. Results are shown as means ± standard deviation (SD) (n = 10) of three different preparations. Abbreviation: *Đ = dispersity.

Samples	Average diameter (nm) ± SD	Đ*	Z-potential (mV) ± SD
Blank NDs	210.1 ± 5.1	0.28	- 61.3 ± 3.5
Oxy-NDs	244.9 ± 2.3	0.19	- 62.5 ± 4.3
GEM-NDs	208.5 ± 3.1	0.29	- 23.6 ± 4.1
Oxy-GEM-NDs	215.2 ± 3.6	0.29	- 26.9 ± 2.6
Cur-NDs	213.9 ± 4.2	0.23	- 60.8 ± 4.7
Oxy-Cur-GEM-NDs	236.8 ± 4.7	0.27	- 27.2 ± 1.8

Encapsulation efficiency and loading capacity

The encapsulation efficiency (EE) and the loading capacity (LC) were calculated using Equation 1 and Equation 2 (presented in Methods) and are reported in Table 7. The Gemcitabine was able to be incorporated in the GEM-NDs and Oxy-GEM-NDs with an efficiency of about 66% in both cases. These results are in line with the dialysis process to which the samples are subjected to eliminate the no-loaded drug after their preparation. Besides, the presence of the oxygen in the core of the NDs did not affect the interaction of the drug and the polymeric shell.

Table 7. Encapsulation efficiency and drug loading of GEM loaded in GEM-NDs and Oxy-GEM-NDs. Abbreviations: *EE = encapsulation efficiency; §LC = loading capacity.

Samples	EE* (%)	LC§ (%)
GEM-NDs	65.8 ± 0.6	9.4 ± 0.7
Oxy-GEM-NDs	66.6 ± 0.9	8.2 ± 0.5

Echogenic Properties of nanodroplet formulations

The nanodroplet formulations were visualized under ultrasound application, demonstrating their echogenic properties. For this purpose, all the ND formulations were evaluated at 37 °C. As an example, a representative image of the echogenic properties of GEM-NDs is reported in Figure 1. The visualization of NDs is related to the phase-shift from the liquid nanodroplets to the gas microbubbles, due to a phenomenon called acoustic droplet vaporization (ADV). The increase in volume enables the visualization of newly formed bubbles. This technique can be promising for both early cancer detection and treatment monitoring, using nanodroplets as effective theranostic nanotools [15].

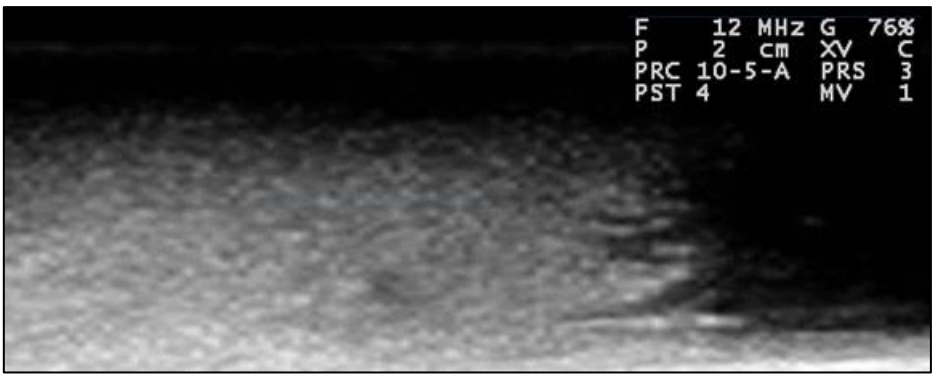

Figure 1. Echogenic images of GEM-NDs, visualized using MyLab 25Gold (Esaote, Genova, Italy) sonograph. The frequency was 12 MHz and the Mechanical Index 1.1.

Gemcitabine *in vitro* release kinetics

The *in vitro* percentage of Gemcitabine released over time was evaluated for GEM-NDs and Oxy-GEM-NDs in Figure 3. These results showed a sustained drug release effect and suggested that Gemcitabine-loaded nanodroplets can represent an effective drug reservoir. A slow release kinetic profile was evaluated until 28 hours of the study. After 24 hours, the drug released from the formulations was around 45%, while its free form solution was around 80%. The oxygen encapsulation did not affect Gemcitabine release over time. Moreover, the release of Gemcitabine was followed after Ultrasound application (frequency 2.5 ± 0.1 MHz) for 1 minute. As reported in Figure 1 (orange line), Gemcitabine was released from US-activated GEM-NDs with a larger extent than the same formulation not subjected to US. The maintained prolonged release proved that the insonation conditions did not disrupt the nanodroplet structure.

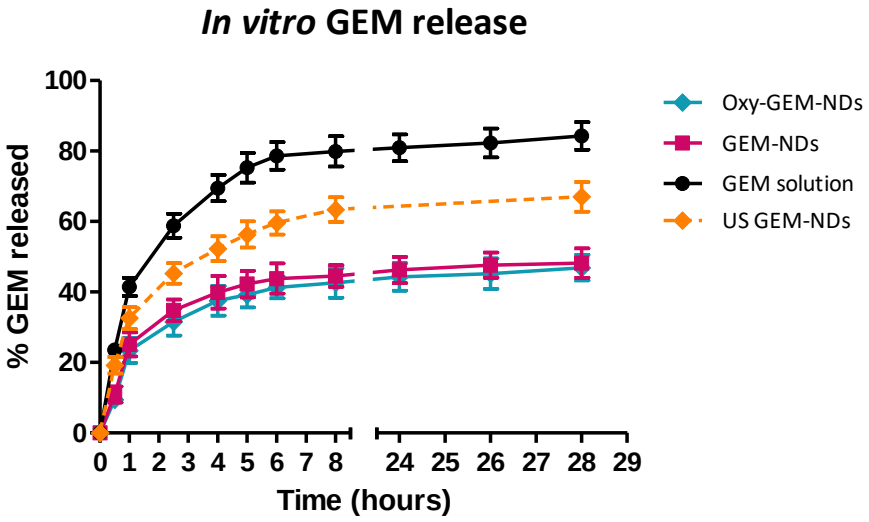

Figure 2. *In vitro* release study of GEM-NDs, Oxy-GEM-NDs, and free Gemcitabine solution as control. The release was also evaluated for Ultrasound (US)-activated GEM-NDs. Gemcitabine release was evaluated for 28 hours. Results are presented as mean ± SD (n=3).

In vitro oxygen release kinetics

The *in vitro* oxygen release study of Oxy-NDs and Oxy-GEM-NDs is presented in Figure 3. Sustained release of oxygen at 37 °C was observed up to 24 hours, suggesting that they could work as an effective reservoir of oxygen. The prepared nanodroplets showed a good oxygen-loading capacity due to the 2H,3H-decafluoropentane as ND core. Moreover, the presence of the drug in the ND shell affected very slightly the oxygen release kinetics.

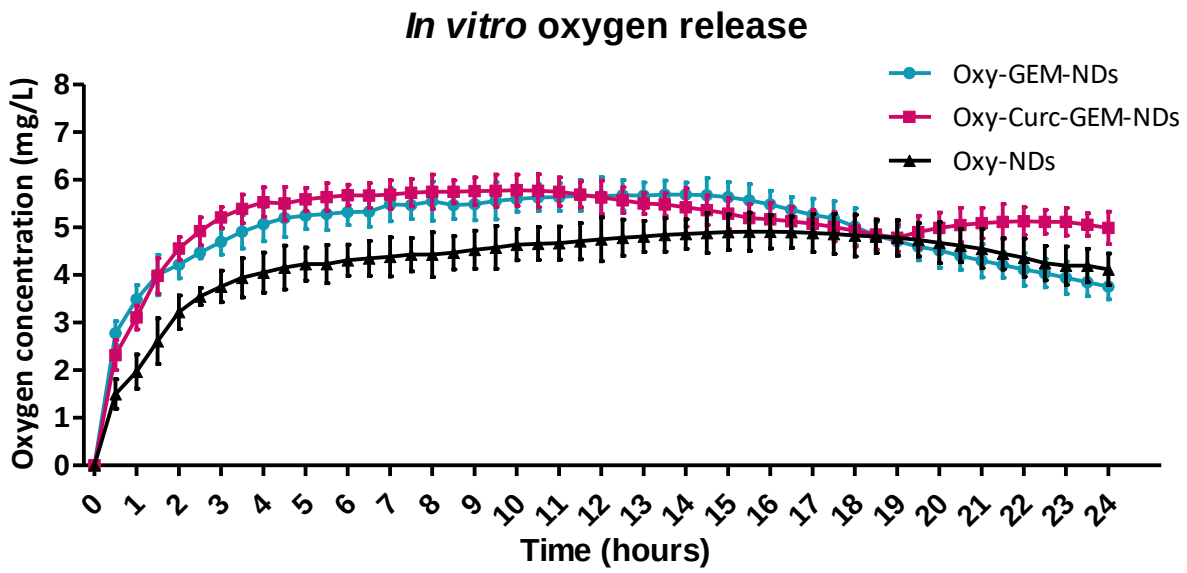

Figure 3. *In vitro* oxygen release from Oxy-ND, Oxy-GEM-ND and Oxy-Curc-GEM-ND formulations over time measured at 37 °C by HQ40d model (Hach) oximeter. Data are reported as mean ± SD (n=3).

Nanodroplets are biocompatible

Nanodroplet biocompatibility was investigated with a hemolysis assay. The diluted whole blood was incubated for 90 minutes at 37 °C with different dilutions of blank NDs (1:10 – 1:400 v/v) in saline solution. After the incubation time, the samples were centrifuged and the supernatants read to the spectrophotometer. As it is depicted in Figure 4, the NDs did not cause significant hemolysis, thus validating their biocompatibility. These results are in line with the biocompatibility of dextran sulfate coated nanobubbles assessed by Cavalli *et al.* [13].

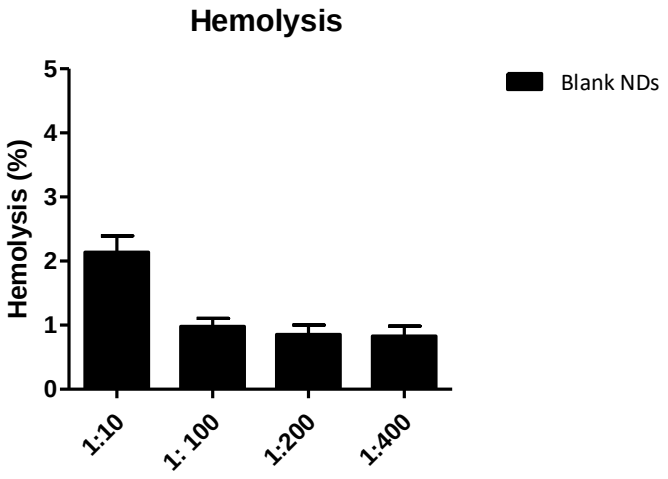

Figure 4. Hemolysis of murine erythrocytes after incubation at 37 °C for 90 minutes with different dilutions of blank nanodroplet formulation. The results presented a negligible hemolytic activity. Each point represents the mean ± SD of the three different experiments (n=3).

Cell viability assay

In order to evaluate the *in vitro* efficiency of the different ND formulations, a cell viability assay was performed. The PDAC cells were incubated for 48 hours with blank NDs, to check the biocompatibility of the system, GEM-NDs and GEM solution as a control. The experiments were conducted in normoxic and hypoxic conditions, to mimic the oxygen-depleted milieu of pancreatic cancer and to assess their activity under that condition. In normoxia as in hypoxia, blank NDs did not show significant cytotoxicity on PDAC cells, thus confirming the biological compatibility of the nanodroplet platform (Figure 5) [32]. After 48 hours, the GEM solution demonstrated to have higher cytotoxicity than GEM-NDs. Indeed, the nanodroplets act as drug reservoirs, and once internalized by the cells, they can release their cargo with a prolonged profile [11]. Moreover, their internalization is probably mediated by endocytosis, thus the NDs need to disrupt the endosomes to release the drug in the cytoplasm. On the other hand, the Gemcitabine solution is immediately available by cell metabolism when it is uptaken by the nucleoside transporters that mediate its internalization. Inside the cells, free GEM can be directly activated to its active triphosphate form, which inhibits the synthesis of DNA or induces cell apoptosis [33]. Besides, Curc-NDs were tested, and they did not show significant cytotoxicity. Curc-GEM-NDs presented a comparable cytotoxic profile than GEM-NDs, confirming that Curcumin does not affect modifying the cell viability.

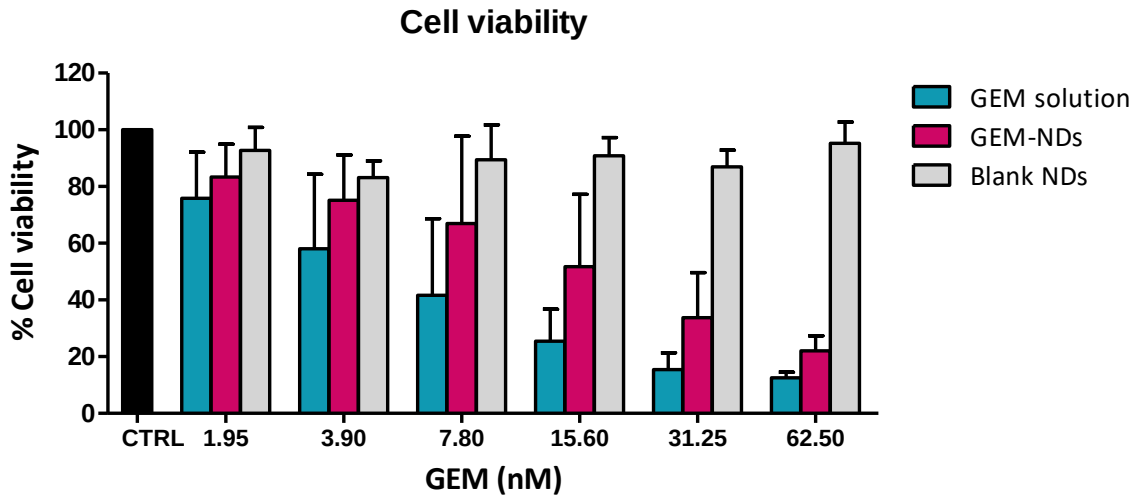

Figure 5. *In vitro* cell viability on PDAC cell line under normoxic conditions. PDAC cells were tested with different concentrations of GEM solution and GEM-NDs, assessing their cytotoxicity activity. Each bar represents the mean ± SD of three different experiments.

Invasion assay

The invasiveness of the PDAC cells was evaluated upon treatment with GEM solution and GEM-NDs on PDAC seeded on Transwells. After 48 hours, the invasion capacity was measured, once the cells were fixed and stained. As shown in Figure 6, both GEM solution and GEM-NDs inhibited the invasiveness of the cancer cells comparably.

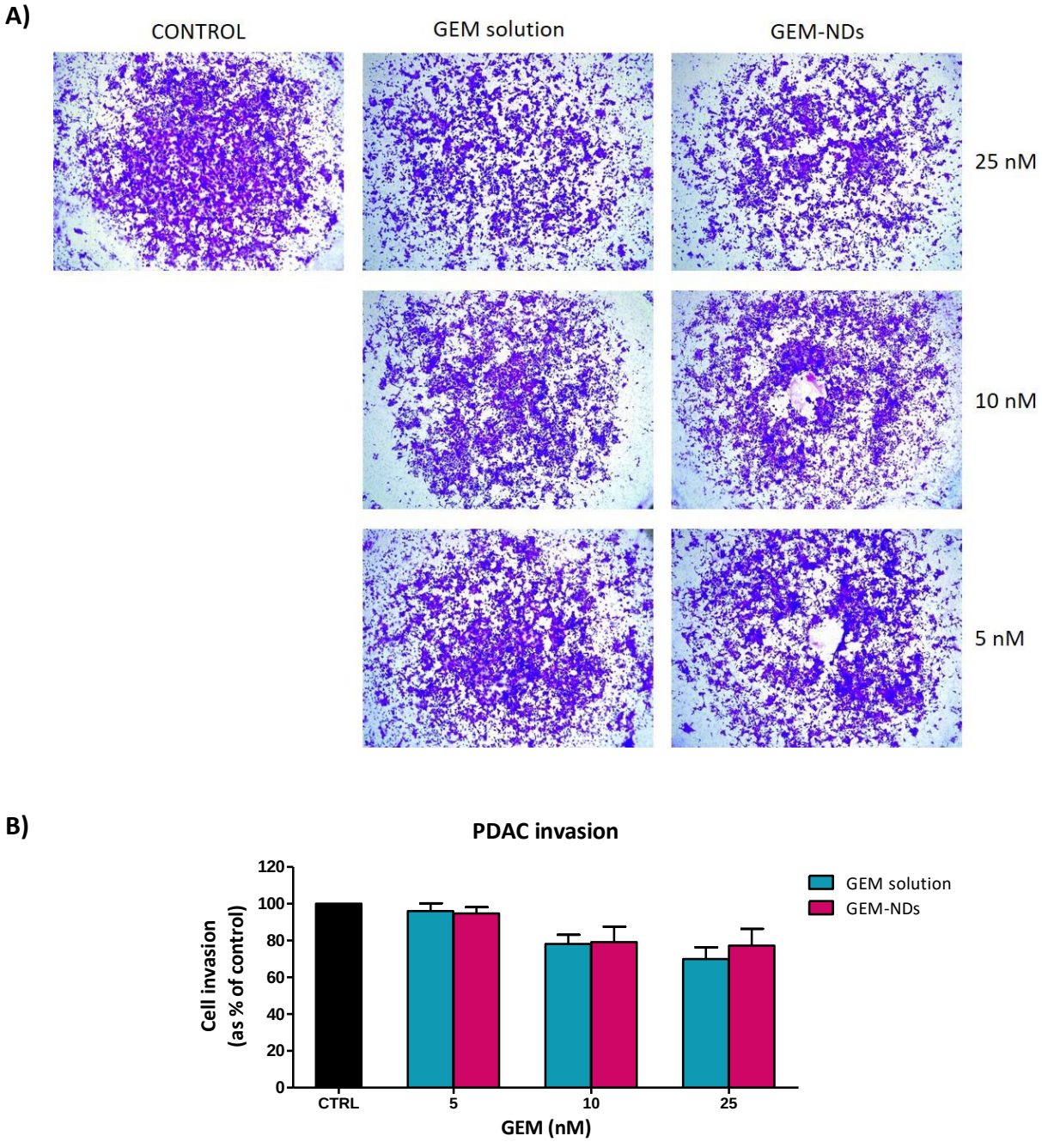

Figure 6. Invasion inhibition by GEM solution and GEM-NDs on PDAC cells using Transwell. **A**) Representative images of PDAC invasion; **B**) Quantification of cell invasiveness upon treatment. Data are expressed as mean ± SD and the experiments were repeated in triplicate (n=3).

Gemcitabine-loaded NDs hampered spheroid invasion

PDAC cells were cultured to form spheroids following the hanging drop method. Spheroid pictures were taken before starting the treatment with GEM-NDs, Oxy-GEM-NDs, and GEM solution, and after 1, 6 and 7 days. As shown in Figure 7, the spheroids reduced constantly their perimeters overtime for the groups treated with GEM solution, GEM-NDs and Oxy-GEM-NDs respected to control.

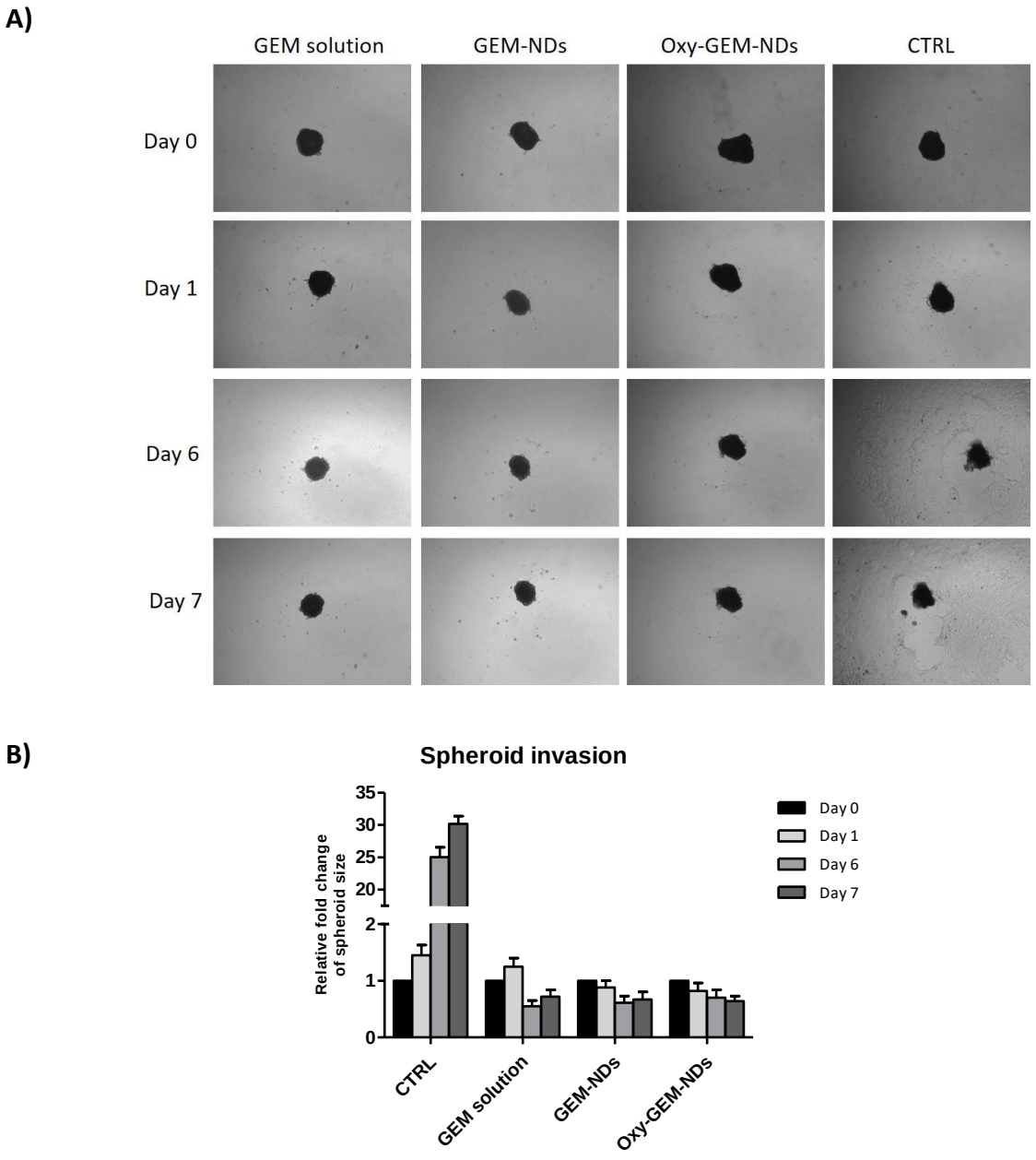

Figure 7. Gemcitabine-loaded NDs and GEM solution hampered the spheroid invasiveness. Size changes in PDAC spheroids treated with GEM-NDs, Oxy-GEM-NDs, and GEM solution were followed for 7 days. The control was only medium. The concentration of GEM for the different preparations was 25 nM. Spheroid sizes were respectively compared with that on day 0. **A**) Pictures of spheroids were taken with Leica DM1400B microscope (objective 5X) until day 7. **B**) Perimeter analysis of spheroids was performed at days 0, 1, 6 and 7 and represented in a graph as mean ± SD. The analysis was performed using Image J software and measurements were performed from two independent experiments in two replicates.

Oxygen-loaded Nanodroplets have a role in restoring normoxia

Reduced level of oxygen occurs under various physiological (embryonic development, adaptation to high altitudes, wound healing) as well as pathological (ischemic diseases, cancer) conditions. In order to deal with hypoxia, organisms undergo several systemic and local changes to reestablish the homeostasis and limit the effect of low oxygen levels. In particular, in response to hypoxia, cells activate HIF-1α, which induces the expression of different factors involved in cancer progression, such as extracellular matrix remodeling, angiogenesis, cell migration, and metastasis. To evaluate if oxygen-loaded nanodroplets could efficiently revert the hypoxic conditions, typical of the pancreatic tumor, PDAC cells were previously incubated for three hours at 37 °C with 5% CO_2 and 1% O_2. Then, different dilutions of nanodroplet formulations were added. At first, different time-lapses of incubation were tested to find the optimal condition. With this purpose, the cells were treated for 1, 3, 6, 12, 24 and 48 hours with Oxy-NDs. After that, the RNA was extracted from the different samples to evaluate by Real Time-RT-PCR analysis the expression of some genes regulated by HIF-1α, specifically Carbonic anhydrase 9 (CA9), Glucose transporter 1 (GLUT1), and Tyrosine-protein kinase Met (c-MET). The CA9 and GLUT1 genes are downstream targets of HIF-1α [34]. CA9 is a transmembrane isozyme involved in the control of cell proliferation and is involved in maintaining the acidic pH. Its expression is strongly induced by hypoxia and plays an important role in tumor progression and survival under normoxic and hypoxic conditions [35]. GLUT1, instead, facilitates the transport of glucose across the cellular membrane, thus favoring a metabolic adaptation of cells to hypoxia [36]. The tyrosine kinase receptor c-MET is an important cell surface mediator of hypoxia-induced migration, invasion, and metastasis [37].
As shown in Figure 8, it was found that after 3 hours of incubation in hypoxic conditions the PDAC cells presented an overexpression of the genes related to hypoxia, compared to the cells cultured in normoxia. Moreover, the supply of oxygen delivered by Oxy-NDs contributed to significantly revert the gene expression of CA9, GLUT1, and c-MET. Considering the *in vitro* ability of Oxy-NDs to restore normoxia, these nanoplatforms may be considered as promising oxygen delivery systems.

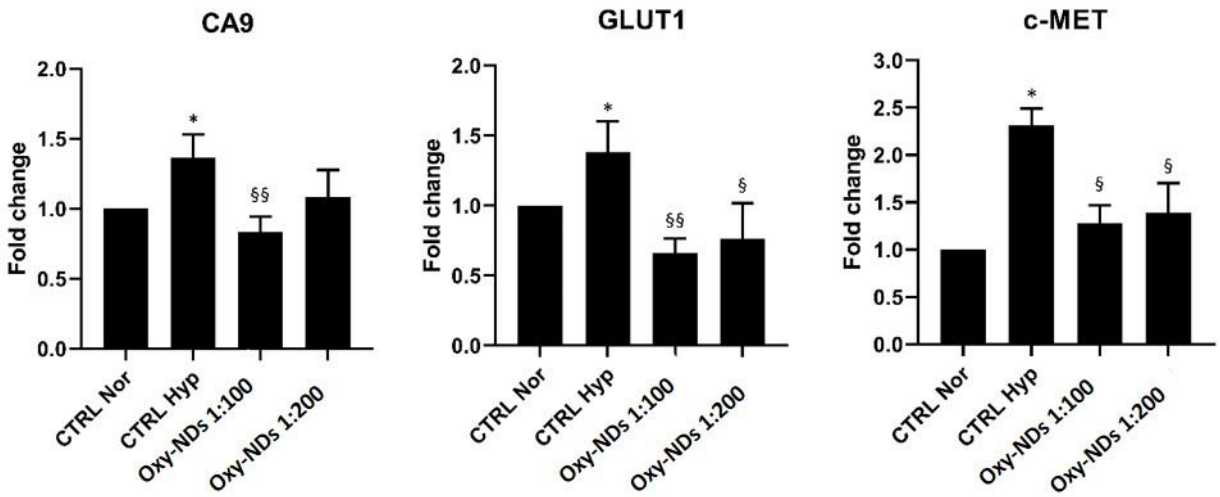

Figure 8. Analysis of gene expression by Real Time-RT-PCR of Carbonic anhydrase 9 (CA9), Glucose transporter 1 (GLUT1), and Mesenchymal–epithelial transition factor (c-MET). PDAC cells were incubated for 3 hours under hypoxic conditions (incubator 37°C, 5% CO_2, 1% O_2) with Oxy-NDs at different dilutions (1:100 and 1:200 v/v). All values are expressed as mean ± SD of four experiments (n = 3) in duplicate. *p≤0.05; ***p ≤ 0.001 versus CTRL Nor (untreated cells in normoxic conditions); §p≤0.05; §§p≤0.01 versus CTRL Hyp (untreated cells in hypoxic conditions).

Reactive Oxygen Species detection in cells

To verify if the supply of oxygen with nanodroplets could lead to an adverse increment of oxidative stress to the cells, an analysis for the detection of reactive oxygen species (ROS) was performed. PDAC cells were incubated for 3 and 24 hours, under hypoxic conditions, with different dilutions of Oxy-NDs and Oxy-GEM-NDs. As it is depicted in Figure 9, after 3 hours of incubation the ROS content did not increase in the cells. On the other hand, after 24 hours there was a slight increment of ROS for all the samples, but not significant to determine oxidative stress.

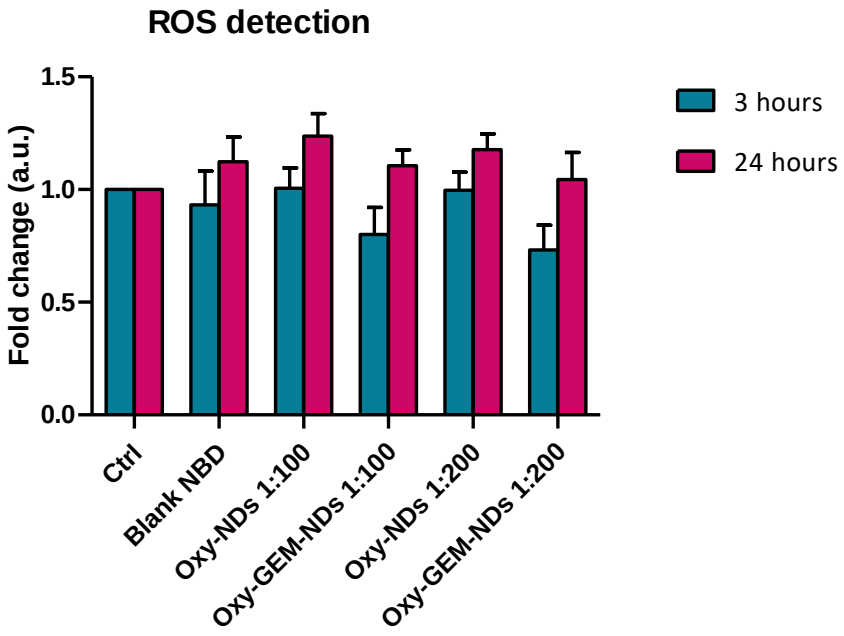

Figure 9. ROS detection in PDAC cells under hypoxic conditions. Cells were treated with different dilutions of Oxy-NDs, Oxy-GEM-NDs, blank NDs and only cell medium as control. The results are expressed as mean ± SD (n=2) in arbitrary units (a.u.), where control values were set as 1.

Conclusions

In this PhD project, novel nanodroplet formulations for the triple co-delivery of Oxygen, Curcumin and Gemcitabine were designed and prepared. Different components were stably incorporated in the nanodroplet structure and their contribution to hampering pancreatic cancer cells was *in vitro* evaluated. Gemcitabine loaded in NDs showed to have an *in vitro* prolonged release and a cytotoxic profile in PDAC cells, thus hypothetically reducing the high doses usually employed for the treatment. Moreover, the resistance induced by Gemcitabine in the cancer cells may be attenuated by the presence of Curcumin, a natural polyphenol derivative that has the capacity to inhibit several resistance-related pathways in cancer cells. Finally, the oxygen-loaded NDs showed to restore normoxia regulating the expression of some genes related to HIF-1α, activated by the cells in response to low oxygen levels. In addition, the theranostic features of the formulations may represent a promising advantage in the diagnosis and treatment of this malignancy. Indeed, nanodroplets as theranostic nanotool have the potential to improve the outcomes of the disease. Taken together, these results indicate that Oxy-Cur-GEM-NDs may potentially be considered as a novel nanoplatform for a combinational therapy aimed at addressing thorny pancreatic cancer.

References

[1] J. Kleeff, M. Korc, M. Apte, C. La Vecchia, C.D. Johnson, Pancreatic cancer, (2016). doi:10.1038/nrdp.2016.22.

[2] B. Muz, P. de la Puente, F. Azab, A.K. Azab, The role of hypoxia in cancer progression, angiogenesis, metastasis, and resistance to therapy, Hypoxia. (2015) 83. doi:10.2147/hp.s93413.

[3] M. Erkan, M. Kurtoglu, J. Kleeff, The role of hypoxia in pancreatic cancer: A potential therapeutic target?, Expert Rev. Gastroenterol. Hepatol. 10 (2016) 301–316. doi:10.1586/17474124.2016.1117386.

[4] V. Petrova, M. Annicchiarico-Petruzzelli, G. Melino, I. Amelio, The hypoxic tumour microenvironment, Oncogenesis. 7 (2018). doi:10.1038/s41389-017-0011-9.

[5] F. Hajizadeh, I. Okoye, M. Esmaily, M. Ghasemi Chaleshtari, A. Masjedi, G. Azizi, M. Irandoust, G. Ghalamfarsa, F. Jadidi-Niaragh, Hypoxia inducible factors in the tumor microenvironment as therapeutic targets of cancer stem cells, Life Sci. 237 (2019) 116952. doi:10.1016/j.lfs.2019.116952.

[6] P. Michieli, P. Michieli, Hypoxia, angiogenesis and cancer therapy: To breathe or not to breathe?, 4101 (2009). doi:10.4161/cc.8.20.9741.

[7] I. Moen, L.E.B. Stuhr, Hyperbaric oxygen therapy and cancer — a review, (2012) 233–242. doi:10.1007/s11523-012-0233-x.

[8] R. Jahanban-Esfahlan, M. de la Guardia, D. Ahmadi, B. Yousefi, Modulating tumor hypoxia by nanomedicine for effective cancer therapy, J. Cell. Physiol. 233 (2018) 2019–2031. doi:10.1002/jcp.25859.

[9] M. Iijima, N. Gombodorj, Y. Tachibana, K. Tachibana, T. Yokobori, K. Honma, T. Nakano, T. Asao, R. Kuwahara, K. Aoyama, H. Yasuda, M. Kelly, H. Kuwano, D. Yamanouchi, Development of single nanometer-sized ultrafine oxygen bubbles to overcome the hypoxia-induced resistance to radiation therapy via the suppression of hypoxia-inducible factor-1α, Int. J. Oncol. 52 (2018) 679–686. doi:10.3892/ijo.2018.4248.

[10] M.S. Khan, J. Hwang, Y. Seo, K. Shin, K. Lee, C. Park, Y. Choi, J.W. Hong, J. Choi, Engineering oxygen nanobubbles for the effective reversal of hypoxia, Artif. Cells, Nanomedicine Biotechnol. 46 (2018) S318–S327. doi:10.1080/21691401.2018.1492420.

[11] C. Greve, L. Jorgensen, Therapeutic Delivery, Ther. Deliv. 7 (2016) 117–138. doi:10.4155/tde.15.92.

[12] P.N. Bhandari, Y. Cui, B.D. Elzey, C.J. Goergen, C.M. Long, J. Irudayaraj, Oxygen nanobubbles revert hypoxia by methylation programming, Sci. Rep. 7 (2017) 1–14. doi:10.1038/s41598-017-08988-7.

[13] R. Cavalli, A. Bisazza, P. Giustetto, A. Civra, D. Lembo, G. Trotta, C. Guiot, M. Trotta, Preparation and characterization of dextran nanobubbles for oxygen delivery, Int. J. Pharm. 381 (2009) 160–165. doi:10.1016/j.ijpharm.2009.07.010.

[14] L. Duan, L. Yang, J. Jin, F. Yang, D. Liu, K. Hu, Q. Wang, Y. Yue, N. Gu, Micro/nano-bubble-

assisted ultrasound to enhance the EPR effect and potential theranostic applications, Theranostics. 10 (2020) 462–483. doi:10.7150/thno.37593.

[15] M.T. Burgess, T.M. Porter, Control of Acoustic Cavitation for Efficient Sonoporation with Phase-Shift Nanoemulsions, Ultrasound Med. Biol. 45 (2019) 846–858. doi:10.1016/j.ultrasmedbio.2018.12.001.

[16] A.L.Y. Kee, B.M. Teo, Biomedical applications of acoustically responsive phase shift nanodroplets: Current status and future directions, Ultrason. Sonochem. 56 (2019) 37–45. doi:10.1016/j.ultsonch.2019.03.024.

[17] F. Yang, Z.-Y. Chen, Y. Lin, Advancement of Targeted Ultrasound Contrast Agents and their Applications in Molecular Imaging and Targeted Therapy, Curr. Pharm. Des. 19 (2013) 1516–1527. doi:10.2174/1381612811319080019.

[18] M.S. Khan, J. Hwang, K. Lee, Y. Choi, K. Kim, H.J. Koo, J.W. Hong, J. Choi, Oxygen-carrying micro/nanobubbles: Composition, synthesis techniques and potential prospects in photo-triggered theranostics, Molecules. 23 (2018) 1–19. doi:10.3390/molecules23092210.

[19] C. Kang, D. Kim, Nanoconfinement-mediated cancer theranostics, Arch. Pharm. Res. 43 (2020) 110–117. doi:10.1007/s12272-020-01217-2.

[20] V.S. Madamsetty, A. Mukherjee, S. Mukherjee, Recent trends of the bio-inspired nanoparticles in cancer theranostics, Front. Pharmacol. 10 (2019) 1–12. doi:10.3389/fphar.2019.01264.

[21] K. Samanta, S. Setua, S. Kumari, M. Jaggi, M.M. Yallapu, S.C. Chauhan, Gemcitabine combination nano therapies for pancreatic cancer, Pharmaceutics. 11 (2019) 1–25. doi:10.3390/pharmaceutics11110574.

[22] M. Amrutkar, I.P. Gladhaug, Pancreatic cancer chemoresistance to gemcitabine, Cancers (Basel). 9 (2017) 1–23. doi:10.3390/cancers9110157.

[23] A. Manzur, A. Oluwasanmi, D. Moss, A. Curtis, C. Hoskins, Nanotechnologies in pancreatic cancer therapy, Pharmaceutics. 9 (2017). doi:10.3390/pharmaceutics9040039.

[24] A.B. Kunnumakkara, P. Anand, B.B. Aggarwal, Curcumin inhibits proliferation, invasion, angiogenesis and metastasis of different cancers through interaction with multiple cell signaling proteins, Cancer Lett. 269 (2008) 199–225. doi:10.1016/j.canlet.2008.03.009.

[25] O. Naksuriya, S. Okonogi, R.M. Schiffelers, W.E. Hennink, Curcumin nanoformulations: A review of pharmaceutical properties and preclinical studies and clinical data related to cancer treatment, Biomaterials. 35 (2014) 3365–3383. doi:10.1016/j.biomaterials.2013.12.090.

[26] B.L. Tan, M.E. Norhaizan, Curcumin combination chemotherapy: The implication and efficacy in cancer, Molecules. 24 (2019) 1–21. doi:10.3390/molecules24142527.

[27] R. Cavalli, M. Argenziano, E. Vigna, P. Giustetto, E. Torres, S. Aime, E. Terreno, Preparation and in vitro characterization of chitosan nanobubbles as theranostic agents, Colloids Surfaces B Biointerfaces. 129 (2015) 39–46. doi:10.1016/j.colsurfb.2015.03.023.

[28] M.E. Gilles, F. Maione, M. Cossutta, G. Carpentier, L. Caruana, S. Di Maria, C. Houppe, D. Destouches, K. Shchors, C. Prochasson, F. Mongelard, S. Lamba, A. Bardelli, P. Bouvet, A. Couvelard, J. Courty, E. Giraudo, I. Cascone, Nucleolin targeting impairs the progression of pancreatic cancer and promotes the normalization of tumor vasculature, Cancer Res. 76

(2016) 7181–7193. doi:10.1158/0008-5472.CAN-16-0300.

[29] C.T. Rueden, J. Schindelin, M.C. Hiner, B.E. DeZonia, A.E. Walter, E.T. Arena, K.W. Eliceiri, ImageJ2: ImageJ for the next generation of scientific image data, BMC Bioinformatics. 18 (2017) 1–26. doi:10.1186/s12859-017-1934-z.

[30] A.S. Nunes, A.S. Barros, E.C. Costa, A.F. Moreira, I.J. Correia, 3D tumor spheroids as in vitro models to mimic in vivo human solid tumors resistance to therapeutic drugs, Biotechnol. Bioeng. 116 (2019) 206–226. doi:10.1002/bit.26845.

[31] M. Daga, C. Ulllio, M. Argenziano, C. Dianzani, R. Cavalli, F. Trotta, C. Ferretti, G.P. Zara, C.L. Gigliotti, E.S. Ciamporcero, P. Pettazzoni, D. Corti, S. Pizzimenti, G. Barrera, GSH-targeted nanosponges increase doxorubicin-induced toxicity “in vitro” and “in vivo” in cancer cells with high antioxidant defenses, Free Radic. Biol. Med. 97 (2016) 24–37. doi:10.1016/j.freeradbiomed.2016.05.009.

[32] M. Argenziano, G. Banche, A. Luganini, N. Finesso, V. Allizond, G.R. Gulino, A. Khadjavi, R. Spagnolo, V. Tullio, G. Giribaldi, C. Guiot, A.M. Cuffini, M. Prato, R. Cavalli, Vancomycin-loaded nanobubbles: A new platform for controlled antibiotic delivery against methicillin-resistant Staphylococcus aureus infections, Int. J. Pharm. 523 (2017) 176–188. doi:10.1016/j.ijpharm.2017.03.033.

[33] L. De Sousa Cavalcante, G. Monteiro, Gemcitabine: Metabolism and molecular mechanisms of action, sensitivity and chemoresistance in pancreatic cancer, Eur. J. Pharmacol. 741 (2014) 8–16. doi:10.1016/j.ejphar.2014.07.041.

[34] D.I. Vitoratou, M. Tolia, P. Liakos, N. Tsoukalas, C. Giaginis, M. Nikolaou, G. Nikolaou, G. Rigas, K. Psarianos, A. Lioupis, G. Kyrgias, Clinical value of significance of hypoxia inducible factor-1α, glucose transporter-1 and carbonic anhydrase IX in rectal cancer after preoperative chemoradiotherapy, J. B.U.ON. 24 (2019) 456–463.

[35] N. Robertson, C. Potter, A.L. Harris, Role of carbonic anhydrase IX in human tumor cell growth, survival, and invasion, Cancer Res. 64 (2004) 6160–6165. doi:10.1158/0008-5472.CAN-03-2224.

[36] C.C. Barron, P.J. Bilan, T. Tsakiridis, E. Tsiani, Facilitative glucose transporters: Implications for cancer detection, prognosis and treatment, Metabolism. 65 (2016) 124–139. doi:10.1016/j.metabol.2015.10.007.

[37] L. Dong, S. You, Q. Zhang, S. Osuka, N.S. Devi, S. Kaluz, J.H. Ferguson, H. Yang, G. Chen, B. Wang, H.E. Grossniklaus, E.G. Van Meir, Arylsulfonamide 64B inhibits hypoxia/ HIF-induced expression of c-Met and CXCR4 and reduces primary tumor growth and metastasis of uveal melanoma, Clin. Cancer Res. 25 (2019) 2206–2218. doi:10.1158/1078-0432.CCR-18-1368.

CHAPTER 2

LOW-DOSE CURCUMINOID-LOADED IN DEXTRAN-BASED NANODROPLETS CAN PREVENT METASTATIC SPREADING IN PROSTATE CANCER CELLS

Introduction

In this second project, the Curcuminoid delivery in nanodroplets as adjuvant therapy for prostate cancer was investigated. Prostate cancer is one of the most diffuse pathologies in elderly men. Due to its very slow development and the chance of predicting it in advance, by monitoring the serum concentration of the prostate specific antigen (PSA), more than 3 over 4 patients recovers following surgical excision or radical radiotherapy [1]. However, in the cases of prostate cancer at high risk, that are often predictable as based on cancer histology, PSA values, patients are at risk of developing local or metastatic (mainly in bones) recurrences, which can evolve in the almost non-curable castration resistant prostate cancer [2]. To prevent or delay recurrences, such patients are normally treated with adjuvant therapies (i.e. concomitant or just following radical surgery or radiotherapy) mainly based on androgen deprivation therapies (ADT). Moreover, for adjuvant ADT in high risk patients neither conclusive support for benefits [3] nor standard recommendations exist [4]. Since hormonal therapies have many collateral toxic effects, especially for elderly or multi-diseased patients, there is a need for alternative and safe compounds for developing new adjuvant therapies. Among other substances of natural origin suitable as candidate for adjuvant therapies, curcumin has been largely investigated.

Curcumin is a natural polyphenol molecule derived from the *Curcuma longa* L. plant. Much research on curcumin showed its properties as antioxidant, anti-inflammatory, anti-angiogenic, anti-diabetic, hepatoprotective agent in cell culture and animal studies [5]. Moreover, current pre-clinical and clinical studies revealed that curcumin also exerts antiproliferative and proapoptotic effects against various tumors *in vitro* and *in vivo* [6]. Moreover, several preclinical studies demonstrated that curcumin is also able to inhibit chemically induced carcinogenesis, both at initial and progression stages [7]. Curcumin can interfere with the tumor cell cycle and inhibit tumor cell invasion through regulation of cytokines, growth factors, and their receptors, enzymes, and adhesion molecules. It induces apoptosis in cancer cells by inhibiting various intracellular transcription factors and secondary messengers such as NF-kB, AP-1, c-Jun, the Jak-STAT pathway and various others [8]. Interestingly, in the past decade, research about the bioactivity of turmeric components of curcumin has been broadened, opening new perspectives about chemical entities different from Curcuminoids (Curc). Curcumin-free extracts from turmeric, demonstrate different biological activities such as anti-diabetic, anticancer, antimicrobial and anti-inflammatory effects [9]. Several investigations have been focused on the pharmacological properties of the lipophilic fraction (turmeric oil), mainly composed of aromatic (ar)-turmerone, alfa-turmerone, beta-turmerone, curlone, sesquiphellandrene, and zingiberene. This field of research was corroborated by the potent anticancer and anti-inflammatory activities discovered [10–12]. Although the biological effects of turmeric oil have been reported, its role as an isolated fraction or as an extract component is still not completely clarified. A synergistic effect of the whole phytocomplex with Curcuminoids seems to enhance the curcumin bioavailability [13].

Depending on the cultivar, on the origin and in general on the growing conditions, Curcuminoid content in *Curcuma longa* L. ranges from 2% to 9% [14, 15]. With such a low concentrated matrix, an efficient extraction procedure is mandatory, also considering the critical stability profile of Curcuminoids, given their proneness to photo- and oxidative degradation [16]. For these reasons, microwave-assisted extraction (MAE) has been selected. Microwaves were introduced in the eighties for analytical samples preparation using domestic ovens [17]. MAE differs from

conventional techniques because of the direct interaction of dielectric heating with the in situ water and other polar components within the cells of the plant material. These waves are made up of two perpendicular oscillating fields which are used as energy carriers. The application of microwaves includes its interaction with the specific materials which can absorb a part of its electromagnetic energy and can convert it into heat. The electromagnetic waves generate thermal energy by dipole rotation and ion traffic increasing the penetrating efficiency of the solvents into the plant matrix with consequent cell membranes and walls rupture and the release of target compounds [18]. The efficiency of microwaves to be converted into heat is expressed by the dielectric properties of the material, and for this reason, particular importance is played by the solvent [19].

In conventional processes, heat moves from the hot solvent to the inner part of the matrix, whilst in MAE the heat is transferred volumetrically within the irradiated medium, allowing fast treatments and avoiding degradation. All these features allow a synergistic combination of heat and mass transport phenomena, leading to extraction acceleration and increasing selectivity and yields.

However, there are also some drawbacks. Besides its positive properties, curcumin possesses poor water solubility, lack of stability, and presents a rapid degradation by hydrolysis and then it undergoes molecular fragmentation [20]. As a consequence, it exhibits low bioavailability. Moreover, it displays rapid intestinal and hepatic metabolism, approximately 60%–70% of an oral dose of curcumin gets eliminated in the feces [21]. Several clinical studies showed that only a few patients responded to curcumin despite high doses used.

Based on these premises, the solubility, stability and consequently the bioavailability of curcumin can be enhanced by encapsulation in nanoparticles. Therefore, suitable delivery vehicles have been designed for curcumin. In the literature, many nanocarriers have already been proposed to deliver either curcumin alone or associated with antitumoral drugs. A WoS investigation found about 20 relevant related original papers. Among them, experiments were performed on PCa cell lines (mainly LNCaP, PC-3 and DU-145) at various curcumin doses from 5 up to 600 μM. Direct curcumin administration produced dose-dependent inhibition of cellular proliferation [22, 23], induction of apoptosis [23, 24] and direct cell toxicity at doses higher than 50 μM [25–28]. Such effects were detected also when curcumin was delivered by nanocarriers [25] but also other important features were underlined, as effective internalization [28] and enhanced anticancer effect [29–31]. Different theranostic nanocarriers have also been proposed so far based on the correlated imaging techniques mainly MRI [26, 32–35] and optical [36–39].

Among other nanodelivery systems, nanobubbles are innovative nanoplatform developed to enhance the effectiveness of treatments, control drug release, modify pharmacokinetics and biodistribution, decrease the administered doses of encapsulated drugs, overcome biological barriers, target specific cells and decrease the occurrence of side effects. Nanobubbles are core-shell structure and present spherical shape. Their shell mainly consists of lipids, proteins, polymers or biocompatible polysaccharide (i.e. chitosan, or dextran sulfate); instead, the core can be filled up with various gases, such as perfluorocarbons, sulfur hexafluoride, and carbon dioxide. Nanobubbles have been deeply investigated as drug and nucleic acid delivery systems [40] and displayed effective oxygen storing capacity [41]. In addition to their drug loading capability, nanobubbles are ultrasound (US) responsive nanocarriers [42]. Being US sensitive, this nanotechnology has been used for the development of externally triggered nanocarriers that provide controlled payload release. Interestingly, nanosized bubbles can extravasate from blood vessels into surrounding tissues, thus improving the delivery efficiency and target. Furthermore, nanoscale dimensions offer

some advantages, such as the ability to accumulate within tumor tissues via the enhanced permeability and retention effect (EPR). In addition to the accumulation via passing targeting, nanobubbles can be functionalized and provide active targeting. Indeed, binding antibodies to the nanobubble surface can direct the nanosystems in the target tissue, improving the therapeutic therapy efficacy.

These formulations have been referred to as nanobubbles for the sake of simplicity, but it would be more correct to use the term nanodroplets, being perfluoropentane liquid at room temperature.

In this project, nanodroplets with dextran sulfate-shell and perfluoropentane core were designed and tuned to efficiently encapsulate Curcuminoids in a large amount. Therefore, Curcuminoid-loaded nanodroplets (Curc-NDs) were developed as innovative delivery systems, able to carry and to release Curcuminoids to the target site. Moreover, nanodroplet nanosuspensions can protect Curcuminoids from degradation and chemical instability that occur under physiological conditions [43]. Indeed, nanodroplets are interesting nanotools that can store and enhance the stability of the carried drug or active compound [40]. Being Curc-NDs detectable using ultrasound (US) imaging [44] and MRI [42], they are effective theranostic tools. In the present work, the effect of highly concentrated Curc extracts has been investigated both free and carried in nanodroplets as Curc-NDs.

Aim of the project

In order to provide a proof-of-concept about the effectiveness of Curcuminoids as adjuvant therapy to prevent prostatic cancer recurrence after radical prostatectomy or radiotherapy, when a small number of viable cancer cells are expected dextran-sulfate shelled Curcuminoids-loaded nanodroplets (Curc-NDs) were designed and developed. The nanodroplet nanoformulation confers higher stability to the Curcuminoid compounds, that can be delivered more efficiently to the tumor target site. Moreover, since the nanodroplets express echogenic properties, they can be exploited as theranostic nanotools. Curcuminoid effect both in solution and as Curc-NDs was *in vitro* evaluated on cell viability, colony formation, apoptosis, adhesion and migration properties in two prostatic cancer cell lines.

The results of this work were published as

BESSONE, Federica, *et al.* Low-dose curcuminoid-loaded in dextran nanobubbles can prevent metastatic spreading in prostate cancer cells. *Nanotechnology*, **2019**, *30* (21), p. 214004

Materials and methods

Materials

The substances and laboratory reagents were from Sigma-Aldrich (St Louis, MO, US), unless otherwise specified. Soybean lecithin (Epikuron 200®) was kindly gifted by Cargill (Wayzata, MI, US). Perfluoro-n-pentane min. 98% and was sourced from Strem Chemical (Newburyport, MA, US). Ultrapure water was obtained using a 1–800 Millipore system (Molsheim, France). The tubular semi-permeable cellulose membrane was from Carl Roth (Karlsruhe, Germany). Cell culture reagents were purchased from Gibco/Invitrogen (Life Technologies, Paisley, UK) except where otherwise indicated. All reagents were of analytical grade.

Methods

Preparation and characterization of Curcuminoids

Curcuma longa L. rhizome powder (2 mm average size) was transferred into a 40 ml glass vessel. Hydroalcoholic solution (70% ethanol) was added keeping a solid-liquid ratio of 1:10. Extraction was performed into a multimodal microwave autoclave reactor (Synthwave, Milestone). With a fixed maximum power of 1500 W, the sample was irradiated for 5 min at 80 °C under magnetic stirring (650 rpm). The system was pressurized with N_2 (2 bar) to prevent solvent evaporation and Curcuminoids degradation. The crude extract was filtered on sintered glass and dried under vacuum. Total Curcuminoids concentration was measured by HPLC with an external standard calibration curve. The analysis was performed with a Waters 1525 binary HPLC pump equipped with 2998 PDA, and a Phenomenex Kinetex® Column (5 µm C18 100 Å, 250 × 4.6 mm). Data acquisition was accomplished using Empower PRO (Waters Associates, Milford, CT, US). CH_3CN: 5% acetic acid aqueous solution was used as mobile phase. The chromatographic separation was performed in isocratic (50:50, v/v) at 25 °C with a flow rate of 1 mL/min. Injection volume was 10 µL, while sample detection was carried out at 425 nm; Curc standard solutions (from 0.02 to 2 mg/mL) were analyzed by HPLC (10 µL injection) to give linear regressions with $R^2 > 0.999$. Before the injection, all samples were dissolved in MeOH, giving concentrations of between 10 and 20 mg/mL. All samples were filtered through 0.2 µm membrane filters before injection into the HPLC apparatus.

Preparation of Curcuminoid solution

The solubility issue of Curcuminoids is a limitation for the preparation of a solution. Since Curc are poorly water soluble, an organic solvent is required. Moreover, the choice of the solvent should be taken considering its application in biological studies. For this purpose, N-methyl-2-pyrrolidone was selected. Curc solution was obtained by firstly solving a weighted amount of Curc at a concentration of 0.5 M in N-methyl-2-pyrrolidone. Then, the solution was diluted in a mixture of N-methyl-2-pyrrolidone/0.9% NaCl in a ratio 1:1 v/v, to obtain a final concentration of 3 mM. The Curcuminoids concentration of the solution was determined by a RF-551 Spectrofluorometer (Shimadzu, Kyoto, Japan) using the method described below. Once obtained, the Curc solution was stored at 4 °C.

Preparation of Nanodroplet formulations

Unloaded Nanodroplets

The nanodroplets (NDs) were obtained by tuning a previously described method [44–46]. Briefly, NDs were prepared using perfluoropentane as inner core component and dextran sulfate (MW of 100 kDa) for the shell. In the beginning, an ethanol solution containing Epikuron® 200 (1.5% w/v) was added to perfluoropentane forming a pre-emulsion. Then, ultrapure water was added and the mixture was homogenized using an Ultra-Turrax® homogenizer (IKA, Konigswinter, Germany) for 2 minutes and heat at 37 °C for 15 minutes. After that, an aqueous solution of the dextran sulfate (2% w/v) was added dropwise under mild magnetic stirring. Blank NDs were used as control in the following experiments.

Curcuminoid loaded Nanodroplets

Curc-NDs were prepared adding to an ethanol solution containing Epikuron® 200 (1.5% w/v) Curcurcuminoids (8.5% w/v). After the addition of perfluoropentane and ultrapure water, the mixture was homogenized using an Ultra-Turrax® homogenizer for 2 min and heat at 37 °C for 15 min. Then, an aqueous solution of the dextran sulfate salt (2% w/v) was added dropwise under mild magnetic stirring. The final concentration of loaded Curcuminoids in the formulation was 3 mM, determined by Spectrofluorometer analysis using the method described below.

Characterization of Nanodroplet formulations

The different ND formulations were physico-chemically characterized. The nanosuspensions were previously diluted in deionized filtered water. Then, the average diameters and dispersity of the various diluted nanodroplet formulations were measured by photocorrelation spectroscopy using a 90 Plus instrument (Brookhaven, NY, US) with a scattering angle of 90° at 25 °C.

The zeta potential was determined by the same instrument. The diluted samples, placed in an electrophoretic cell, were subjected to an electric field of around 15 V cm^{-1}. The analyses were conducted in triplicate of three different batches.

Spectrofluorometer quantitative Curcuminoid determination method

Curcuminoid concentration was determined using a RF-551 Spectrofluorometer (Shimadzu, Kyoto, Japan). The excitation wavelength was set at 422 nm and the emission spectrum was recorded in a wavelength range between 350 and 650 nm. The peak area correlated linearly with Curcuminoid concentration in the range of 5–30 ng/mL (R^2 = 0.9994). To calculate Curc concentration, a linear calibration curve was set up with a concentration range of 2.5–30 ng/mL (R^2 = 0.9994).

Echogenic properties of Nanodroplet formulations

Echogenic images were visualized using MyLab 25Gold (Esaote, Genova, Italy) instrument. The frequency was 7.5 MHz, the Mechanical Index 1.1; contrast Res modality.

Encapsulation efficiency and loading capacity of Curcuminoids in Nanodroplet

Curc-ND encapsulation efficiency was determined with a centrifugal filter system. For this purpose, 100 µLof Curc-ND formulations were put in a centrifugal filter device (Amicon® Ultra-0.5) and then centrifuged at 20000 rpm for 15 minutes with a Beckman Coulter Allegra 64R Centrifuge. The filtered solution was collected and the amount of free Curcuminoids in the nanosuspension was quantified by a spectrofluorometer. The encapsulation efficiency was calculated as follows:

Encapsulation Efficiency (EE):

$$EE = \frac{Total_{Curc} - Free_{Curc}}{Total_{Curc}} \times 100$$

(Equation 1)

Freeze-dried ND samples were used for the determination of the loading capacity of Curc-NDs. A weighted amount of freeze-dried Curc-NDs was suspended in water. The sample was firstly sonicated and centrifuged, and then the supernatant was analyzed. The loading capacity of Curcuminoids in Curc-NDs was calculated as follows.

Loading Capacity (LC):

$$LC = \frac{Total_{Curc}}{ND\ weight} \times 100$$

(Equation 2)

In vitro Curcuminoid release from Curc-NDs

The *in vitro* release of Curcuminoids from nanodroplet formulation was carried out by the use of a multi-compartment rotating cell. Curc-NDs and Curc solution as control were respectively placed in the donor chambers, separated from the receiving chamber by a semipermeable cellulose membrane (cut-off 14 kDa). The receiving phase consisted of a H_2O/EtOH 1:1 v/v mixture. At fixed time intervals, the samples were collected and the same volume was replaced with the fresh receiving phase. Then, the samples were analyzed and Curcuminoid concentration was determined by a spectrofluorometer, following the method described above.

In vitro evaluation of the stability of Curcuminoid solution and Curc-NDs over time

The stability of Curcuminoids was evaluated in N-methyl-2-pyrrolidone/0.9% NaCl solution and carried in nanodroplets. The Curcuminoid concentration was evaluated over time by spectrofluorometry, following the method described above. The samples were stored at 4 °C and analyzed up to 30 days.

Cells

Human umbilical vein endothelial cells (HUVEC) were isolated from human umbilical veins by collagenase treatment (1%) and cultured in M199 medium with the addition of 20% fetal calf serum (FCS) 100 UI/mL penicillin, 100 µg/mL streptomycin, 5 UI/mL heparin, 12 µg/mL bovine brain extract and 200 mM glutamine. HUVEC were grown to confluence in flasks and used from the second to the fifth passage [47]. The use of HUVEC was approved by the Ethics Committee of the "Presidio Ospedaliero Martini" of Turin and conducted following the Declaration of Helsinki. Written informed consent was obtained from all donors.

The study was performed on two prostate cell lines, PC-3 and DU-145. The human cancer cells were both obtained from ATCC (Milan, Italy). The cell lines were grown in culture dishes as a monolayer in RPMI 1640 medium supplemented with 10% FCS, 100 UI/mL penicillin, and 100 µg/mL streptomycin at 37 °C in a 5% CO_2 humidified atmosphere.

Curcuminoids-nanodroplet cell uptake

PC-3 cells were seeded onto Corning® cover glasses (Sigma-Aldrich) in a 24-well plate (4×10^4 cells per well) and incubated overnight at 37 °C in a 5% CO_2 atmosphere. Then, the media was replaced with a fresh media mixture containing Curc-NDs and free Curc in solution, both at the final concentration of 5 µM. After 1 hour of incubation, the cells were washed with PBS, and fixed in 4% paraformaldehyde at room temperature for 15 minutes. Fixed cells were washed with PBS and stained with 4',6-diamidine-2-phenylindole. Finally, coverslips were mounted. Image acquisition was performed with a TCS SP2 AOBS confocal microscope (Leica, Wetzlar, Germany), equipped with 63X/1.40 HCX Plan-Apochromat oil-immersion objective.

In vitro cytotoxicity studies

PC-3 and DU-145 cells (8×10^2/well) were seeded in 96-well plates and incubated at 37 °C, 5% CO_2 for 24 h in RPMI 1640 media. Then, the cells were treated with blank NDs, Curc solution and Curc-NDs at a concentration in the range 1–15 µM. After 24–72 hours of incubation, viable cells were evaluated by 2,3-bis[2-methoxy-4-nitro-5sulphophenyl]-2H-tetrazolium-5carboxanilide (MTT) inner salt reagent at 570 nm, as described by the manufacturer's protocol. The control cells were normalized to 100%, and the readings from treated cells were expressed as % of viability inhibition. Eight replicates were used to determine each data point and five different experiments were performed.

Colony-forming assay

PC-3 and DU-145 cells (8×10^2/well) were seeded into 6-well plates and treated with blank NDs, Curc solution and Curc-NDs (1–15 µM). The medium was changed after 3–24 hours and cells were cultured for additional 10 days. After that, cells were fixed and stained with a solution of 80% crystal violet and 20% methanol. Colonies were washed and 30% acetic acid was added to induce a complete dissolution of the crystal violet. Absorbance was recorded at 595 nm by a 96-well plate ELISA reader. Five different experiments were performed. The untreated cells (control) were

normalized to 100%, and the readings from treated cells were expressed as % of viability.

Cell apoptosis assay

The cell apoptosis was detected by using the FITC Annexin V Apoptosis Detection Kit (BD Biosciences Cat N° 556 547). Briefly, PC-3 cells (1.2×10^5/well) were seeded into 6-well plates and treated with blank NDs, Curc solution, or Curc-NDs (10 and 15 µM). After 24 hours, adherent and non-adherent treated and control cells were harvested and stained with FITC-Annexin V and PI, according to the manufacturer protocol. The samples were analyzed with a FACScan cytometer (Becton Dickinson, Accuri).

Cell adhesion assay

HUVEC were grown to confluence in 24-well plates. Then, cells were pre-treated for 30 minutes with blank NDs, Curc solution and Curc-NDs at a concentration of 5 µM and then were stimulated with TNF-α 10 ng/mL. After 18 hours, HUVEC cells were washed twice with fresh medium and tumor cells (1×10^5/well) were seeded and left to adhere with HUVEC for 1 hour, as previously reported [48]. Unattached tumor cells were washed away and the number of adherent cells was evaluated by the Image Pro Plus Software for micro-imaging (Media Cybernetics, version 5.0, Bethesda, MD, US). The viability of the unattached cells was evaluated by the Trypan Blu test. Five different experiments were performed. Data are shown as percentages of the adhesion of treated cells. Control adhesion was 49 ± 4 cells per microscope field for PC-3 cells and in a similar range (54 ± 5 cells) for DU-145 (mean ± standard error of the mean (SEM)).

Cell motility assay

In the Boyden chamber invasion assay, cells (5×10^3) were plated onto the apical side as previously reported [49] in serum-free medium with blank NDs, Curc solution and Curc-NDs (5 µM). Medium containing PMA 100 ng/mL or FCS 20% were placed in the basolateral chamber as chemoattractants. After 18 hours, cells on the apical side were wiped off with Q-tips. Cells on the bottom of the filter were stained with crystal violet and counted (all fields of each triplicate filter) with an inverted microscope. Five different experiments were performed. Data are shown as percentages of the migration of treated cells. Control migration was 52 ± 4 cells per microscope field for PC-3 cells and 66 ± 5 for DU-145 cells.

Data analysis

Data are shown as mean ± SEM. Statistical analyses were performed with GraphPad Prism 5.0 software (San Diego, CA, US). One way ANOVA was performed, followed by Tukey's multiple comparison post test when needed. Only P values < 0.05 were considered significant.

Results

Preparation and characterization of the Curcuminoids

The highly efficient MW-assisted extraction procedure afforded 20.76% of Curcuminoids (12.49% Curcumin, 4.77% demethoxycurcumin, 3.50% bisdemethoxycurcumin) in the dry extract. The reported yield represents nearly 90% of the total content in rhizomes. The fast process and the controlled atmosphere helped to preserve the stability of the final extract, which has been used without any further purification.

Preparation and physico-chemical characterization of Nanodroplet formulations

Nanodroplets (NDs) with dextran sulfate-shell and perfluoropentane core were obtained for the delivery of Curcuminoids. Novel ND formulations were tuned to efficiently encapsulate Curcuminoids in a large amount. Curc-NDs were developed as innovative delivery systems, able to carry and to release Curcuminoids to the target site. Moreover, ND nanosuspensions can protect Curc from degradation and chemical instability that occur under physiological conditions [40]. Indeed, NDs are interesting nanotools that can store and enhance the stability of the carried drug or compound [41, 46]. Curc-NDs were formulated and blank NDs were used as control. The average diameters, dispersity, zeta potentials, and pH of Curc-loaded and unloaded ND formulations are reported in Table 1. Curc-NDs and blank NDs both presented a mean diameter of less than 350 nm and negative Z-potential, due to the negative charges of dextran sulfate. The pH of the nanosuspensions is accepted and applied in biological systems.

Table 1. Physico-chemical characteristics of nanodroplet formulations. Results are shown as means ± SD (n = 3) of three different preparations. Abbreviations: standard deviation (SD); and dispersity (Đ).

Nanodroplet formulations	Average diameter ± SD (nm)	Đ	Z-potential ± SD (mV)	pH
Blank NDs	328.01 ± 5.10	0.19	−44.71 ± 4.22	6.90
Curc-NDs	348.45 ± 7.30	0.20	−53.27 ± 5.96	7.40

Encapsulation efficiency and loading capacity of Curcuminoids in Nanodroplets

NDs were able to efficiently encapsulate Curcuminoids, with an encapsulation efficiency of 97% (Equation 1). On the other hand, the loading capacity of Curc-NDs was 14.20% (Equation 2).

In vitro Curcuminoids release from Curc-NDs

The *in vitro* Curcuminoid release from Curc-NDs and Curc solution was comparatively evaluated over time up to 28 hours. Curc-NDs displayed a slower and prolonged Curcuminoid release over time, with respect to Curc solution (Figure 1). After 24 hours, only 25% of the Curcuminoid was released from Curc-NDs. Thus, it might be hypothesized that Curc-NDs act as a reservoir of the compound until they reach the target site.

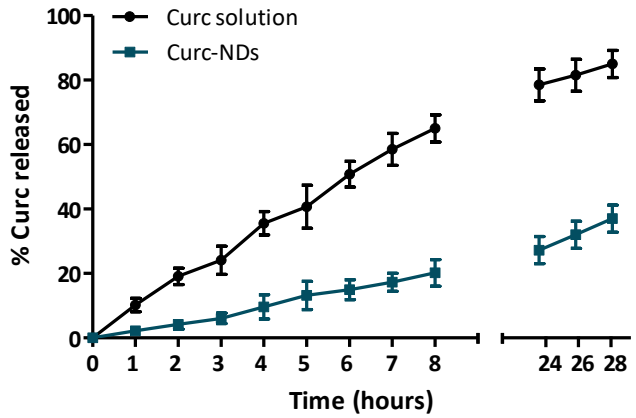

Figure 1. *In vitro* release study of Curc-NDs and Curcuminoid solutions as control up to 28 hours. Curc-NDs released Curcuminoids in a sustained and prolonged manner over time. The results are presented as mean ± SD of three different experiments (n = 3).

In vitro evaluation of the stability of Curcuminoids

Curcuminoid stability was evaluated in N-methyl-2-pyrrolidone solution and when loaded in NDs. The Curcuminoid concentration in the NDs was stable up to 1 month. This result confirmed that the encapsulation of Curcuminoids in the ND nanoformulations increased the stability of the compounds compared to free Curcuminoid solution (Figure 2). Indeed, the decrease in absorbance over time occurred much faster for the Curcuminoid solution, that reduce of a 60% its stability after 30 days.

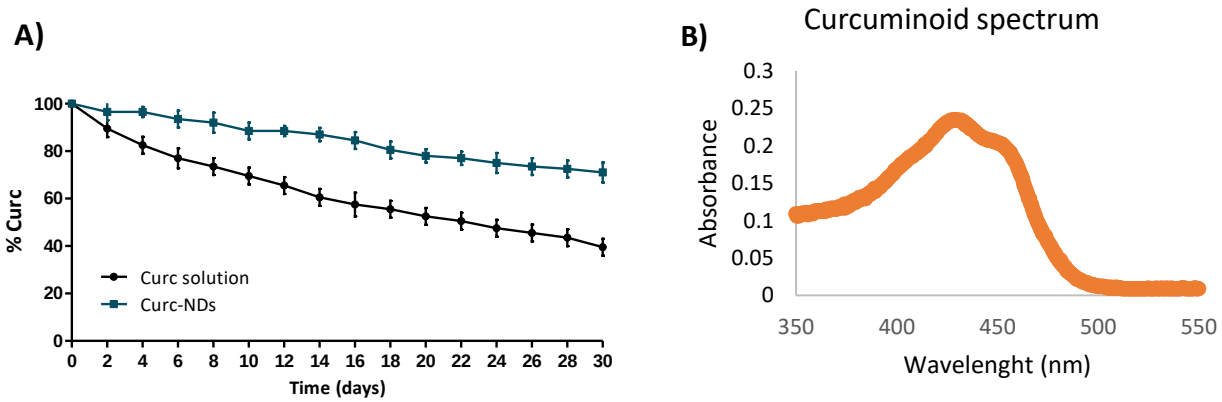

Figure 2. Curcuminoids encapsulated in NDs presented higher chemical stability over time. The stability (expressed as percent of Curcuminoids remained) up to 30 days of Curcuminoids in solution and loaded in NDs was investigated. The results are shown as mean ± SD of three different experiments (n = 3). **B**) Absorption spectrum of Curcuminoids in EtOH/H_2O (1:1 v/v).

Curcuminoids-loaded Nanodroplets display echogenic properties

Curc-loaded ND echogenic properties were visualized by Ultrasound imaging (Figure 3). The visualization of the NDs was due to the acoustic droplet vaporization (ADV) process. Because of this phenomenon, a phase-shift from liquid perfluoropentane nanodroplets to vapor microbubbles occurs, increasing their echogenic properties.

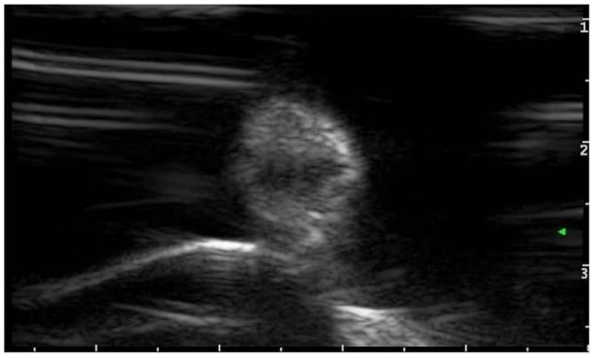

Figure 3. Echogenic image of NDs, visualized using MyLab 25Gold (Esaote, Genova, Italy) sonograph. The frequency was 7.5 MHz, and the Mechanical Index was 1.1.

Curcuminoids-loaded Nanodroplets cell internalization

In order to evaluate the biological uptake, Curc-NDs and Curc solution were incubated at a concentration of 5 µM with PC-3 cell line for 1 hour. Curc fluorescence per se was exploited for the evaluation of the internalization of the NDs by confocal microscopy. Indeed, Curc presented a λ_{ex}=422 nm and a λ_{em}=550 nm, as shown in Figure 4A [50]. As reported in Figure 4B, Curc-NDs were avidly internalized by the cells compared to free Curc solution.

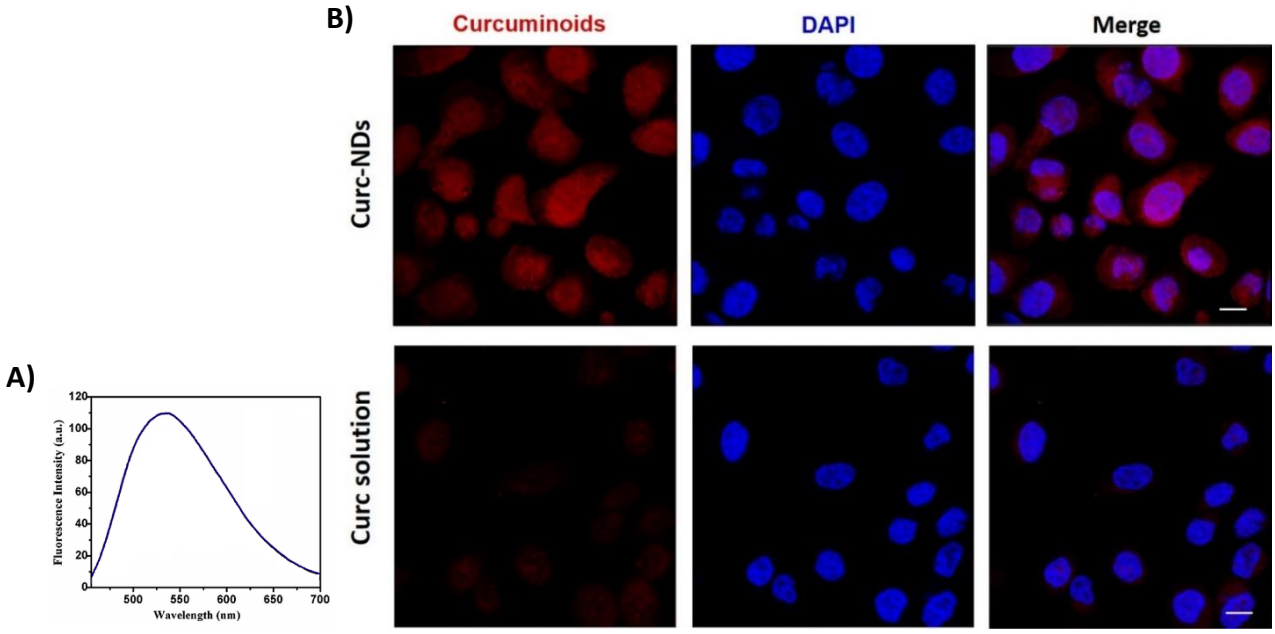

Figure 4. A) Fluorescence spectrum of Curc, modified from Prabu *et al.* [50]. **B**) Curc-NDs are avidly internalized by PC-3 cells. Curcuminoid-loaded NDs and Curcuminoid solution were internalized into PC-3 cells after 1 hour of incubation. Images are representative of three fields per condition (n = 3).

Viability test

The effect of Curcuminoid solution and Curc-NDs on the viability of PC-3 and DU-145 cells was *in vitro* investigated. Figure 5 shows that in both cell lines Curc-NDs inhibited cell viability with a higher extent than Curcuminoid solution. The effect was concentration- and time-dependent with a small difference between the two cell lines. Curc-NDs were more efficient than Curcuminoid solution in terms of timing, maximal inhibition and effective doses. At low doses, on the contrary, Curcuminoids are almost non-toxic either in free form or encapsulated. Blank NDs did not affect tumor cell viability at all the concentrations and the times tested.

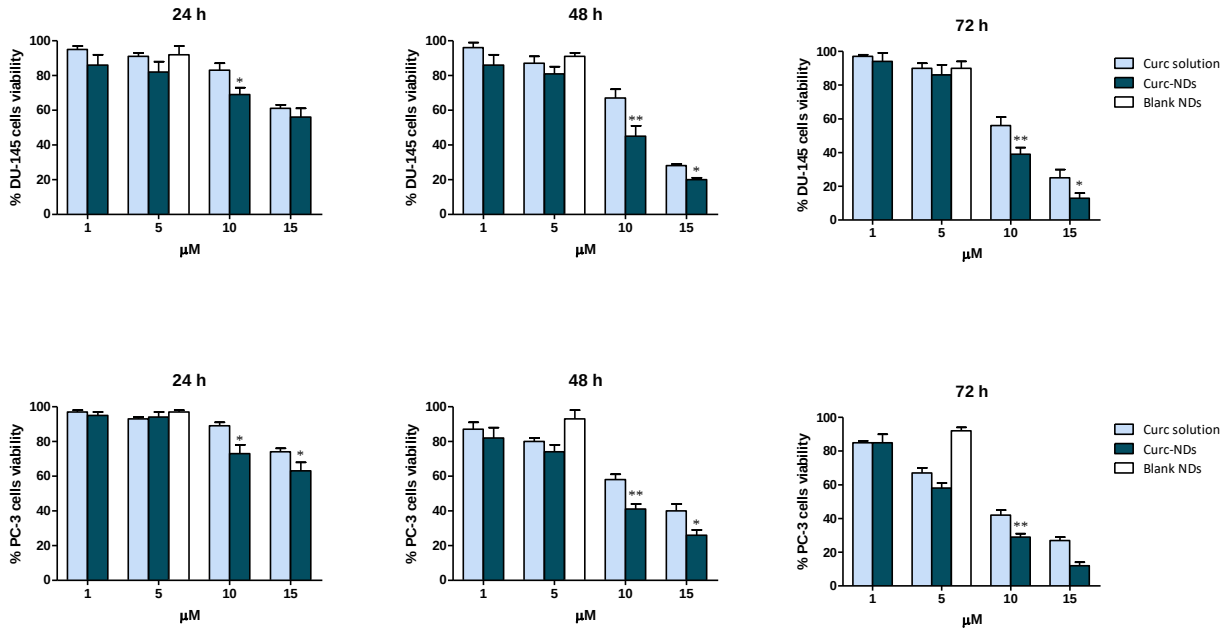

Figure 5. Cell viability of DU-145 and PC-3 after the incubation of Curc solution and Curc-NDs for 24, 48 and 72 hours. Data are expressed as mean ± SD (n=3). *p<0.05, **p<0.01 vs Curcuminoid solution.

Colony-forming assay

To validate cell viability results, an *in vitro* cell survival assay based on the capability of a single cell to grow into a colony was performed. The cells were incubated for 3 and 24 hours with the Curc-NDs and Curcuminoids solution. After that, the cells were washed with PBS, fresh cell medium was added, and the cells were allowed to grow for additionally 7 days. As shown in Figure 6, there is a significant difference between PC-3 cells treated with Curc solution and Curc-NDs already after 3 hours at 15 µM. Whereas, the higher efficacy of Curc-NDs becomes constant at all the concentrations tested after 24 hours (Figure 6A). Similar results were obtained with DU-145 cell line (data not shown), demonstrating the higher and faster internalization of the Curcuminoid loaded in NDs than Curcuminoid solution. Figure 6B shows assay photos from a representative experiment.

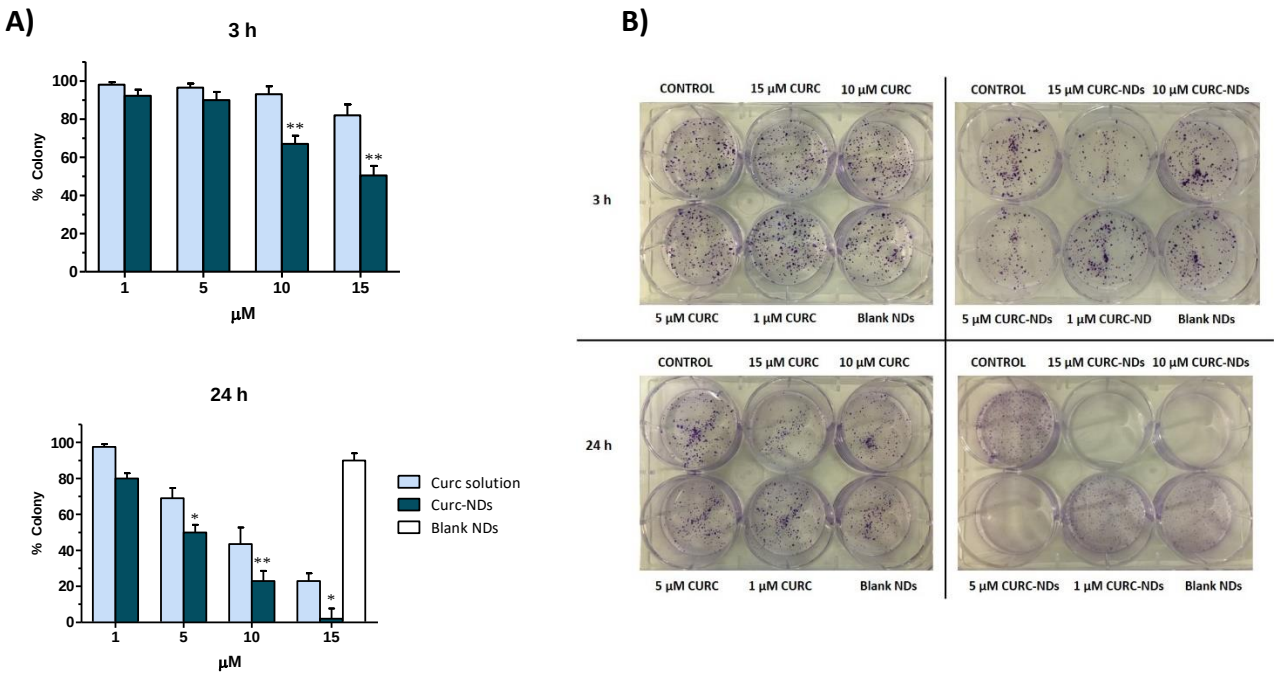

Figure 6. Colony-forming assay by Curc solution and Curc-NDs. PC-3 cells were treated with 1–15 μM of Curc solution and Curc-NDs, or untreated (control) for 3 or 24 hours. Then, the cells were washed and allowed to grow for 7 days. Moreover, the cells were treated with blank NDs, at the dilution corresponding to that of Curc-NDs 15 μM. **A**) Percent colony-formed. The control (untreated cells) was normalized to 100%, and the readouts from treated cells were expressed as % of viability and are the mean ± SD. *p<0.05, **p<0.01 vs Curc solution. **B**) Representative experiments of colony-forming were photographed.

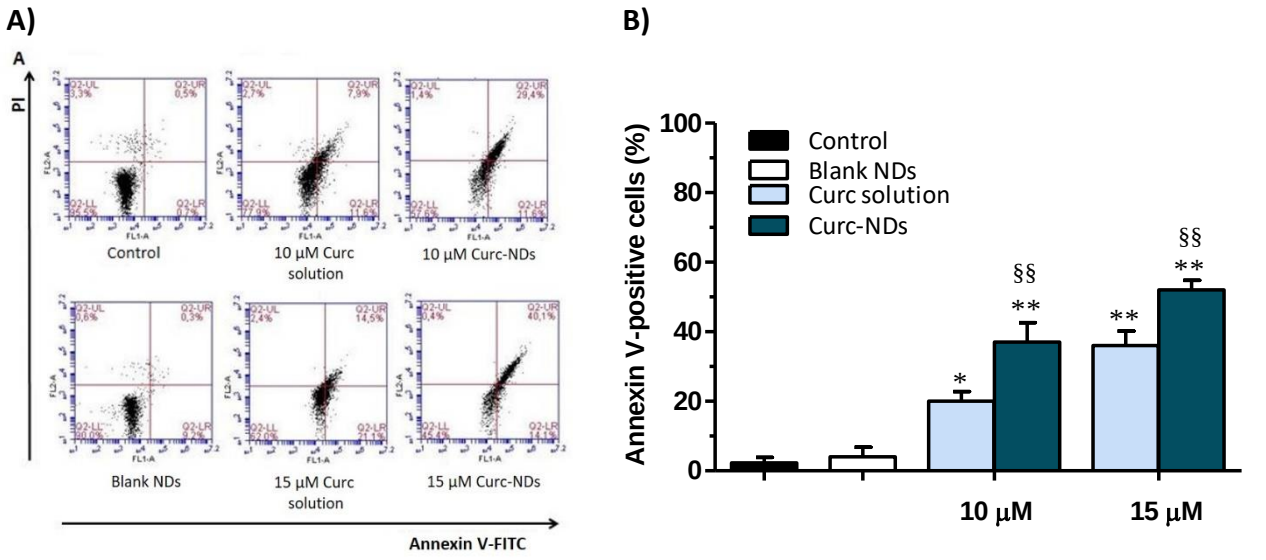

Figure 7. Determination of apoptosis using a flow cytometry-based Annexin V/IP assay. PC-3 cells were treated with 10 and 15 μM of Curc solution and Curc-NDs, or untreated (control) for 24 hours. Moreover, the cells were treated with blank NDs, at the dilution corresponding to that of Curc-NDs 15 μM. **A**) Fow cytometry profiles of a representative experiment. **B**) Summary of the Annexin V-FITC Apoptosis assay results of three independent experiments. Data are expressed as mean ± SD. *p<0.05, **p<0.01 vs control; §§p<0.01 vs Curc solution.

Cell apoptosis

The Annexin V-FITC/IP Apoptosis assay results are presented in Figure 7. The flow cytometry profiles of a representative experiment are shown in panel A of Figure 7. The PC-3 untreated cells and the cells exposed to blank NDs, at the dilution corresponding to that of Curc-NDs 15 µM, showed a cell viability of 95.5% and 90%, respectively. Treatment with 10 and 15 µM Curc solution induced a significant increase of Annexin V-positive cells (19.6% and 35.6%, respectively). The percentage of apoptotic cells was further increased when the cells were treated with Curc-NDs at the same concentrations (41% and 54.2% in Curc-NDs at 10 µM and at 15 µM, respectively). In Figure 7B, the summary of the Annexin V-FITC Apoptosis assay results of three independent experiments is shown.

Adhesion test

Adhesion of tumor cells to vascular endothelium and their migration to the target organs are key steps for metastasis formation. *In vitro* experiments were performed on adhesion to HUVEC and motility of tumor cells to compare the potential of free Curc and Curc-NDs. In the adhesion experiments, HUVEC were pre-treated for 30 minutes with blank NDs, Curc solution, and Curc-NDs and then were stimulated with TNF-α 10 ng/mL. After 18 hours, tumor cells were seeded and left to adhere with HUVEC for 1 hour. The concentration of 5 µM of Curc solution and Curc-NDs was selected in the experiments of adhesion and migration because this concentration resulted to be non-toxic for tumor cells. Figure 8 shows that Curcuminoids at low doses can completely reverse the pro-adhesion effect of TNF-α in DU-145 and PC-3 cells, being Curc-NDs significantly more effective than free Curcuminoids.

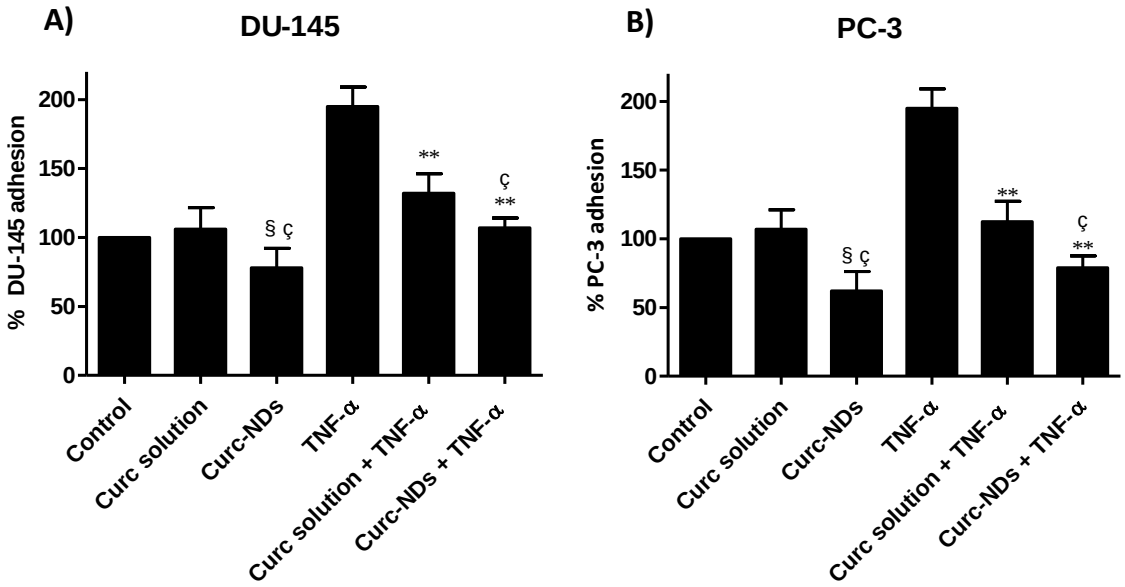

Figure 8. Tumor cell adhesion to HUVEC induced by Curcuminoid solution and Curc-NDs. DU-145 (**A**) and PC-3 cells (**B**) were treated with 5 µM of Curc solution and Curc-NDs, or untreated (control) for 30 minutes and then stimulated with TNF-α 10 ng/mL. After 18 hours, tumor cells were seeded and left to adhere for 1 hour. Data are expressed as the percentage of tumor cell adhesion on HUVEC and are the mean ± SEM. $^{§}p<0.05$ Curc-NDs vs control; $^{**}p<0.01$ vs TNF-α; $^{ç}p<0.05$ vs Curc solution.

Migration test

Cell motility was assessed using a Boyden chamber assay evaluating the directional migration of cells. DU-145 and PC-3 cells were seeded in the upper chamber of a Boyden chamber in a serum-free medium, to avoid cell proliferation, in the presence of blank NDs or 5 µM of Curc solution or Curc-NDs. Then, cells were allowed to migrate for 18 hours to the lower chamber containing PMA, used as chemoattractant. Figure 9 shows that cell migration is dramatically reduced per se and in presence of a pro-migration substance at low Curcuminoid concentrations. Moreover, the effect was higher when Curcuminoids were loaded in nanodroplets, in both DU-145 and PC-3 cell lines.

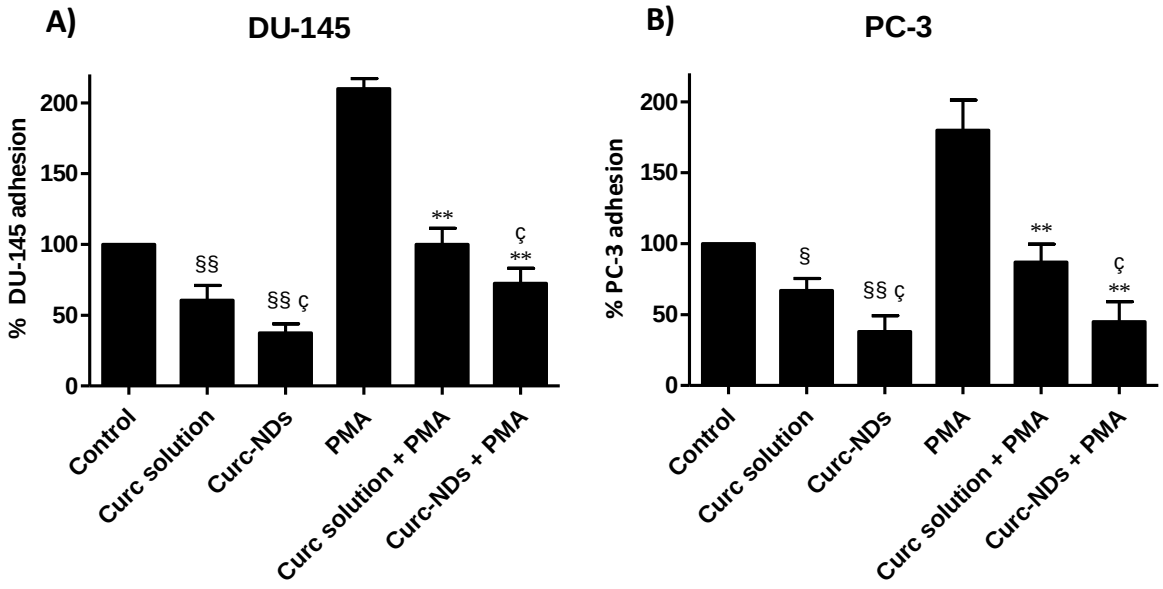

Figure 9. Tumor cell migration induced by Curc and Curc-NDs. DU145 (**A**) and PC-3 cells (**B**) were treated with 5 µM of Curc solution and Curc-NDs, or untreated (control) and seeded in the upper chamber of a Boyden chamber in a serum-free medium. The cells were allowed to migrate for 18 hours to the lower chamber containing PMA 10 ng/mL. Data are expressed as the percentage of tumor cell migration and are the mean ± SD. $^{§}p<0.05$, $^{§§}p<0.05$ vs control; **p<0.01 vs PMA; $^{ç}p<0.05$ vs Curc solution.

Discussion

Curcumin is currently administered orally but its low bioavailability needs high doses. In this work, we would like to overcome these drawbacks with a two-fold approach: the use of a Curcuminoid extract and its incorporation in a nanocarrier. The first problem is a non-trivial one. Indeed, in food and pharmaceutical applications a restricted number of solvents are allowed for the extraction process (FAO/WHO and European Commission sources), comprising ethanol, methanol, acetone, hexane and ethyl acetate [51]. Ethanol is commonly the most preferred solvent in turmeric extraction, ensuring good yields and purity in curcumin [14]. Among the enabling technologies that can ensure a rapid and cost-effective recovery of bioactives from vegetal matrices [52], microwave irradiation represents a promising method to enhance extraction efficiency and selectivity [53] compared to conventional thermal heating, boosting extraction and reducing time and solvents. Fast protocols are critical in handling labile metabolites and avoiding losses or degradations. Here, we tuned a new extraction method to obtain Curc extract with high purity and safety.

The second point was focused on selecting dextran sulfate-based nanodroplets, a versatile nanotool suitable for different administration routes and with echogenic properties. NDs are spherical nanoparticles with a core-shell structure filled up with a gas, which gives them acoustically active properties. With this aim, NDs were largely proposed as theranostic agents, combining the modality of therapy and diagnostic imaging [42, 54, 55]. In particular, polymer-shelled NDs were designed as multifunctional agents to provide tumor cell targeting, Ultrasound imaging and US-triggered cancer therapy [56–58]. The theranostic approach offers the potential to image the pathological tissues and simultaneously to monitor the delivery kinetics and biodistribution of an active compound. The nanodroplet formulations can easily extravasate the bloodstream to reach the tumor site because of their nanosize. Once there, the exposition to US leads to a phase transition from liquid nanodroplets to gas microbubbles, in a process called acoustic droplet vaporization (ADV) [59].

Previously, curcumin was delivered in PEG-PCL nanodroplets showing an enhanced anticancer effect in mice [60]. Once injected, these nanodroplets based on perfluoropentane accumulated in sarcoma tumor tissue and were disrupted by the US, releasing curcumin. Curcumin-loaded nanodroplets significantly reduced the primary tumor volume compared to the control, in a greater extent when activated by US. Nevertheless, no *in vitro* studies were carried out and the possible rule of the nanodroplets on the occurrence of metastasis was not investigated.

More recently, microbubbles loading curcumin were synthesized using bovine serum albumin as shell component and perfluorobutane as gas core [61]. Curcumin uptake by HeLa cells increased when the active compound was carried on the microbubbles. Moreover, the cell viability reduced significantly when the microbubbles were used with US supply. Besides, microbubbles cannot passively extravasate from blood vessels into surrounding tissues due to their size.

In this work, we focused the attention on prostatic cell lines, PC-3 and DU-145, designing nanoscale systems for potentially impairing metastatic spread. It is worth noting that, in order to prevent or delay recurrences, the patients are normally treated with adjuvant therapies (radical surgery or radiotherapy), although frequently they are not conclusive.

In vitro results showed that Curcuminoids alone were effective in inhibiting prostate cancer cell growth, colony-forming ability, endothelial adhesion and migration. The concomitant presence of demethoxycurcumin, bisdemethoxycurcumin and other bioactive lipophilic compounds presented in *Curcuma longa* L. extract can play a role in the enhanced effectiveness of Curcuminoids with respect to curcumin. In particular, the Curcuminoid effect at the highest concentration tested is detectable after 24 hours of incubation, while after 48–72 hours also 10 µM concentration is effective. In addition, Curcuminoids were able to reduce cell colony-forming at all dosages, but only

after 24 hours of incubation. Moreover, Curcuminoid extract prevented adhesion to HUVEC and migration in the presence of promoting agents (TNF-α and PMA respectively) already at low concentration. Interestingly, at low doses Curc-NDs showed a higher effect than Curcuminoid solution on cell motility, showing that Curc-NDs may play a role against a possible metastatic spread. Based on this evidence, ND nanoformulation is able to incorporate and efficiently release Curcuminoids in a prolonged manner. Moreover, the Curc-NDs are fast internalized by the cells.

These results are complementary with those reported by Dorai *et al.* [24], that showed that curcumin was able to interfere with the osteoblastic as well as the osteoclastic component of the highly metastatic C4–2B PCa cell line, by interfering with the growth factor receptor pathways and by inhibiting the NF-kappaB activation process. Such a result was confirmed by further investigations on PC-3 PCa cells, where the chemotactic activity of the CC motif ligand 2 was severely reduced by curcumin, inhibiting their pro-metastatic effectiveness [62].

More recently, it was observed that curcumin abrogated HGF-induced cell scattering and invasion in DU-145 cells by downregulating the expression of phosphorylated c-Met, extracellular signal-regulated kinase and Snail [63].

Conclusions

Based on the results of this study, Curc-NDs might be proposed as a safe and potential effective adjuvant tool for preventing metastatic spread as an alternative to the androgen deprivation therapy. Since it has been reported that Cur-NDs have theranostic properties, their administration can be monitored and properly tailored in order to reach an effective release of Curcuminoids when residual cancer cells are suspected. Moreover, Cur-NDs presented the capability to *in vitro* inhibit prostate cancer cell growth, colony-forming, endothelial adhesion and migration. Future *in vivo* studies are required to assess whether an effective dose can be reached in pancreatic cancer cells following systemic and/or local administration.

References

[1] Stura I, Ditaranto S, Gabriele D, Migliaretti G and Guiot C 2017 A new predictive tool for the post-surgical risk of recurrence of prostate cancer potentially unveiling hidden residual disease J. Pros. Cancer 2 2

[2] Attard G, Parker C, Eeles R A, Schröder F, Tomlins S A, Tannock I, Drake C G and de Bono J S 2016 Prostate cancer Lancet 387 70–82

[3] Kumar S, Shelley M, Harrison C, Coles B, Wilt T J and Mason M D 2006 Neo-adjuvant and adjuvant hormone therapy for localised and locally advanced prostate cancer Cochrane Database Syst. Rev. 4 CD006019

[4] NCCN-Evidence-Based Cancer Guidelines, Oncology Drug Compendium, Oncology Continuing Medical Education www.nccn.org (accessed: 13 February 2019)

[5] Bansal S S, Goel M, Aqil F, Vadhanam M V and Gupta R C 2011 Advanced drug delivery systems of curcumin for cancer chemoprevention Cancer Prevention Res. 4 1158–71

[6] Bachmeier B E, Killian P H and Melchart D 2018 The role of curcumin in prevention and management of metastatic disease Int. J. Mol. Sci. 19 1716–34

[7] Thangapazham R L, Sharma A and Maheshwari R K 2006 Multiple molecular targets in cancer chemoprevention by curcumin AAPS J. 8 E443–9

[8] Anand P et al 2008 Biological activities of curcumin and its analogues (congeners) made by man and mother nature Biochem. Pharmacol. 76 1590–611

[9] Gupta S C, Sung B, Kim J H, Prasad S, Li S and Aggarwal B B 2013 Multitargeting by turmeric, the golden spice: from kitchen to clinic Mol. Nutrition Food Res. 57 1510–28

[10] Aratanechemuge Y, Komiya T, Moteki H, Katsuzaki H, Imai K and Hibasami H 2002 Selective induction of apoptosis by ar-turmerone isolated from turmeric (curcuma longa L) in two human leukemia cell lines, but not in human stomach cancer cell line Int. J. Mol. Med. 9 481–4

[11] Yue G G L, Chan B C L, Hon P-M, Lee M Y H, Fung K-P, Leung P-C and Lau C B S 2010 Evaluation of in vitro anti- proliferative and immunomodulatory activities of compounds isolated from curcuma longa Food Chem. Toxicol. Int. J. Publ. Br. Ind. Biol. Res. Assoc. 48 2011–20

[12] Sandur S K, Pandey M K, Sung B, Ahn K S, Murakami A, Sethi G, Limtrakul P, Badmaev V and Aggarwal B B 2007 Curcumin, demethoxycurcumin, bisdemethoxycurcumin, tetrahydrocurcumin and turmerones differentially regulate anti-inflammatory and anti-proliferative responses through a ROS-independent mechanism Carcinogenesis 28 1765–73

[13] Aggarwal B B, Yuan W, Li S and Gupta S C 2013 Curcumin- free turmeric exhibits anti-inflammatory and anticancer activities: identification of novel components of turmeric Mol. Nutrition Food Res. 57 1529–42

[14] Esatbeyoglu T, Huebbe P, Ernst I M A, Chin D, Wagner A E and Rimbach G 2012 Curcumin–from molecule to biological function Angew. Chem., Int. Ed. Engl. 51 5308–32

[15] Priyadarsini K I 2014 The chemistry of curcumin: from extraction to therapeutic agent Molecules 19 20091–112

[16] Peram M R, Jalalpure S S, Palkar M B and Diwan P V 2017 Stability studies of pure and mixture form of curcuminoids by reverse phase-HPLC method under various experimental stress conditions Food Sci. Biotechnol. 26 591–602

[17] Ganzler K, Salgó A and Valkó K 1986 Microwave extraction. A novel sample preparation method for chromatography. J. Chromatogr. 371 299–306

[18] Chemat F and Cravotto G 2013 Microwave-assisted Extraction for Bioactive Compounds: Theory and Practice (New York, Heidelberg, Dordrecht, London: Springer)

[19] Akhtar I, Javad S, Yousaf Z, Iqbal S and Jabeen K 2019 Microwave assisted extraction of phytochemicals an efficient and modern approach for botanicals and pharmaceuticals Pak. J. Pharm. Sci., 32 223-230

[20] Mondal S 2016 Stability of curcumin in different solvent and solution media: UV-visible and steady-state fluorescence spectral study J. Photochem. Photobiol. B 158 212–8

[21] Pan M H, Huang T M and Lin J K 1999 Biotransformation of curcumin through reduction and glucuronidation in mice Drug Metab. Dispos. Biol. Fate Chem. 27 486–94

[22] Dorai T, Dutcher J P, Dempster D W and Wiernik P H 2004 Therapeutic potential of curcumin in prostate cancer: IV. Interference with the osteomimetic properties of hormone refractory C4-2B prostate cancer cells Prostate 60 1–17

[23] Hong J H, Ahn K S, Bae E, Jeon S S and Choi H Y 2006 The effects of curcumin on the invasiveness of prostate cancer in vitro and in vivo Prostate Cancer Prostatic Dis. 9 147–52

[24] Mukerjee A and Vishwanatha J K 2009 Formulation, characterization and evaluation of curcumin-loaded PLGA nanospheres for cancer therapy Anticancer Res. 29 3867–75

[25] Adahoun M A, Al-Akhras M-A H, Jaafar M S and Bououdina M 2017 Enhanced anti-cancer and antimicrobial activities of curcumin nanoparticles Artif. Cells Nanomed. Biotechnol. 45 98–107

[26] Barick K C, Ekta, Gawali S L, Sarkar A, Kunwar A, Priyadarsini K I and Hassan P A 2016 Pluronic stabilized Fe3O4 magnetic nanoparticles for intracellular delivery of curcumin RSC Adv. 6 98674–81

[27] Salehi P, Makhoul G, Roy R, Malhotra M, Mood Z A and Daniel S J 2013 Curcumin loaded NIPAAM/VP/PEG-A nanoparticles: physicochemical and chemopreventive properties J. Biomater. Sci. Polym. Ed. 24 574–88

[28] Serri C et al 2017 Nano-precipitated curcumin loaded particles: effect of carrier size and drug complexation with (2-hydroxypropyl)-β-cyclodextrin on their biological performances Int. J. Pharm. 520 21–8

[29] Rao W et al 2014 Thermally responsive nanoparticle- encapsulated curcumin and its combination with mild hyperthermia for enhanced cancer cell destruction Acta Biomater. 10 831–42

[30] Thangavel S, Yoshitomi T, Sakharkar M K and Nagasaki Y 2015 Redox nanoparticles inhibit curcumin oxidative degradation and enhance its therapeutic effect on prostate cancer J. Control. Release Off. J. Control. Release Soc. 209 110–9

[31] Yallapu M M, Dobberpuhl M R, Maher D M, Jaggi M and Chauhan S C 2012 Design of curcumin loaded cellulose nanoparticles for prostate cancer Curr. Drug Metab. 13 120–8

[32] Sivakumar B, Aswathy R G, Romero-Aburto R, Mitcham T, Mitchel K A, Nagaoka Y, Bouchard R R, Ajayan P M, Maekawa T and Sakthikumar D N 2017 Highly versatile SPION encapsulated PLGA nanoparticles as photothermal ablators of cancer cells and as multimodal imaging agents Biomater. Sci. 5 432–43

[33] Khalkhali M, Sadighian S, Rostamizadeh K, Khoeini F, Naghibi M, Bayat N, Habibizadeh M and Hamidi M 2015 Synthesis and characterization of dextran coated magnetite nanoparticles for diagnostics and therapy BioImpacts 5 141–50

[34] Yallapu M M, Othman S F, Curtis E T, Bauer N A, Chauhan N, Kumar D, Jaggi M and Chauhan S C 2012 Curcumin-loaded magnetic nanoparticles for breast cancer therapeutics and imaging applications Int. J. Nanomed. 7 1761–79

[35] Yallapu M M, Othman S F, Curtis E T, Gupta B K, Jaggi M and Chauhan S C 2011 Multi-functional magnetic nanoparticles for magnetic resonance imaging and cancer therapy Biomaterials 32 1890–905

[36] Mukerjee A, Ranjan A P and Vishwanatha J K 2016 Targeted nanocurcumin therapy using annexin A2 anitbody improves tumor accumulation and therapeutic efficacy against highly metastatic breast cancer J. Biomed. Nanotechnol. 12 1374–92

[37] Xue P, Liu D, Wang J, Zhang N, Zhou J, Li L, Guo W, Sun M, Han X and Wang Y 2016 Redox-sensitive citronellol- cabazitaxel conjugate: maintained in vitro cytotoxicity and self-assembled as multifunctional nanomedicine Bioconjug. Chem. 27 1360–72

[38] Gong G, Pan Q, Wang K, Wu R, Sun Y and Lu Y 2015 Curcumin-incorporated albumin nanoparticles and its tumor image Nanotechnology 26 045603

[39] Verderio P, Pandolfi L, Mazzucchelli S, Marinozzi M R, Vanna R, Gramatica F, Corsi F, Colombo M, Morasso C and Prosperi D 2014 Antiproliferative effect of ASC-J9 delivered by PLGA nanoparticles against estrogen- dependent breast cancer cells Mol. Pharm. 11 2864–75

[40] Cavalli R, Bisazza A, Trotta M, Argenziano M, Civra A, Donalisio M and Lembo D 2012 New chitosan nanobubbles for ultrasound-mediated gene delivery: preparation and in vitro characterization Int. J. Nanomed. 7 3309–18

[41] Cavalli R, Bisazza A, Giustetto P, Civra A, Lembo D, Trotta G, Guiot C and Trotta M 2009 Preparation and characterization of dextran nanobubbles for oxygen delivery Int. J. Pharm. 381 160–5

[42] Cavalli R, Argenziano M, Vigna E, Giustetto P, Torres E, Aime S and Terreno E 2015 Preparation and in vitro characterization of chitosan nanobubbles as theranostic agents Colloids Surf. B 129 39–46

[43] Kharat M, Du Z, Zhang G and McClements D J 2017 Physical and chemical stability of curcumin in aqueous solutions and emulsions: impact of pH, temperature, and molecular environment J. Agric. Food Chem. 65 1525–32

[44] Capece S, Chiessi E, Cavalli R, Giustetto P, Grishenkov D and Paradossi G 2013 A general strategy for obtaining biodegradable polymer shelled microbubbles as theranostic devices Chem. Commun. 49 5763–5

[45] Marano F, Argenziano M, Frairia R, Adamini A, Bosco O, Rinella L, Fortunati N, Cavalli R and Catalano M G 2016 Doxorubicin-loaded nanobubbles combined with extracorporeal shock waves: basis for a new drug delivery tool in anaplastic thyroid cancer Thyroid Off. J. Am. Thyroid Assoc. 26 705–16

[46] Argenziano M et al 2017 Vancomycin-loaded nanobubbles: a new platform for controlled antibiotic delivery against methicillin-resistant staphylococcus aureus infections Int. J. Pharm. 523 176–88

[47] Gigliotti C L et al 2016 In vitro and in vivo therapeutic evaluation of camptothecin-encapsulated β-cyclodextrin nanosponges in prostate cancer J. Biomed. Nanotechnol. 12 114–27

[48] Gigliotti C L et al 2017 Enhanced cytotoxic effect of camptothecin nanosponges in anaplastic thyroid cancer cells in vitro and in vivo on orthotopic xenograft tumors Drug Deliv. 24 670–80

[49] Dianzani C et al 2014 B7h triggering inhibits the migration of tumor cell lines J. Immunol. 192 4921–31

[50] Prabu S et al 2020 Curcumin/beta-cyclodextrin inclusion complex as a new “turn-off” fluorescent sensor system for sensitive recognition of mercury ion J. Mol. Struct 1204 127528

[51] Anon 2010 Scientific Opinion on the re-evaluation of curcumin (E 100) as a food additive EFSA J. 8 1679

[52] Chemat F, Vian M A and Cravotto G 2012 Green extraction of natural products: concept and principles Int. J. Mol. Sci. 13 8615–27

[53] Cravotto G, Boffa L, Mantegna S, Perego P, Avogadro M and Cintas P 2008 Improved extraction of vegetable oils under high-intensity ultrasound and/or microwaves Ultrason. Sonochem. 15 898–902

[54] Zullino S, Argenziano M, Stura I, Guiot C and Cavalli R 2018 From micro- to nano-multifunctional theranostic platform: effective ultrasound imaging is not just a matter of scale Mol. Imaging 17 1–16

[55] Ayodele A T, Valizadeh A, Adabi M, Esnaashari S S, Madani F, Khosravani M and Adabi M 2017 Ultrasound nanobubbles and their applications as theranostic agents in cancer therapy: a review Biointerface Res. Appl. Chem. 7 2253–62

[56] Li Y, Wan J, Zhang Z, Guo J and Wang C 2017 Targeted soft biodegradable glycine/PEG/RGD-modified poly (methacrylic acid) nanobubbles as intelligent theranostic vehicles for drug delivery ACS Appl. Mater. Interfaces 9 35604–12

[57] Shen X, Li T, Chen Z, Geng Y, Xie X, Li S, Yang H, Wu C and Liu Y 2017 Luminescent/magnetic PLGA-based hybrid nanocomposites: a smart nanocarrier system for targeted codelivery and dual-modality imaging in cancer theranostics Int. J. Nanomed. 12 4299–322

[58] Bosca F, Bielecki P A, Exner A A and Barge A 2018 Porphyrin-loaded pluronic nanobubbles: a new US-activated agent for future theranostic applications Bioconjug. Chem. 29 234–40

[59] Hu H-J, Lin X-L, Liu M-H, Fan X-J and Zou W-W 2016 Curcumin mediates reversion of HGF-induced epithelial- mesenchymal transition via inhibition of c-Met expression in DU145 cells Oncol. Lett. 11 1499–505

[60] Ji G, Yang J and Chen J 2014 Preparation of novel curcumin- loaded multifunctional nanodroplets for combining ultrasonic development and targeted chemotherapy Int. J. Pharm. 466 314–20

[61] Upadhyay A, Yagnik B, Desai P and Dalvi S V 2018 Microbubble-mediated enhanced delivery of curcumin to cervical cancer cells ACS Omega 3 12824–31

[62] Herman J G, Stadelman H L and Roselli C E 2009 Curcumin blocks CCL2-induced adhesion, motility and invasion, in part, through down-regulation of CCL2 expression and proteolytic activity Int. J. Oncol. 34 1319–27

[63] Kee A L Y, Teo B M 2019 Biomedical applications of acoustically responsive phase shift nanodroplets: Current status and future directions Ultrason. Sonochem. 56 37–45

CHAPTER 3

HYPOXIA-SENSITIVE LIPOSOMES FOR CO-DELIVERY OF siRNA AND PACLITAXEL

Introduction

The co-delivery of chemotherapeutic drugs and small interfering RNA (siRNA) for improving the outcomes of cancer therapy has been identified as a promising therapeutic modality [1–6]. Chemotherapy alone, indeed, presents many advantages in the fight of cancers but can also provoke several problems. As a matter of fact, anticancer drugs can cause severe side effects to normal cells or contribute to develop multidrug resistance (MDR) in cancer cells. Paclitaxel is a chemotherapeutic drug commonly used in the management of breast, ovarian and non-small cell lung cancers. Besides the effective cytotoxic proprieties on cancer cells, Paclitaxel presents some drawbacks in the use in the clinic. Indeed, it has very poor solubility in water, thus reducing the therapeutically efficiency. In the last years, researchers have been employed many energies to overcome these limitations and several nanodelivery systems to encapsulate and safely deliver the drug have been designed and developed [7]. These efforts have resulted in the entry on the market of Abraxane®. Notably, these Paclitaxel albumin-bound nanoparticles have been approved by the FDA for the first time in 2005 for the treatment of metastatic breast cancer and in 2012 for non-small cell lung cancer. Besides albumin-based nanoparticles, another important platform for the delivery of anticancer drugs is represented by liposomes. In nanomedicine, indeed, phospholipid-based liposomes represent a versatile tool [8] and they have been largely studied also for the delivery of Paclitaxel [9]. One of the main drawbacks of the use of Paclitaxel is that it is a substrate of the permeability-glycoproteins (P-gp). This ABC transporter is typically overexpressed in breast and ovarian cancer cells [10], and it is responsible for the expulsion of the anticancer drugs, thus limiting its accumulation at the tumor site, leading to MDR. For this reason, there is a need for the development of nanodelivery systems able to co-carry the chemotherapeutic drug and an inhibitor [11,12] or a silencing agent [13,14] for the P-gp.

RNA-based technology has been demonstrated to have a promising application in the treatment of several diseases, and among them, cancer is one of the most challenging [15]. RNA interference (RNAi) approach is based on the gene regulatory process. In particular, siRNAs are double-stranded RNA, composed of 21–23 nucleotides, which act as inhibitors of target protein expression. Indeed, siRNAs can be exploited to knockdown pathologically overexpressed or mutated target genes, thus silencing specific sequences [16]. Despite the potential application of RNAi in cancer management, numerous obstacles and barriers limit the *in vivo* delivery of siRNAs. Notably, naked siRNAs present short half-lives, rapid enzymatic degradation by nucleases, poor chemical stability and weak permeability to cell membranes due to their negative charge and hydrophilicity [17].

Based on these considerations, it is necessary to find an appropriate delivery route and carriers for the successful use of RNA-based therapies in the clinic. In order to achieve an efficient delivery, the criteria to follow for an ideal carrier should be: (i) biocompatibility, biodegradability, non-immunogenicity; (ii) increased circulation time, avoiding early clearance; (iii) increased cell uptake; (iv) reduced “off-target” and side effects [18]. Currently, the non-viral delivery systems of siRNA for cancer therapy include i) chemical conjugation; ii) lipid-based systems; iii) polymer-based systems; iv) inorganic nanoparticles; v) co-delivery of siRNA and anticancer drugs [19–21].

Among the polymers, polyethyleneimine (PEI) is commonly used and it is considered the gold-standard as transfection agent in cells [22]. PEI presents positively charged amino groups that can electrostatically interact with negatively charged siRNA, enabling an efficient condensation and the formation of the so-called “polyplex”. The high transfection efficiency of PEI is partially based on its high buffering ability for endosomal escape, thus allowing an accumulation of polyplexes in the cytosol of the cells [23]. However, there are several limitations to the use of PEI in the clinic, including high cellular toxicity, non-degradability, and clearance of the polyplexes after systemic

administration. These drawbacks derive mainly from the molecular weight (MW) of the polymer. Indeed, the higher is the MW, the higher is the transfection efficiency, but also higher the cytotoxicity caused by the excessive positive charges and the nonspecific targets. Conversely, branched PEI (bPEI) of low molecular weight (LMW) preserves moderate transfection efficacy with lower cytotoxicity [24].

To circumvent these problems, many strategies have been suggested, such as the combination of linear or branched LMW PEIs with degradable linkages (i.e. disulfide bridges) [25,26], the lipidation of LMW PEI to increase the uptake by lipophilic cell membranes [27,28], or the modification of the PEI surface with nonionic and hydrophilic polymers like polyethyleneglycol (PEG) [29]. The PEGylation of these PEI-based systems can have several advantages for the final siRNA delivery. Indeed, the PEG grafting improves the circulation time in the bloodstream of the polyplexes, decreasing the interaction with plasma proteins and increasing the possibility for the nanocarriers to reach the tumor site through the enhanced permeability and retention (EPR) effect [30]. PEG also reduces the possible aggregations and decreases the extremely high positive charge density of PEI-based polyplexes, thus lowering the cytotoxicity [31]. Besides these favorable features of PEGylation, this component may also hamper the cell uptake and the endosomal escape, resulting in a loss of gene transfection activity. Indeed, the aqueous phase on the surface of the nanodelivery systems due to PEG moiety reduces the interaction with the cancer cells. However, in gene delivery, the nanocarriers need to accumulate in the target intracellular compartment to be therapeutically efficient. For this reason, appropriate strategies to overcome the so-called “PEG dilemma” have to be considered for the development of efficient siRNA carriers [32–34]. One possibility is the cleavage of PEG from the carrier systems once delivered to the target site [35,36]. Notably, the tumor microenvironment presents peculiar characteristics that differentiate it from a healthy one, such as the severely low oxygen levels. Hypoxia is largely exploited as a tumor target [37,38], and can also play a role in PEG detachment. Perche *et al.* designed a hypoxia-sensitive conjugate for the efficient delivery of siRNA [39]. They studied a system able to be activated in oxygen-deficient conditions, developing a nanocarrier containing PEG, an azobenzene group (Azo), PEI, and 1,2-dioleoyl-sn-glycero-3-phosphoethanolamine (DOPE) units (in short PAPD). In a tumor hypoxic microenvironment, reductive enzymes reduce the azobenzene, thus provoking the cleavage of the nanoparticle in two parts. The siRNA is complexed to PEI and protected from early degradation with a PEG layer. At the tumor target site, the PEG portion is cleaved and the positive charges of PEI, now exposed to the nanocarrier surface, promote the internalization in cancer cells and the endosomal escape.

Aim of the project

During my PhD, I spent six months in the laboratory of Professor Vladimir Torchilin at the Center for Pharmaceutical Biotechnology and Nanomedicine at Northeastern University (Boston, MA, US). There, I had the pleasure to join an international and hard-worker group, whit whom members I developed and designed hypoxia-sensitive liposomes for the co-delivery of siRNA and Paclitaxel.
The aim of the project was to design a liposomal formulation able to reach the tumor site without early clearance and to efficiently deliver a chemotherapeutic and a siRNA-mediated knockdown of P-glycoprotein (siMDR1). Paclitaxel-loaded liposomes were coated with a hypoxia-sensitive PEG-azobenzene-PEI-DOPE conjugate. The PEG shield contributes to give long-circulating time to the formulation, but at the hypoxic tumor environment, the azobenzene group would cleave. In this way, the positive charges of PEI, that complexes the siMDR1, are exposed, thus facilitating the entrance of the liposomes inside the cells. Once there, the surface charge of PEI also contributes to the endosomal escape of the liposomes, allowing the release of the siMDR1 and paclitaxel in the cytoplasm. The downregulation of the overexpressed efflux pumps and the simultaneous co-administration of Paclitaxel should maximize the efficiency of chemotherapy. Indeed, hampering the resistance of cancer cells, the anticancer drug can accumulate inside the cells and be more effective. Moreover, the use of a conjugate that is activated just in response to tumor milieu can represent a promising approach to reduce the non-specific toxicity and lead to better outcomes of the treatment.

Material and Methods

Material

Egg phosphatidylcholine (ePC), cholesterol (Chol) and N-(glutaryl)-1,2-dioleoyl-sn-glycero-3-phosphoethanolamine (NGPE) were purchased from Avanti Polar Lipids (Alabaster, AL, US). Methoxy-poly-(ethyleneglycol) (mPEG-NH_2) was acquired from Corden Pharma International (Plankstadt, Germany). Branched polyethyleneimine (bPEI) with a molecular weight of 1800 Da was purchased from Polysciences, Inc. (PA, US) and Paclitaxel (PTX) was from LC Laboratories (Woburn, MA, US). MCF7 sensitive, MCF7 ADR (Adriamycin-resistant), and A2780 ADR cell lines were from Sigma (ECACC, UK). Dulbecco's Modified Eagle Medium (DMEM) with 1 and 4.5 g/L of glucose and RPMI media were purchased from Cellgro (VA, US). Bovine serum albumin (BSA), Lipofectamine RNAiMAX, non-targeting control siRNA (siSCR), Ambion™ siRNA targeting MDR-1 (siMDR-1): 5'-GGAAAAGAAACCAACUGUCdTdT-3' (sense) [14], E-Gel™ General Purpose Agarose Gel (2%) were purchased from Thermo-Fisher Scientific (Cambridge, MA, US). Nuclease-free water was from Qiagen (MD, US). CellTiter-Blue® cell viability assay was obtained from Promega Corp. (Madison, WI, US). The antibodies were acquired from Abcam (Cambridge, MA, US).

Methods

Synthesis of the polyethyleneimine–phospholipid conjugate (bPEI-PE)

For the coating of the liposomes, the bPEI-PE conjugate was synthesized starting from the components reported in Table 1. N-(3-dimethylaminopropyl)-N'-ethylcarbodiimide HCl (EDCI) (92.60 mg) and N-hydroxysuccinimide (NHS) (55.60 mg), previously dissolved in methanol, were used to activate a chloroform solution containing N-(glutaryl)-1,2-dioleoyl-sn-glycero-3-phosphoethanolamine (NGPE, 20 mg). The NHS/EDCI solution was added drowise to NGPE and let on stirring for 1 hour at room temperature. Branched polyethyleneimine (bPEI) was solubilized in triethanolamine and chloroform (ratio 1:80) and added dropwise to the activated solution of NGPE under magnetic stirring. The agitation was continued overnight at room temperature. The day after, the organic solvent was removed by rotary evaporation and the conjugate was placed under lyophilization for 3 hours. Then, the conjugate was suspended in RNAse free water with gentle vortex and purified from free bPEI with dialysis (membrane MWCO 2000 Da) against excess deionized water for 24 hours. After that, the conjugate was freeze-dried again, resuspended in chloroform and stored at -80 °C. The synthesized bPEI-PE conjugate was characterized by thin-layer chromatography.

Table 1. List of components for the synthesis of the bPEI-PE conjugate.

Components	MW	Ratio
NGPE	828.04	1
EDCI	191.70	20
NHS	115.09	20
bPEI	600	2

2,4,6-Trinitrobenzene Sulfonic Acid assay

2,4,6-Trinitrobenzene Sulfonic Acid (TNBS) assay was performed to determine the amount of free amine groups present in the bPEI-PE conjugate. The sample was diluted with 0.1 M sodium bicarbonate at pH 8.5 (1:100). Then, 2.5% (v/v) TNBS reagent (30 mM), previously diluted in water, was added and the reaction was incubated for 30 minutes. After that, the absorbance of the reaction product was recorded at 420 nm using a microplate reader (BioTek, Model EL800, Winooski, VT). The quantification of amine groups was determined by using a standard curve (R^2=0.9954) using 0.39-50 µg/mL concentration of bPEI.

PEG-Azo-PEI-DOPE Synthesis

PEG-Azo-PEI-DOPE (PAPD) conjugate was synthesized as described in Perche *et al.* [40]. The list of the components is reported in Table 2.

1) Azobenzene-4,4'-dicarboxylic acid (Azo, 5.4 mg) was dissolved in 1 mL of pyridine, and EDCl (5.4 mg), NHS (2.3 mg) and a catalytic amount of dimethylaminopyridine (DMAP) were added under stirring. The agitation was maintained for 1 hour under nitrogen atmosphere. Then, in this reagent mixture, methoxy-poly-(ethyleneglycol) (mPEG-NH_2, 20 mg) dissolved in chloroform ($CHCl_3$) was added dropwise and the reaction was stirred overnight. The day after, the organic solvent was removed through rotary evaporation and the sample was lyophilized. After, the sample was suspended in 10 mL of water, vortexed and centrifuged for 10 minutes at 2000x g. The supernatant was collected, filtered (0.2 µM filter), and dialyzed against water (MWCO 1 K) for 2 days. The dialysate was lyophilized and a PEG-Azo-Acid in the form of fluffy yellow solid was obtained.
2) PEG-Azo-Acid (12 mg) was dissolved in 1 mL of deuterated chloroform ($CDCl_3$) and pyridine (1:1 ratio). To this mixture, EDCl (2.0 mg), NHS (1.2 mg) and a catalytic amount of dimethylaminopyridine (DMAP) were added under stirring. The agitation was maintained for 1 hour under nitrogen atmosphere. Then, bPEI (11.5 mg) in $CHCl_3$ was added dropwise and stirred overnight under nitrogen. The day after, the organic solvent was evaporated by rotary evaporation and the sample was dissolved in water, dialyzed against water (cellulose ester membrane, MWCO 3.5 K), and freeze-dried. PEG-Azo-PEI conjugate was obtained.
3) Triethylamine (30 µL) was added to a solution of NGPE (6.6 mg), EDCl (4.3 mg) and NHS (2.6 mg) in $CDCl_3$ and the mixture was stirred for 1 hour. Then, PEG-Azo-PEI (30 mg) in chloroform was added dropwise and stirred overnight. The day after, the organic solvent was removed, the sample was suspended in water and dialyzed against water (cellulose ester membrane, MWCO 3.5 K) overnight. The sample was finally lyophilized and PEG-Azo-PEI-DOPE was obtained and stored at -80 °C. Before the use, it was suspended in chloroform.

Table 2. List of components for the synthesis of PEG-Azo-PEI-DOPE conjugate.

PEG-Azo-Acid			**PEG-Azo-PEI**			**PEG-Azo-PEI-DOPE**		
Components	**MW**	**Ratio**	**Components**	**MW**	**Ratio**	**Components**	**MW**	**Ratio**
Azo	182.23	1	**PEG-Azo-Acid**		1	**PEG-Azo-PEI**		1
EDCl	191.70	1	**EDCl**	191.70	2	**NGPE**	828.04	1
NHS	115.09	1	**NHS**	115.09	2	**EDCl**	191.70	3
DMAP	122.17	---	**DMAP**	122.17	---	**NHS**	115.09	3
mPEG-NH_2	2000	---	**bPEI**	1800	---			

Preparation and characterization of liposome formulations

Different liposome formulations were designed as described below. Once prepared, all the formulations were filtered through 0.22 mm PES membranes for their sterilization. Then, the liposome and micelle formulations were characterized by measuring size, dispersity and zeta potential by dynamic light scattering (DLS) in a Zetasizer Nano ZS 90 (Malvern Instruments, UK). The samples were previously diluted with ultrapure water.

Plain liposomes

Liposomes were prepared using the thin-film formation method followed by extrusion. Plain liposomes were prepared to start from egg phosphatidylcholine (ePC) and cholesterol (Chol). ePC and Chol (90:10 mol%) were mixed, and chloroform was removed to form a thin film of lipids. The film was lyophilized for 1 hour and then rehydrated with phosphate buffer saline (PBS) at pH 7.4, in order to obtain a concentration of lipids of 15 mg/mL. After that, the suspension was extruded 15 times through 200 nm and subsequently 100 nm pore-sized polycarbonate membrane filter (Avanti Polar Lipids) using a Mini-Extruder (Avanti Polar Lipids). The plain liposomes were stored at 4 °C.

Paclitaxel-loaded liposomes

Paclitaxel-loaded liposomes (PTX-liposomes) were prepared adding Paclitaxel (4% w/w) to a solution of ePC and Chol (90:10 mol%). The organic mixture was then evaporated to have a thin film. After that, the preparation followed as previously described.

Rhodamine b-loaded liposomes

Rhodamine b-liposomes were prepared to exploit Rhodamine b fluorescence in the following experiments. Rhodamine b (0.1 mol%) was added to a chloroform solution of ePC and Chol (90:10 mol%). Then, the organic mixture was evaporated to obtain a thin film. Subsequently, the preparation followed as previously described.

bPEI-PE and PAPD conjugate-coated liposomes

Liposomes were coated with bPEI-PE and PAPD conjugates. Respectively, bPEI-PE and PAPD films (1mol% ratio of bPEI-PE : liposomal lipids) were formed by chloroform evaporation under nitrogen flux. Then, HEPES-buffered Glucose (HBG) (10 mM HEPES, 5% D-glucose) was added to rehydrated the films, forming micelles. After 1 hour of incubation at 37 °C under mild agitation, plain liposomes, PTX-liposomes, and Rhodamine b-liposomes were added to bPEI-PE and PAPD micelle nanosuspensions. For a stable post-insertion of bPEI-PE and PAPD micelles into the lipid bilayer, the formulations remained in incubation at 37 °C under mild agitation for 4 hours.

siRNA-loaded liposomes

Firstly, chloroform was evaporated from bPEI-PE and PAPD conjugate solutions, forming a film. After that, siRNA targeting MDR1 (siMDR1) or scrambled siRNA for negative control (siSCR) were incubated separately with bPEI-PE and PAPD films in equal volumes of HBG at 37 °C for 1 hour. The final concentration of siRNA in the formulations was 2000 nM. In this way, siRNA/bPEI-PE and siRNA/PAPD polyplexes were prepared. Then, plain liposomes and PTX-liposomes were added to the micelles (1 mol% ratio of bPEI-PE: liposomal lipids) and incubated for 4 hours at 37 °C under mild agitation for a stable post-insertion. siRNA/bPEI-PE-liposomes and siRNA/PAPD-liposomes were obtained.

Encapsulation efficiency and loading capacity of PTX-liposomes

The encapsulation efficiency of PTX-liposomes was determined by a validated reversed-phase HPLC method using a Hitachi Elite LaChrome HPLC system equipped with an auto-sampler (Pleasanton, CA) and diode array detector. The analysis was conducted with an Xbridge C18 (4.6 mm x 250 mm) reverse phase column (Waters Corporation, Milford, MA) at a flow rate of 1 mL/min. The Paclitaxel was detected at a wavelength of 227 nm. To determine the drug concentration, a calibration curve was obtained with a concentration range of 3.13–50 µg/mL (R^2 = 0.999).
A part of drug-loaded liposomes before (total PTX) and after (loaded PTX) extrusion was analyzed. The samples were diluted in the mobile phase (60% v/v acetonitrile, 40% v/v water) to disrupt the liposome structure. Before the injection in the HPLC, the samples were filtered. All the samples were analyzed in triplicate. The encapsulation efficiency was calculated as follows (Equation 1).

Encapsulation Efficiency (EE):

$$EE = \frac{Loaded_{PTX}}{Total_{PTX}} \times 100$$

(Equation 1)

The loading capacity of PTX-liposomes was determined by the amount of PTX loaded in liposomes and the total amount of lipid, as reported in Equation 2.

Loading capacity (LC):

$$LC = \frac{Loaded_{PTX}}{Total_{LIPIDS}} \times 100$$

(Equation 2)

Hypoxic conditions

Hypoxia was produced by bubbling 100% nitrogen gas in line.

Gel retardation analysis

To evaluate the complexation efficiency of siRNA with bPEI-PE-liposomes, PAPD-liposomes and PAPD-micelles, a gel retardation study was performed. For this experiment, a fixed amount of siRNA was incubated separately with variable amounts of bPEI-PE and PAPD. To find the optimum ratio of complexation, different amine/phosphate (N/P) ratios were tested. The N/P ratio was calculated assuming that 43.1 g/mol corresponds to each repeating unit of PEI containing one amine, and 316 g/mol corresponds to each repeating unit of siRNA containing one phosphate. The samples were prepared as previously described and a gel electrophoresis analysis using an E-Gel™ General Purpose Agarose Gel (2%) containing Ethidium Bromide (Invitrogen, MA, US) was carried out. Free siRNA (900 ng) was used as control. After the run (60 mV for 30 minutes), siRNA bands were visualized under UV light.

Cell cultures

The Adriamycin-resistant human ovarian carcinoma A2780 ADR cells were cultured in RPMI. The multidrug-resistant breast cancer MCF7 ADR cells were cultured in low glucose (1 g/L) DMEM, while MCF7 sensitive cells in high glucose (4.5 g/L) DMEM. All the cell media were supplemented with 10% v/v FBS and antibiotics (100 IU/mL streptomycin). The cells were incubated at 37 °C, in a 5% CO_2 atmosphere. To maintain the resistance, A2780 ADR and MCF7 ADR were cultured in media containing 100 nM doxorubicin hydrochloride twice a week.

Cytotoxicity assay

In order to evaluate the *in vitro* cytotoxicity of the formulations, A2780 ADR, MCF7 ADR and MCF7 sensitive cell lines were seeded in 96-well plates ($3x10^3$ cells/well). The day after, the cells were treated with Paclitaxel solution, bPEI-PE-liposomes and bPEI-PE/PTX-liposomes in serum complete media at a range concentration of Paclitaxel from 0.2 to 50 μg/mL. After 48 hours of incubation, CellTiter-Blue® (Promega, WI, US) was added. After 1 hour of incubation, the cytotoxicity profiles were measured by recording the fluorescence intensity (λ_{ex}=560 nm, λ_{em}=590 nm) in a microplate reader (BioTek, Model EL800, Winooski, VT).

Cytotoxicity assay for the combinational effect of siMDR1/PAPD-liposomes and PTX solution

The cells were treated with free Paclitaxel solution and siMDR1/PAPD-liposomes, both in normoxic and hypoxic conditions, to evaluate the *in vitro* cytotoxicity due to the downregulation of MDR1. A2780 ADR cells were previously seeded ($3x10^3$ cells/well) in 96-well plates. The day after, the cells were treated with siMDR1/PAPD-liposomes (N/P = 40; siMDR1/well = 100 nM) for 4 hours and then the media was replaced with fresh one. After 20 hours, the cells were treated for additional 48 hours with different concentrations of Paclitaxel solution. Then, the cell viability was evaluated with CellTiter-Blue® assay, as previously described.

Transfection efficiency

To evaluate the transfection efficiency of siMDR1/PAPD-liposomes for the downregulation of MDR1 in resistant cancer cell lines, two different techniques were exploited: western blot and flow cytometry analysis.

Western blot

The transfection efficiency of siMDR1/PAPD-liposomes was evaluated in MCF7 ADR cells, both in hypoxic and normoxic conditions. The cells were seeded into 6-well plates at $2x10^5$ cells/well. siMDR1/PAPD complexes were prepared at N/P=40. Free siMDR1, as positive control, and siSCR, as negative control, were incubated with Lipofectamine RNAiMAX to facilitate their entry into cells. MCF7 ADR cells were treated with 100 nM of siRNA/well for 4 hours and then the media was replaced with fresh one. Cells were incubated for an additional 20 and 44 hours. Then, the cells were detached with trypsin, centrifuged and washed with ice-cold PBS. For the protein extraction, a mixture of RIPA buffer/protease inhibitors/EDTA (98:1:1 ratio) was added for 30 minutes at 4°C. After that, the samples were centrifuged at 14,000×g for 15 minutes to pellet the cell debris. The supernatants were transferred and the protein concentration was determined by BCA Protein Assay (Thermofisher Scientific, MA, US). The diluted samples were incubated with a mixture of A and B

reagents (1:50 ratio) for 30 minutes at 37°C, according to the manufacturer protocol. In order to determine the protein concentration, a calibration curve was obtained with serial dilutions of Bovine Serum Albumin (BSA; 2-200 μg/mL, R^2 = 0.996). After the incubation, the samples were measured using a spectrophotometer microplate reader (BioTek, Model EL800, Winooski, VT) at λ=562 nm. The western blot analysis was then conducted. The protein lysates were separated by SDS-PAGE electrophoresis with a polyacrylamide/bisacrylamide gradient gel (4–20%) and transferred to nitrocellulose membrane (Hybond-C Extra, Amersham Biosciences). After the blocking with 5% BSA (w/v) in Tris-buffered saline (TBS), membranes were incubated with primary antibody (Ab) for 1 hour at room temperature or overnight at 4°C. We used the following Abs: rabbit polyclonal anti-P-gp (1:2000, Abcam), mouse polyclonal anti-β-actin (1:200, Abcam). After the incubation with a secondary peroxidase-conjugated anti-rabbit (1:20000, Abcam), or anti-mouse (1:5000, Abcam) antibody, the proteins were detected with ECL (Western Lightning Plus, Perkin-Elmer). The relative intensity of the signal of each protein band was determined by means of a Bio-Rad Chemi-Doc and Quantity One Program by following the manufacturer's instructions.

Flow cytometry analysis

The transfection efficiency of siMDR1/PAPD-liposomes and siMDR1/PAPD-micelles was evaluated in A2780 ADR cells, both in hypoxic and normoxic conditions. The cells were seeded into 6-well plates at $2x10^5$ cells/well. siMDR1/PAPD complexes were prepared at N/P=40. Free siMDR1, as positive control, and siSCR, as negative control, were incubated with Lipofectamine RNAiMAX to facilitate their entry into cells. The siRNA concentration in each well was 150 nM. After 4 hours of treatment, the cells were washed and fresh complete media was added. After 20 and 44 hours, the cells were washed with ice-cold PBS and detached with enzyme-free cell disassociation buffer (EMD Millipore). After centrifugation, the cells were resuspended in with 2% BSA (w/v) in PBS pH 7.4 and incubated for 30 minutes. Then, a phycoerythrin-labeled anti-P-glycoprotein antibody was added (UIC2, ab93590, Abcam) was added and the samples were incubated for 45 minutes on ice. Cells were then washed twice with ice-cold PBS and resuspended in the same solution for immediate flow cytometer analysis. The cell-associate fluorescence was quantified by Becton Dickinson FACScan™ (Becton Dickinson, San Jose, CA) at the λ_{em}=488 nm. The data were analyzed with the CellQuest software (Becton Dickinson).

Cell uptake studies

To evaluate the *in vitro* cell uptake of the different liposome formulations, a qualitative and a quantitative experimental approach was carried out. MCF7 ADR cells were previously seeded ($2x10^5$ cells/well) in a 6-well plate. Then, the cells were treated with plain liposomes, Rhodamine b-loaded liposomes and only media as the control for 4 hours. After that, the cell uptake was differently evaluated as follows, exploiting the Rhodamine b fluorescence.

Fluorescence microscopy

After the incubation with plain liposomes, Rh/PEI-PE-liposomes and Rh/PAPD-liposomes, under normoxic and hypoxic conditions, the cells were washed twice with PBS and visualized by KEYENCE Fluorescence Microscope (40X obj).

Flowcytometry analysis

After 4 hours of incubations with the formulations, the cells were detached, washed and resuspended in PBS pH 7.4. Then, the flowcytometry analysis was carried out and the cell fluorescence was recorded at λ_{em} = 488 nm. A total of 10,000 gated live cell events were collected.

The fold increase in geometric mean fluorescence intensity (gMFI) was calculated between the treated cells and the untreated ones.

Statistical analysis

Results are expressed as mean ± standard deviation (SD). The statistical significance was evaluated with GraphPad prism 6 (GraphPad Software, Inc., San Diego, CA). A 2-tailed Student's t-test was performed to analyze the statistical significance between two groups.

Results and discussion

Preparation and characterization of the formulations

In this work, different types of liposomal formulations were designed and developed, as summarized in Table 3. The liposomes were prepared and coated with bPEI-PE or PEG-azobenzene-PEI-DOPE (PAPD) conjugates, in the presence or absence of Paclitaxel (PTX). The polymeric coating stabilized the formulations. Moreover, the siRNA (siMDR1 or siSCR) was loaded by electrostatic interaction to the conjugated polymer, thus combining the delivery of a chemotherapeutic and a transfection agent. Rhodamine b (Rh)-loaded liposomes were prepared in order to study the internalization of the liposomes inside the cells.

Table 3. Experimental design of the different liposomal formulations. (+) indicates the presence and (-) the absence of the component.

Samples	**Components**					
	Liposomes	bPEI-PE	PAPD	PTX	siRNA	Rh
Plain liposomes	+	-	-	-	-	-
bPEI-PE-liposomes	+	+	-	-	-	-
bPEI-PE-PTX-liposomes	+	+	-	+	-	-
siRNA/bPEI-PE-liposomes	+	+	-	-	+	-
PAPD-liposomes	+	-	+	-	-	-
siRNA/PAPD-liposomes	+	-	+	-	+	-
PAPD micelles	-	-	+	-	-	-
siRNA/PAPD micelles	-	-	+	-	+	-
Rh/bPEI-PE-liposomes	+	+	-	-	-	+
Rh/PAPD-liposomes	+	-	+	-	-	+

The formulations were physico-chemical characterized by measuring size, dispersity and surface charge (Table 4). All the liposomes presented a mean diameter between 150 nm and 164 nm. The dispersity was less than 0.10 for all the liposomes, while was higher for the PAPD-micelles. After the deposition of b-PEI-PE, the zeta potential of the formulations turned to positive, thus proving the interaction between the liposomes and the cationic polymer (Table 4A). On the other hand, the coating of PAPD provided a slightly negative charge to the liposomes (Table 4B). This behavior is ascribed to the PEG chains grafted onto the polymer surface.

Table 4A. Physico-chemical characterization of uncoated and bPEI-PE-coated liposomes. The data are expressed as mean ± SD, n = 5. Abbreviation: * Đ = dispersity.

Samples	Average diameter (nm) ± SD	Đ*	Z-potential (mV) ± SD
Plain liposomes	150.4 ± 0.5	0.06	- 12.2 ± 0.4
bPEI-PE-liposomes	153.3 ± 0.6	0.09	16.3 ± 0.2
PTX-liposomes	160.2 ± 0.8	0.08	- 4.9 ± 0.5
bPEI-PE-PTX-liposomes	163.5 ± 0.7	0.10	18.2 ± 0.3

Table 4B. Physico-chemical characterization of PEG-azobenzene-PEI-DOPE (PAPD)-coated micelles and liposomes. The data are expressed as mean ± SD, n = 3. Abbreviation: * Đ = dispersity.

Samples	Average diameter (nm) ± SD	Đ*	Z-potential (mV) ± SD
PAPD-micelles	146.4 ± 1.3	0.28	-0.30 ± 0.1
PAPD-liposomes	163.6 ± 0.7	0.03	-2,80 ± 0.2
PAPD-PTX-liposomes	160.4± 0.5	0.04	-2,60 ± 0.1

Encapsulation efficiency and loading capacity of paclitaxel in liposomes

Paclitaxel was efficiently loaded in bPEI-PE-liposomes, with a mean encapsulation efficiency of 87% (Equation 1). The loading capacity of bPEI-PE-PTX-liposomes was of 2.7% (Equation 2).

Cell viability

The *in vitro* cytotoxicity of bPEI-PE-liposomes, bPEI-PE-PTX-liposomes and Paclitaxel solution was evaluated on human breast cancer MCF7 sensitive cells, MCF7 ADR and human ovarian cancer A2780 ADR cells (Figure 1). After 48 hours of incubation, plain bPEI-PE-liposomes did not show any toxicity on cells, thus confirming the safety of this nanocarrier system. For MCF7 sensitive cells, there was not a significant difference between the treatment with PTX solution or encapsulated in liposomes (Figure 1A). On the other hand, an enhanced cytotoxic effect of PTX-loaded liposomes was observed in the Adriamycin-resistant cells (Figure 1B and C). Indeed, in this case, the cells presented an overexpression of P-glycoprotein (P-gp), responsible for the pumping-out of the chemotherapeutic from cells. Paclitaxel is a substrate of P-gp, and when it is administrated alone can be easily eliminated from the cells. Otherwise, the liposomes enable a prolonged release of the drug directly inside the cancer cells, interfering with the P-gp activity.

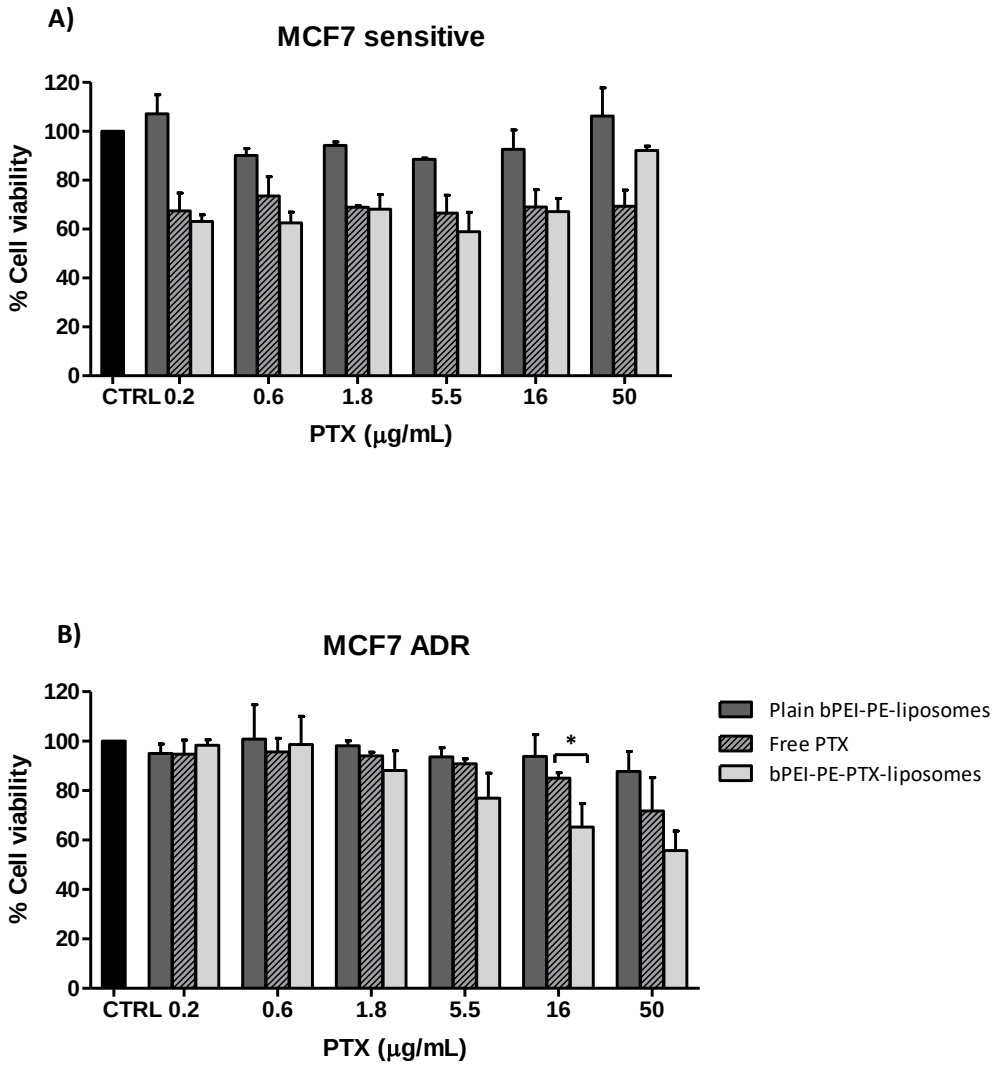

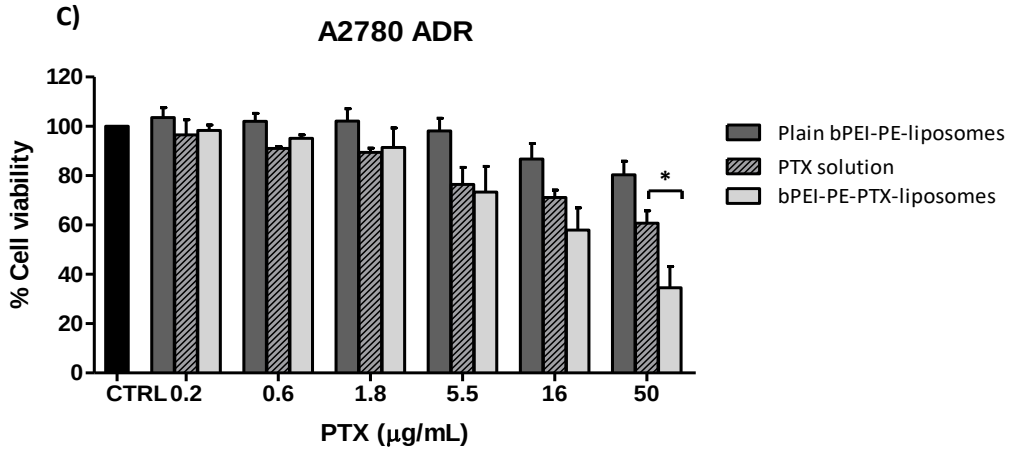

Figure 1. Cell viability of Paclitaxel solution (PTX), bPEI-PE-liposomes, and bPEI-PE-PTX-liposomes on MCF7 sensitive (**A**), MCF7 ADR (**B**), and A2780 ADR (**C**) cells. The formulations were incubated for 48 hours with the cells, and then the cell viability was measured. Results are expressed as mean ± standard deviation (SD) of triplicate. *p≤0.05 bPEI-PE-PTX-liposomes versus free PTX.

siRNA complexation efficiency

The capacity of bPEI-PE and PAPD-coated liposomes to form stable polyplexes with siSCR (negative control siRNA) at different N/P ratios was confirmed by gel retardation assay. The polyplexes were prepared at N/P ratios between 1 and 40 and their complexation efficiency was tested by electrophoresis using an agarose gel (2%). Whereas free siRNA (900 ng) was clearly visible in the agarose gel, the polyplexes showed a reduced ability to migrate, which is relative to the ratio of bPEI-PE and PAPD used (Figure 2). For the siRNA/bPEI-PE liposomes, the maximum of complexation efficiency was obtained at an N/P ratio of 10 (Figure 2A). While, the retardation of siRNA for PAPD-conjugate was evaluated at N/P ratios of 25 and 40 [39], in normoxic or hypoxic conditions (Figure 2B). In both cases, PAPD showed a high complexation efficiency, either coated on liposomes or tested alone in micelles. Moreover, since PAPD conjugate is sensible to hypoxia, the experiment was also conducted in mimic hypoxic conditions. Even under hypoxia, the siRNA remained condensed to PAPD, thus confirming that the cleavage of the PEG portion of the polymer did not affect the complexation of siRNA to the PEI portion.

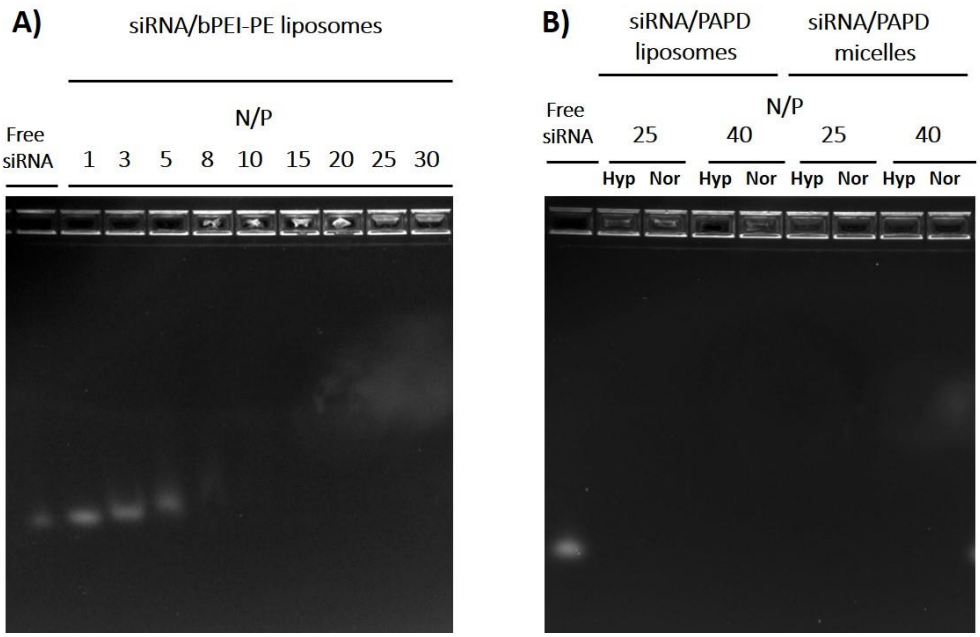

Figure 2. Gel electrophoresis image (2% agarose gel) showed the capability of bPEI-PE and PAPD-coated liposomes to complex siRNA. siRNA/bPEI-PE liposomes reached full complexation at N/P ratio 10 (**A**). PAPD, either coated on liposomes or in micelle form, resulted to complex with high efficiency siRNA at N/P of 25 and 40, in hypoxic (*Hyp*) or normoxic (*Nor*) conditions (**B**).

siMDR1/PAPD liposomes efficiently downregulated P-gp

P-glycoprotein (P-gp) is mainly involved in the mechanisms for the development of multidrug resistance in cancer cells [10]. Its overexpression mediates the extrusion of the chemotherapeutics from the cells, thus reducing their efficiency and the therapeutical outcomes of the treatment. To revert the resistance in MCF7 ADR cells, the MDR1 gene was silenced using a small interfering RNA condensed with PAPD-coated liposomes. Since PAPD conjugate is sensible to reduced oxygen levels, the experiment was also conducted in hypoxia. As shown in Figure 3, after 24 hours of incubation siMDR1/PAPD liposomes in mimic hypoxic conditions downregulated P-gp comparably to the siMDR1 control. This confirmed that thanks to the cleavage of the PEG-Azo group, the liposomes were easily internalized in the cells and were effective in the transfection.

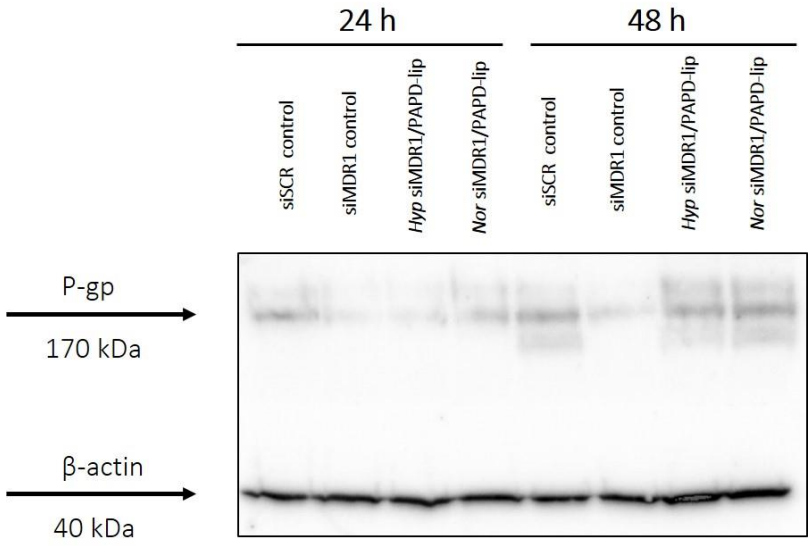

Figure 3. siMDR1/PAPD liposomes silenced P-gp expression in MCF7 ADR cells after 24 hours of incubation. Western blot analysis of lysates of MCF7 ADR transfected with siMDR1/PAPD liposomes, under hypoxic (*Hyp*) or normoxic (*Nor*) conditions. β-actin was used as internal standard. Free siSCR as negative control and free siMDR1 as positive control were transfected with Lipofectamine RNAiMAX.

siRNA-mediated P-gp downregulation by PAPD-coated liposomes was investigated also in the A2780 ADR cells by flowcitometry analysis. The cells were incubated with siMDR1/PAPD liposomes, in hypoxic and normoxic conditions, and siMDR1/PAPD micelles, under hypoxia. As shown in Figure 4, after 24 hours of incubation the P-gp expression was not downregulated by the siMDR1-loaded formulations, while the siMDR1 positive control presented activity of about 40% (Figure 4A). On the other hand, after 48 hours siMDR1/PAPD liposomes showed a significantly silencing of P-gp, under normoxia (around 37%) and even more under hypoxia (around 48%) (Figure 4B). Furthermore, siMDR1/PAPD micelles downregulated the P-gp for about 15%. These results supported the proposal that the PEG cleavage facilitates the entrance in the cells of the formulations. Finally, the PAPD-coated liposomes showed to have a higher transfection efficiency compared to PAPD-micelles, proving to be a more promising nanocarrier tool.

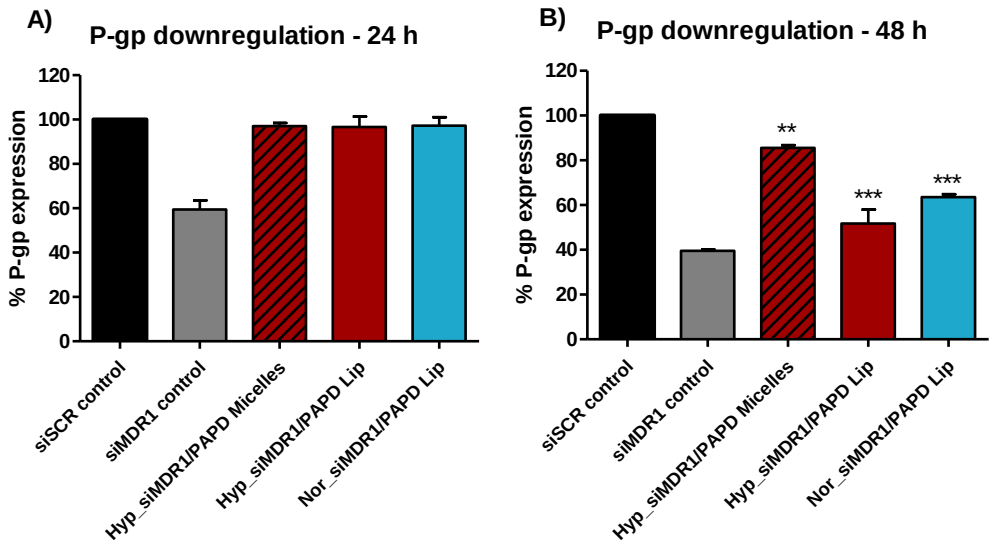

Figure 4. Flowcitometry analysis of P-gp downregulation in A2780 ADR cells treated with siMDR1/PAPD micelles and liposomes in hypoxic and normoxic conditions for 24 and 48 hours. Data are shown as mean ± SD (n=3). **p<0.01, ***p<0.001 vs siSCR control.

The combinational efficiency of siMDR1/PAPD liposomes and Paclitaxel

In order to evaluate the combinational effect of the downregulation of P-gp mediated by siMDR1/PAPD liposomes and paclitaxel, a preliminary *in vitro* cytotoxicity test was performed. P-gp overexpressed A2780 ADR cells were used to assess the dual therapy with a small interfering RNA and a chemotherapeutic. The cells were previously incubated for 4 hours with siMDR1/PAPD liposomes and the day after were treated for additionally 48 hours with different concentrations of Paclitaxel solution. As shown in Figure 5, the co-delivery of the two different cargos at the lowest concentration of PTX significantly inhibited the cell viability with respect to the free drug. This preliminary result needs more investigations, but the synergistic effect of the downregulation of P-gp and the chemotherapeutic PTX may represent a promising combination for counteracting the chemoresistance.

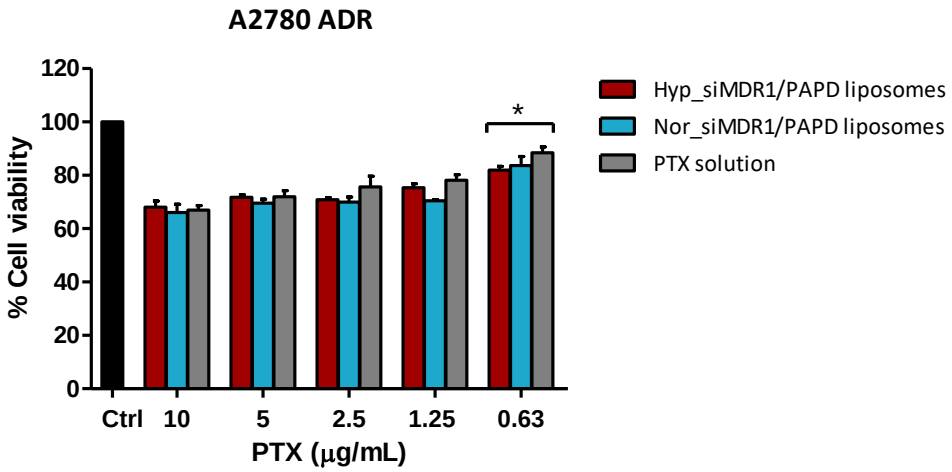

Figure 5. The combination of siMDR1/PAPD liposomes and free PTX hampered A2780 ADR viability. The cancer cells were treated for 4 hours with 100 nM siMDR1/PAPD liposomes in normoxic and hypoxic conditions. At 24 hours, the cells were incubated with different concentrations of free PTX for additional 48 hours. The results indicate the mean ± SD (n=3). *p≤0.05 vs Paclitaxel solution.

Cell uptake

In order to evaluate the internalization of the different nanoformulations, two different uptake studies were performed. In parallel, MCF7 ADR cells were seeded and treated with Rhodamine b-loaded bPEI-PE-liposomes and PAPD-liposomes, both in normoxic and hypoxic conditions. Firstly, after 4 hours of incubation, the cells were washed twice with PBS and visualized under KEYENCE Fluorescence Microscope, exploiting the Rhodamine b fluorescence. As shown in Figure 6A, Rh/bPEI-PE-liposomes and Rh/PAPD-liposomes in hypoxic conditions were avidly internalized by the cells. On the other hand, Rh/PAPD-liposomes in normoxic conditions were less internalized. This qualitative result was also corroborated by flowcytometry analysis. In Figure 6B, the graph expressed as fold increase in geometric mean fluorescence intensity (gMFI) recorded at λ_{em}=488 nm demonstrates that Rh/bPEI-PE-liposomes and Rh/PAPD-liposomes in hypoxic conditions were internalized around 4 times more with respect to the control. Whereas, Rh/PAPD-liposomes in normoxic conditions were uptaken about 3.5 times more. These results conciliate with the idea that the positive surface charges of PEI enable the liposomes to enter easily in the cells. Under mimic hypoxic conditions, the PEG portion is cleaved from the conjugate and the positive charges of PEI are exposed. For this reason, the Rh/bPEI-PE-liposomes and Rh/PAPD-liposomes in hypoxic conditions expressed similar internalization behavior. Conversely, under normoxic conditions the PEG moieties remain attached to the surface of the liposomes, thus contributing to reducing their internalization inside the cells.

A)

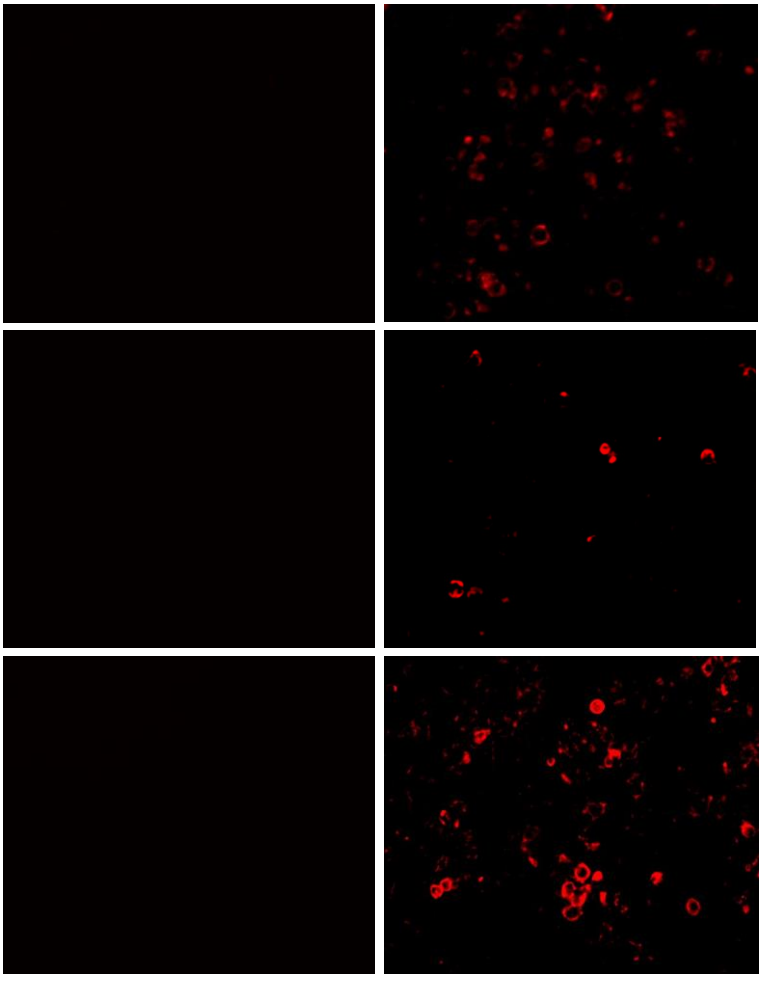

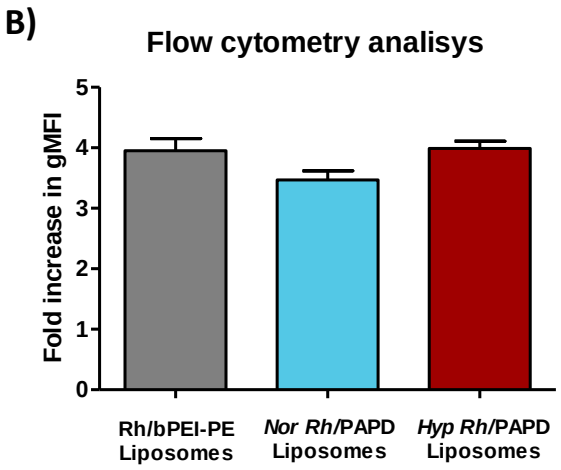

Figure 6. A) Uptake of plain liposomes, Rhodamine b-loaded bPEI-PE-liposomes and PAPD-liposomes, both in normoxic and hypoxic conditions, in MCF7 ADR cells visualized by KEYENCE Fluorescence Microscope (40X obj) after 4 hours of incubation. Results are presented as representatives image from three different preparations. **B**) The graph shows the fold increase in geometric mean fluorescence intensity (gMFI) at the flowcytometry analysis of cells incubated with different liposome formulations. The data are expressed as mean ± SD (n = 3).

Conclusions

The reversal of drug resistance is a current challenge to improve the outcomes of chemotherapy. In this project, novel liposomes coated with a hypoxia sensitive PAPD conjugate were developed. The formulation was studied to efficiently co-deliver a chemotherapeutic, Paclitaxel, and a small interfering RNA against P-glycoprotein. Indeed, the downregulation of P-gp, which is the multidrug resistance-related protein, could represent a promising approach. Moreover, the liposome loading of a chemotherapeutic drug may represent an innovative combinational nanoplatform for the treatment of resistant forms of breast and ovarian cancer. Indeed, the synergic effect of the downregulation of the overexpressed P-glycoprotein and a chemotherapeutic could potentially offer a novel and effective treatment for patients who have established multidrug resistance. Moreover, the use of PAPD conjugate that is activated just in response to tumor milieu can represent a promising approach to reduce the non-specific toxicity and lead better outcomes of the therapeutic treatment.

References

[1] N.S. Gandhi, R.K. Tekade, M.B. Chougule, Nanocarrier mediated delivery of siRNA / miRNA in combination with chemotherapeutic agents for cancer therapy : Current progress and advances, J. Control. Release. 194 (2014) 238–256. doi:10.1016/j.jconrel.2014.09.001.

[2] A.I. Journal, M. Afsharzadeh, M. Hashemi, A. Mokhtarzadeh, Recent advances in co-delivery systems based on polymeric nanoparticle for cancer treatment, Artif. Cells, Nanomedicine, Biotechnol. 46 (2018) 1095–1110. doi:10.1080/21691401.2017.1376675.

[3] A. Babu, A. Munshi, R. Ramesh, Combinatorial therapeutic approaches with RNAi and anticancer drugs using nanodrug delivery systems, 9045 (2017). doi:10.1080/03639045.2017.1313861.

[4] W. Huang, L. Chen, L. Kang, M. Jin, P. Sun, X. Xin, Z. Gao, Y. Han, Nanomedicine-based combination anticancer therapy between nucleic acids and small-molecular drugs ☆, Adv. Drug Deliv. Rev. 115 (2017) 82–97. doi:10.1016/j.addr.2017.06.004.

[5] H. Sun, I. Yarovoy, M. Capeling, C. Cheng, Polymers in the Co-delivery of siRNA and Anticancer Drugs for the Treatment of Drug-resistant Cancers, Top. Curr. Chem. (2017). doi:10.1007/s41061-017-0113-z.

[6] M. Wang, J. Wang, B. Li, L. Meng, Z. Tian, Colloids and Surfaces B : Biointerfaces Recent advances in mechanism-based chemotherapy drug-siRNA pairs in co-delivery systems for cancer : A review, Colloids Surfaces B Biointerfaces. 157 (2017) 297–308. doi:10.1016/j.colsurfb.2017.06.002.

[7] A. Manuscript, NIH Public Access, 4 (2013) 1–35. doi:10.4172/2157-7439.1000164.Paclitaxel.

[8] B.S. Pattni, V. V. Chupin, V.P. Torchilin, New Developments in Liposomal Drug Delivery, Chem. Rev. 115 (2015) 10938–10966. doi:10.1021/acs.chemrev.5b00046.

[9] E. Bernabeu, M. Cagel, E. Lagomarsino, M. Moretton, D.A. Chiappetta, Paclitaxel : What has been done and the challenges remain ahead, Int. J. Pharm. 526 (2017) 474–495. doi:10.1016/j.ijpharm.2017.05.016.

[10] J.I. Fletcher, R.T. Williams, M.J. Henderson, M.D. Norris, M. Haber, ABC transporters as mediators of drug resistance and contributors to cancer cell biology, Drug Resist. Updat. 26 (2016) 1–9. doi:10.1016/j.drup.2016.03.001.

[11] Y. Zhang, S.K. Sriraman, H.A. Kenny, E. Luther, V. Torchilin, E. Lengyel, Reversal of chemoresistance in ovarian cancer by co-delivery of a P-glycoprotein inhibitor and paclitaxel in a liposomal platform, Mol. Cancer Ther. 15 (2016) 2282–2293. doi:10.1158/1535-7163.MCT-15-0986.

[12] C. Sarisozen, A.H. Abouzeid, V.P. Torchilin, The effect of co-delivery of paclitaxel and curcumin by transferrin-targeted PEG-PE-based mixed micelles on resistant ovarian cancer in 3-D spheroids and in vivo tumors, Eur. J. Pharm. Biopharm. 88 (2014) 539–550. doi:10.1016/j.ejpb.2014.07.001.

[13] L.P. Mendes, C. Sarisozen, E. Luther, J. Pan, V.P. Torchilin, Surface-engineered polyethyleneimine-modified liposomes as novel carrier of siRNA and chemotherapeutics for combination treatment of drug-resistant cancers, Drug Deliv. 26 (2019) 443–458. doi:10.1080/10717544.2019.1574935.

[14] J. Pan, L.P. Mendes, M. Yao, N. Filipczak, S. Garai, G.A. Thakur, C. Sarisozen, V.P. Torchilin, Polyamidoamine dendrimers-based nanomedicine for combination therapy with siRNA and chemotherapeutics to overcome multidrug resistance, Eur. J. Pharm. Biopharm. 136 (2019) 18–28. doi:10.1016/j.ejpb.2019.01.006.

[15] A. Singh, P. Trivedi, N.K. Jain, Advances in siRNA delivery in cancer therapy, Artif. Cells, Nanomedicine Biotechnol. 46 (2018) 274–283. doi:10.1080/21691401.2017.1307210.

[16] Y. Dong, D.J. Siegwart, D.G. Anderson, Strategies, design, and chemistry in siRNA delivery systems, Adv. Drug Deliv. Rev. 144 (2019) 133–147. doi:10.1016/j.addr.2019.05.004.

[17] B.L. Davidson, P.B.M. Jr, Current prospects for RNA interference-based therapies, Nat. Publ. Gr. (2011). doi:10.1038/nrg2968.

[18] R.R. Nikam, K.R. Gore, Journey of siRNA: Clinical Developments and Targeted Delivery, Nucleic Acid Ther. 28 (2018) 209–224. doi:10.1089/nat.2017.0715.

[19] W. Tai, Current aspects of siRNA bioconjugate for in vitro and in vivo delivery, Molecules. 24 (2019). doi:10.3390/molecules24122211.

[20] S.W.S. Young, M. Stenzel, Y. Jia-Lin, Nanoparticle-siRNA: A potential cancer therapy?, Crit. Rev. Oncol. Hematol. 98 (2016) 159–169. doi:10.1016/j.critrevonc.2015.10.015.

[21] C. Sarisozen, G. Salzano, V.P. Torchilin, Recent advances in siRNA delivery, Biomol. Concepts. 6 (2015) 321–341. doi:10.1515/bmc-2015-0019.

[22] D. Schermant, B. Demeneixt, J. Behr, A versatile vector for gene and oligonucleotide transfer into cells in culture and in vivo: Polyethylenimine, 92 (1995) 7297–7301.

[23] P. Neuberg, A. Kichler, Recent Developments in Nucleic Acid Delivery with Polyethylenimines, Elsevier, 2014. doi:10.1016/B978-0-12-800148-6.00009-2.

[24] D.F. Costa, V.P. Torchilin, D.F. Costa, Micelle-like nanoparticles as siRNA and miRNA carriers for cancer therapy, (2018).

[25] S. Son, R.A.N. Namgung, J. Kim, K. Singha, W.O.N.J. Kim, Bioreducible Polymers for Gene Silencing and Delivery, 45 (2012). doi:10.1021/ar200248u.

[26] H.J. Mohammad, A. Islam, Degradable Polyethylenimine-Based Gene Carriers, Top. Curr. Chem. (2017). doi:10.1007/s41061-017-0124-9.

[27] R.R. Sawant, S.K. Sriraman, G. Navarro, S. Biswas, R.A. Dalvi, V.P. Torchilin, Biomaterials Polyethyleneimine-lipid conjugate-based pH-sensitive micellar carrier for gene delivery, Biomaterials. 33 (2012) 3942–3951. doi:10.1016/j.biomaterials.2011.11.088.

[28] G. Navarro, S. Essex, R.R. Sawant, S. Biswas, D. Nagesha, S. Sridhar, C.T. De Ilarduya, V.P. Torchilin, Phospholipid-modified polyethylenimine-based nanopreparations for siRNA – mediated gene silencing : Implications for transfection and the role of lipid components, Nanomedicine Nanotechnology, Biol. Med. 10 (2014) 411–419. doi:10.1016/j.nano.2013.07.016.

[29] A. Malek, O. Merkel, L. Fink, F. Czubayko, T. Kissel, A. Aigner, P.E.I. Peg, In vivo pharmacokinetics , tissue distribution and underlying mechanisms of various PEI (– PEG)/ siRNA complexes, Toxicol. Appl. Pharmacol. 236 (2009) 97–108. doi:10.1016/j.taap.2009.01.014.

[30] S. Salmaso, P. Caliceti, Stealth Properties to Improve Therapeutic Efficacy of Drug Nanocarriers, J. Drug Deliv. 2013 (2013) 1–19. doi:10.1155/2013/374252.

[31] A. Koshkaryev, R. Sawant, M. Deshpande, V. Torchilin, Immunoconjugates and long circulating systems : Origins , current state of the art and future directions ☆, Adv. Drug Deliv. Rev. 65 (2013) 24–35. doi:10.1016/j.addr.2012.08.009.

[32] T. Wang, J.R. Upponi, V.P. Torchilin, Design of multifunctional non-viral gene vectors to overcome physiological barriers : Dilemmas and strategies, Int. J. Pharm. 427 (2012) 3–20. doi:10.1016/j.ijpharm.2011.07.013.

[33] H. Hatakeyama, H. Akita, H. Harashima, A multifunctional envelope type nano device (MEND) for gene delivery to tumours based on the EPR effect : A strategy for overcoming the PEG dilemma ☆, Adv. Drug Deliv. Rev. 63 (2011) 152–160. doi:10.1016/j.addr.2010.09.001.

[34] H. Hatakeyama, H. Akita, H. Harashima, Polyethyleneglycol : A Classical but Innovative Material The Polyethyleneglycol Dilemma : Advantage and Disadvantage of PEGylation of Liposomes for Systemic Genes and Nucleic Acids Delivery to Tumors, 36 (2013) 892–899.

[35] Y. Fang, J. Xue, S. Gao, A. Lu, D. Yang, H. Jiang, K. Shi, Cleavable PEGylation : a strategy for overcoming the " PEG dilemma " in efficient drug delivery, Drug Deliv. 0 (2017) 22–32. doi:10.1080/10717544.2017.1388451.

[36] S. Hama, S. Itakura, M. Nakai, K. Nakayama, S. Morimoto, S. Suzuki, K. Kogure, Overcoming the polyethylene glycol dilemma via pathological environment-sensitive change of the surface property of nanoparticles for cellular entry, J. Control. Release. 206 (2015) 67–74. doi:10.1016/j.jconrel.2015.03.011.

[37] Y. Wang, W. Shang, M. Niu, J. Tian, K. Xu, Hypoxia-active nanoparticles used in tumor theranostic, (2019) 3705–3722.

[38] S. Takae, K. Miyata, M. Oba, T. Ishii, PEG-Detachable Polyplex Micelles Based on Disulfide-Linked Block Catiomers as Bioresponsive Nonviral Gene Vectors, (2008) 6001–6009.

[39] F. Perche, S. Biswas, T. Wang, L. Zhu, V.P. Torchilin, Hypoxia-targeted siRNA delivery, Angew. Chemie - Int. Ed. 53 (2014) 3362–3366. doi:10.1002/anie.201308368.

[40] F. Perche, S. Biswas, N.R. Patel, V.P. Torchilin, Hypoxia-responsive copolymer for siRNA delivery. RNA Imaging: Methods and Protocols, 1372 (2016) 14–20. doi:10.1007/978-1-4939-3148-4.

CHAPTER 4

ALBUMIN-BASED NANOPARTICLES FOR IMPROVING INTRACELLULAR DELIVERY OF DOXORUBICIN IN RESISTANT CANCER CELL LINES

Introduction

Resistance to chemotherapy is a major problem that limits the effectiveness of successful treatment of cancer, with over 90% treatment failure rate in metastatic tumors [1]. The use of anticancer drugs is limited by several established mechanisms that confer resistance to one or more chemotherapeutic agents. The resistance can involve single agents, thus allowing possible effective treatment with alternative drugs, or multiple (multidrug resistance, MDR), thereby rendering the tumor refractory to drug treatment [2]. This scenario leads to a poor clinical outcome. The cause of resistance to available systemic therapies is intricate. Nowadays, three prevalent mechanisms predominate: hampered drug uptake through transporters, altered cytotoxicity against cancer cells and increased drug efflux via active pumps [3].

As a matter of fact, doxorubicin-based chemotherapy regimens recurrently fail due to inherent and acquired resistance [4]. The anthracycline Doxorubicin (DOXO), isolated from a culture of *Streptomyces peucetius*, is an antineoplastic agent used in the treatment of a wide range of cancers, such as multiple myeloma, lung, ovarian, gastric, thyroid, breast, sarcoma, and pediatric cancer. Doxorubicin mostly acts by two molecular mechanisms. It impairs DNA replication by DNA intercalation and inhibition of topoisomerase II, and generates free radicals that damage cellular membranes, DNA and proteins [5]. As the majority of chemotherapies, DOXO is renowned for its extensive side-effect profile, in particular the dose-dependent cardiotoxicity, the lack of selectivity for tumor cells and the induced cell resistance [6]. Indeed, DOXO can confer drug resistance in a mechanism that involves an altered or increased expression of ATP-binding cassette (ABC) transporters. Through this mechanism, cancer cells can easily efflux DOXO or other chemotherapeutics through up-regulating efflux transporters, with a consequent decrease in intracellular drug concentration and effectiveness. Thus, to enhance the chemotherapeutic outcome, high drug doses should be used and these always cause severe systemic toxicity [7].

Novel nanomedicines for cancer therapy represent an innovative and promising strategy to overcome the several limitations of conventional small-molecule chemotherapeutics by enhancing drug uptake and selective intracellular accumulation in cancer cells using both passive and active targeting and reducing the toxicity to normal tissues [8–11]. Numerous approaches of combination therapy have been studied to overcome multidrug resistance, including the use of P-gp inhibitor (chemosensitizer) [12–15], protein inhibitor [16] and knockdown agents of markers that control chemoresistance [17–19]. Notably, the first FDA-approved nanodrug in 1995 was Doxil®, a pegylated-liposomal doxorubicin-based formulation for the treatment of ovarian cancer. This first cornerstone of the nanomedicine paved the way for further investigations in this field [20,21]. Doxil®, indeed, was formulated to overcome the drawbacks in DOXO administration, increasing the survival compared to conventional doxorubicin treatment. Doxil® caused the onset of fewer side effects on the patients and presented a long circulation time due to the PEG moieties [22]. However, PEGylated-liposomal doxorubicin can cause the dose-limiting hand-foot syndrome, characterized by skin eruptions on the palms of the hand and soles of the feet, leading to interruption in therapy by at least 2 weeks and decrease in subsequent dosage. Moreover, PEG chains could also impair the entrance of the liposomes inside the cells, thus frustrating the prolonged circulation time benefit [23].

Based on these premises, much research on other nanoformulation has been conducted, included albumin-based nanoparticles [24,25]. Albumin has been considered as one of the most useful and versatile carrier proteins in pharmaceutical and clinical fields. Indeed, albumin is biocompatible and non-toxic, thus can be used as a pharmaceutical carrier more safely versus many synthetic polymers. Albumin-based nanoparticles represent an ideal nanocarrier system because of its low cost, high

availability, easy purification and high drug-loading capacity. Besides, this advanced drug nanodelivery system can interact with both hydrophobic and hydrophilic therapeutic molecules, provide prolonged release of drugs and be easily modified due to the presence of functionally charged surface groups. A variety of albumin-based nanoparticle approaches has been intensively exploited for effective therapies, diagnosis and personalized medicine [26–28].

Aim of the project

In the last part of the PhD project, another nanomedicine-based approach was explored to overcome the resistance that cancer cells develop after the initiation of a chemotherapeutic treatment. In particular, the attention was focused on the design of novel nanoformulations that may counteract *per se* drug resistance. For this purpose, albumin-based nanoparticles carrying doxorubicin were developed with a tuned coacervation method. Moreover, in order to improve the physico-chemical characteristics of the nanoparticles, glycol chitosan was added as a coating layer. In this way, glycol chitosan-coated (GC DOXO-NPs) and un-coated (DOXO-NPs) nanoparticles were obtained. Here, the physico-chemical characterization of the systems was described as well as the *in vitro* evaluation of the NP cytotoxicity on doxorubicin-resistant cancer cells.

Material and Methods

Materials

The substances and laboratory reagents were from Sigma-Aldrich (St Louis, MO, US), unless otherwise specified. Ultrapure water was obtained using a 1–800 Millipore system (Molsheim, France). The tubular semi-permeable cellulose membrane was from Carl Roth (Karlsruhe, Germany). Cell culture reagents were purchased from Gibco/Invitrogen (Life Technologies, Paisley, UK) except where otherwise indicated. All reagents were of analytical grade. Doxorubicin hydrochloride was purchased by Sigma-Aldrich.

Methods

Preformulation studies

In order to obtain stable and reproducible albumin-based nanoparticle formulations, a preformulation study was carried out. Different Bovine Serum Albumin (BSA) concentrations were tested with different amounts of the nonionic surfactant Polysorbate 80 to reach the optimal conditions to load Doxorubicin hydrochloride (DOXO).

Preparation of Albumin-based nanoparticles

Albumin nanoparticles

Once optimized the process, blank albumin nanoparticles were prepared based on a tuned coacervation method. Briefly, 25 mg of Bovine Serum Albumin (BSA) were dissolved in 1 mL of 50 mM TRIS buffer at pH 7.4 containing Polysorbate 80 (2% w/v) as surfactant. Then, ethanol was added dropwise under sonication in a 220-230 V Bransonic® 3510 Ultrasonic Cleaner (Emerson; Saint Louis, MO, US) at 60 °C for 1 hour. When the nanosuspension was obtained, the ethanol was evaporated under nitrogen flux at 60 °C. Moreover, glycol chitosan-coated nanoparticles (blank GC-NPs) were obtained by adding dropwise under constant stirring an aqueous solution of glycol chitosan (2.7% w/v) to the preformed blank BSA-NPs.

Doxorubicin-loaded albumin-based nanoparticles

Albumin nanoparticles carrying DOXO (DOXO-NPs) were obtained by a purposely tuned coacervation method. Briefly, 25 mg of BSA were dissolved in 1 mL of 50 mM TRIS buffer at pH 7.4 containing Polysorbate 80 (2% w/v) as surfactant. DOXO in its hydrochloride form was dissolved in the BSA solution with a concentration of 3 mg/mL. Then, ethanol was added dropwise under sonication in a 220-230 V Bransonic® 3510 Ultrasonic Cleaner (Emerson; Saint Louis, MO, US) at 60 °C for 1 hour. When the nanosuspension was obtained, the ethanol was evaporated under nitrogen flux at 60 °C. In addition, glycol chitosan-coated nanoparticles (GC DOXO-NPs) were obtained by adding dropwise under constant stirring an aqueous of glycol chitosan (2.7% w/v) to the preformed DOXO-loaded nanoparticles.

Physico-chemical characterization of albumin-based nanoparticles

The average diameter, dispersity and zeta potential were determined by photocorrelation spectroscopy using a particle size analyzer at a scattering angle of 90° and a temperature of 25 °C. NP suspensions were diluted in deionized filtered water before measurement. For zeta potential determination, already diluted NP formulations were placed in the electrophoretic cell, where an electric field of approximately 15 V/cm was applied. The morphology of formulations was evaluated by Transmission Electron Microscopy (TEM), using a Philips CM10 (Eindhoven, NL) instrument. Plain NPs and DOXO-NP nanosuspensions were sprayed on Formvar-coated copper grid and air-dried before observation.

Thermal analysis was carried out using a DSC/7 differential scanning calorimeter (Perkin-Elmer, Branford, CT, US) equipped with a TAC 7/DX instrument controller and the Pyris program. A heating rate of 10°C per minute was used in the 25°C–200°C temperature range. Standard aluminium sample pans for solids (Perkin-Elmer) were used and about 20 mg of the freeze-dried nanoparticles weighed. DOXO and BSA-NP were analyzed for comparison purposes. Attenuated Total Reflection (ATR)-Fourier transformed infrared (FTIR) spectra of the DOXO-NPs, GC DOXO-NPs, free DOXO and blank BSA-NPs were obtained using a Perkin Elmer Spectrum 100 FT-IR in the region 4000^{-1}-650^{-1}.

HPLC quantitative Doxorubicin determination

HPLC system consisted of a pump (LC-9A PUMP C, Shimadzu, Japan) equipped with a fluorescence detector (Chrompack, Japan) and analyses were performed using an Agilent TC C18 column (250 mm × 4.6 mm, 5 µm). A degassed solution containing 65% v/v phosphate buffer (pH=1.4), 25% v/v acetonitrile and 10% distilled water was used as mobile phase. The flow rate was 1 mL/min and the fluorimetric detector (Shimadzu) was set at λ_{exc}=480 nm and λ_{em}=560 nm. To calculate the drug concentration, a linear calibration curve was set up with a concentration range of 0.25–2.5 µg/mL with a regression coefficient of 0.999.

Encapsulation efficiency and loading capacity

The encapsulation efficiency of DOXO-NPs and GC DOXO-NPs was determined with a centrifugal filter system. A part of the two nanoformulations was placed in a centrifugal filter device (Amicon® Ultra-0.5) and centrifuged for 15 minutes at 15000 rpm with a Beckman Coulter 64R Centrifuge. Then, the filtered solution containing free DOXO was analyzed at the HPLC as previously described. The encapsulation efficiency of DOXO was quantified by Equation 1.

Encapsulation Efficiency (EE):

$$EE = \frac{Total_{DOXO} - Free_{DOXO}}{Total_{DOXO}} \times 100$$

(Equation 1)

The loading capacity was determined on freeze-dried NP samples. Briefly, a weighted amount of freeze-dried DOXO-NPs and GC DOXO-NPs was suspended in 10 mL of filtered water. After sonication and centrifugation, the supernatant was diluted with mobile phase and analyzed by HPLC. The loading capacity was calculated by Equation 2.

Loading Capacity (LC):

$$LC = \frac{Total_{DOXO}}{NP\ weight} \times 100$$

(Equation 2)

In vitro Doxorubicin release studies

The *in vitro* release of DOXO from the nanoparticles was carried out with a multi-compartment rotating cell. DOXO-NPs, GC DOXO-NPs and DOXO solution as control were used as donors against a receiving phase consisting of TRIS buffer pH 7.4. The chambers were separated with a semi-permeable cellulose membrane (cut-off 14kDa). Samples were drawn at fixed time intervals and the same volume was replaced with fresh medium. Then DOXO concentration was determined using HPLC, as previously described.

Mechanism of Drug Release

In order to assess the mechanism of drug release, *in vitro* release patterns were analyzed using four kinetic models: zero-order kinetic model, first-order kinetic model, simplified Higuchi model, and Korsmeyer-Peppas model [29]. Briefly, for each model, a graph was constructed using Microsoft Excel from which the rate constant and correlation values were obtained by applying a linear regression fit. The zero-order kinetic model was obtained by plotting cumulative % drug release vs time. The first-order kinetic model was analyzed by plotting log cumulative % of drug remaining vs time. The Higuchi model was evaluated by plotting cumulative % drug release vs square root of time, while the Korsmeyer-Peppas model was analyzed by plotting log cumulative % drug release vs log time.

Cells

To evaluate the contribution of doxorubicin-loaded albumin-based nanoparticle, two different cell lines resistant to Doxorubicin were employed. A2780res, human ovarian carcinoma cells, and EMT6/AR10, murine cancer mammary cells, were incubated at 37 °C with 5% CO_2 atmosphere.
EMT6/AR10 cells were cultured in MEM(EBSS) medium, whereas A2780res cells were cultured in RPMI. All the media were supplemented with 10% v/v Fetal Bovine Serum (FBS), 2mM Glutamine and antibiotics. To maintain the resistance, A2780 ADR and MCF7 ADR were cultured in media containing 100 nM doxorubicin HCl twice a week.

Cell viability assay

The cytotoxic effect of DOXO-NPs and GC DOXO-NPs, and of their blank counterparts was evaluated. The EMT6/AR10 and A2780res cells were seeded in a 96-well plate ($3x10^3$ cells/well) and incubated with the albumin-based nanoformulations at different DOXO concentration. After 24 and 48 hours

of incubation, viable cells were evaluated by 3-(4,5-Dimethyl-2-thiazolyl)-2,5-diphenyl-2H-tetrazolium bromide (MTT) inner salt reagent at 570 nm. The readouts from treated cells were expressed as percentage versus control measured on untreated cells.

Colony-forming assay

A2780res cells were seeded into 6-well plates and treated with different concentrations of DOXO-NPs, GC DOXO-NPs and DOXO solution as control. The medium was changed respectively after 3 and 20 hours and cells were cultured for additional 10 days. After that, the cells were fixed and stained with a solution of 80% v/v crystal violet and 20% v/v of ethanol. To induce a complete dissolution of the crystal violet, a solution of 30% v/v acetic acid was added and the absorbance was detected at 595 nm.

Study of DOXO-loaded BSA-NP internalization in A2780res cells

A2780res cells were seeded onto Corning® cover glasses (Sigma-Aldrich) in a 24-well plate (4×10^4 cells/ well) and incubated overnight at 37 °C in a 5% CO_2 atmosphere. Then, the cells were incubated with DOXO-NPs, GC DOXO-NPs and DOXO solution at a final concentration of 5 µg/mL for 1 hour. After that, the cells were washed with PBS, fixed with 4% Paraformaldehyde (PAF) for 15 minutes at room temperature, and stained with 4',6-diamidine-2-phenylindole (DAPI). Finally, coverslips were mounted. The samples were analyzed with a TCS SP2 AOBS confocal microscope (Leica Leica, Wetzlar, Germany) equipped with 63X/1.40 HCX Plan-Apochromat oil-immersion objective.

Statistical analysis

Data are presented as mean ± standard deviation (SD). Statistical analysis was performed by GraphPad Prism program (version 6; GraphPad Software). A 2-tailed Student's t-test was performed to analyze the statistical significance between two groups.

Results and discussion

Albumin-based nanoparticles were purposely designed and developed to obtain stable and reproducible formulations. As reported in the schematic representation of the preparation method in Figure 1, uncoated albumin-based doxorubicin-loaded (DOXO-NPs) and glycol chitosan-coated (GC DOXO-NPs) nanoparticles, and their counterparts were obtained.

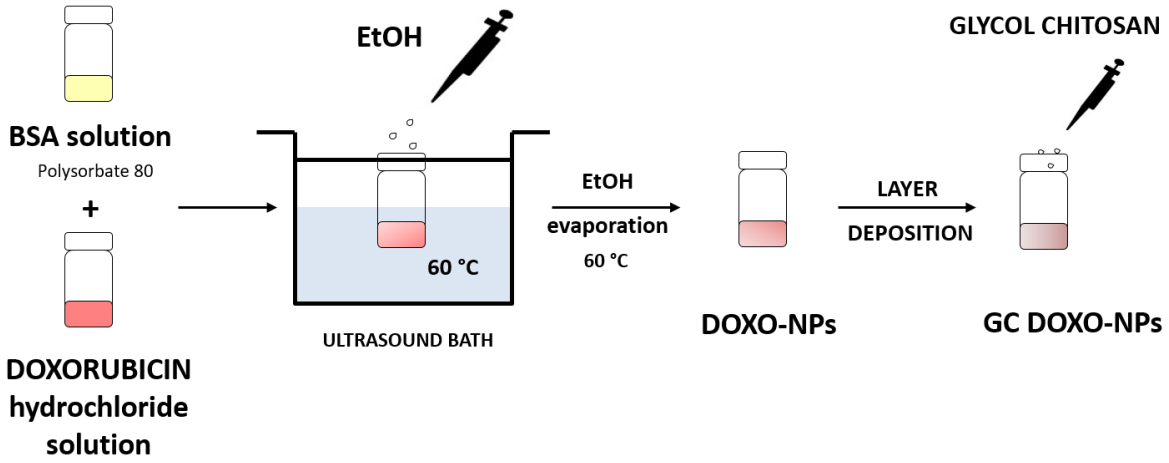

Figure 1. Representative scheme of the tuned preparation method of un-coated (DOXO-NPs) and glycol chitosan-coated (GC DOXO-NPs) DOXO-loaded albumin nanoparticles.

Physico-chemical characterization of nanoparticles

The average diameter, dispersity, zeta potential and pH values of albumin-based nanoparticles (BSA-NPs) are reported in Table 1. All the formulations presented a mean diameter between 360 and 385 nm. The uncoated formulations presented a negative surface charge due to the contribution of the carboxyl groups of albumin. On the other hand, the presence of the coating of glycol chitosan did not modify the dimensions of the nanoparticles but affected their surface charges. Indeed, when coated with glycol chitosan, the zeta potential of the nanoformulations turned to positive because of the amine groups of the polymer. The increased zeta potential confirmed the interaction between the albumin and the polymer. All the formulations presented a physiological pH in the range 6.8-7.4.

Table 1. Physico-chemical characterization of albumin-based nanoparticles. Results are shown as means ± standard deviation (SD) from three different preparations (n=10). Abbreviation: * Đ = dispersity; §EE = encapsulation efficiency.

BSA Nanoparticles	Average diameter (nm) ± SD	Đ*	Z-potential (mV) ± SD	EE§ (%)	EE§ (%)
Blank BSA-NPs	362.1 ± 7.6	0.21	- 27.3 ± 2.3	---	---
DOXO-NPs	380.3 ± 9.5	0.26	- 28.9 ± 4.1	90.2 ± 1.3	6.4 ± 0.8
Blank GC BSA-NPs	365.3 ± 12.8	0.23	7.6 ± 0.9	---	---
GC DOXO-NPs	383.6 ± 10.2	0.21	8.0 ± 0.5	85.2 ± 1.2	4.3 ± 0.4

The spherical morphology of albumin-based nanoformulations and their nanometric sizes were confirmed by Transmission electron microscopy (TEM) analysis. All the nanoparticles presented a reproducible spherical shape. As an example, the morphological appearance of GC DOXO-NPs is reported in Figure 2.

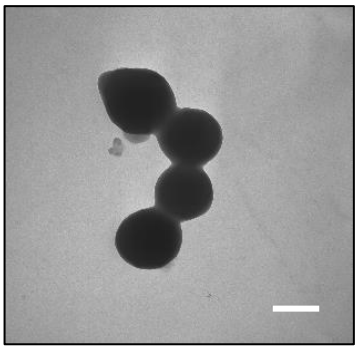

Figure 2. Transmission electron microscopy (TEM) image of GC DOXO-NPs (magnification 28,500×). Results are presented as a representative image from three different preparations. Scale bar, 300 nm.

Differential scanning calorimetry profile and ATR-FTIR analysis of freeze-dried samples of free DOXO, DOXO-NPs, GC DOXO-NPs and blank BSA-NPs were measured. As it is shown in Figure 3, DSC thermograms (Figure 3A) and ATR-FTIR spectra (Figure 3B) confirmed the interaction between the doxorubicin and the nanoformulations.

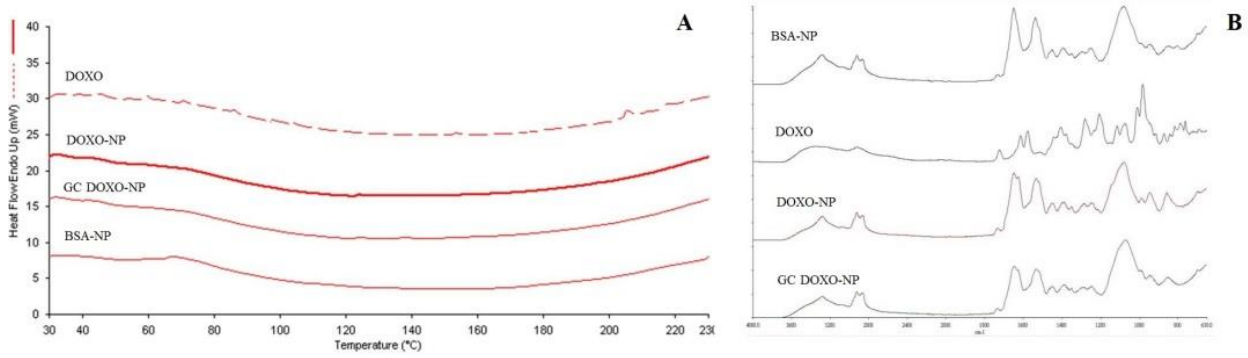

Figure 3. DSC thermograms (**A**) and ATR-FTIR spectra (**B**) of DOXO solution, DOXO-NPs, GC DOXO-NPs and blank BSA-NPs confirmed the interaction between the drug and the nanoparticles.

In vitro release studies

The *in vitro* release kinetics of Doxorubicin from DOXO-NP and GC DOXO-NP formulations was evaluated with a multi-compartment rotating cell. The receiving phase of the study consisted of TRIS buffer at pH 7.4. For both formulations, the release of the drug was slow and prolonged over time, compared to free solution diffusion (Figure 4). After 24 hours, only 30% of the encapsulated drug was released from the DOXO-NPs and GC DOXO-NPs. The coating with glycol chitosan did not affect the Doxorubicin release profile of GC DOXO-NPs. On the other hand, the solution of DOXO hydrochloride passed completely into the receiving phase.
The sustained release may be primarily due to the slow diffusion of Doxorubicin across the albumin matrix of nanoparticles. This could represent a favorable condition to minimize the systemic adverse side effects of Doxorubicin and to enhance the efficiency of nanoparticles at the target site.

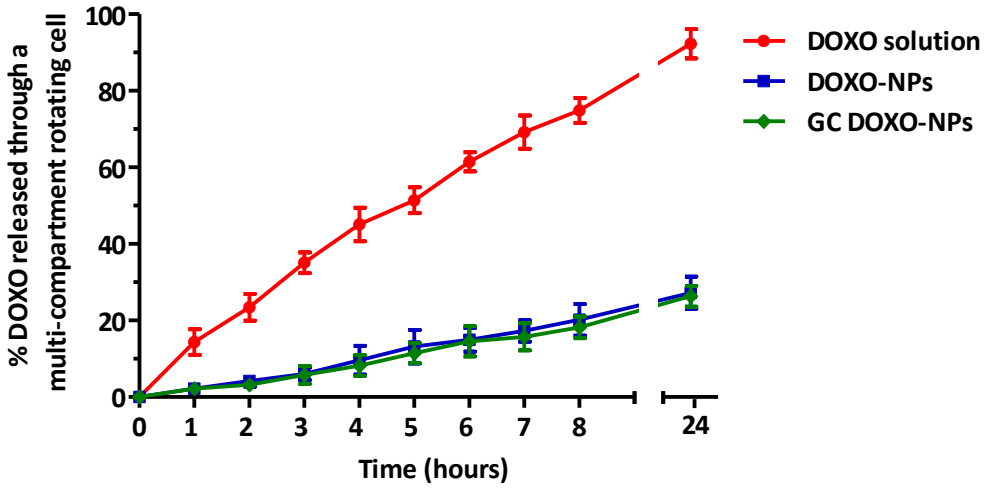

Figure 4. *In vitro* DOXO release from DOXO-NPs and GC DOXO-NPs, and DOXO solution as control, up to 24 hours. Each point represents the mean ± SD of three different formulations.

Moreover, the mechanism of drug release was also analyzed using four kinetic models: zero-order kinetic, first-order kinetic, simplified Higuchi, and Korsmeyer-Peppas modes. For each nanoparticle release profile, a graph was constructed in Microsoft Excel from which the rate constant and correlation values were obtained by applying a linear regression fit (Figure 5). Doxorubicin release was best fitted by the simplified zero-order kinetic for both DOXO-NPs and GC DOXO-NPs. Zero-order kinetics fit with nanostructure forms that do not disaggregate and release the drug slowly.

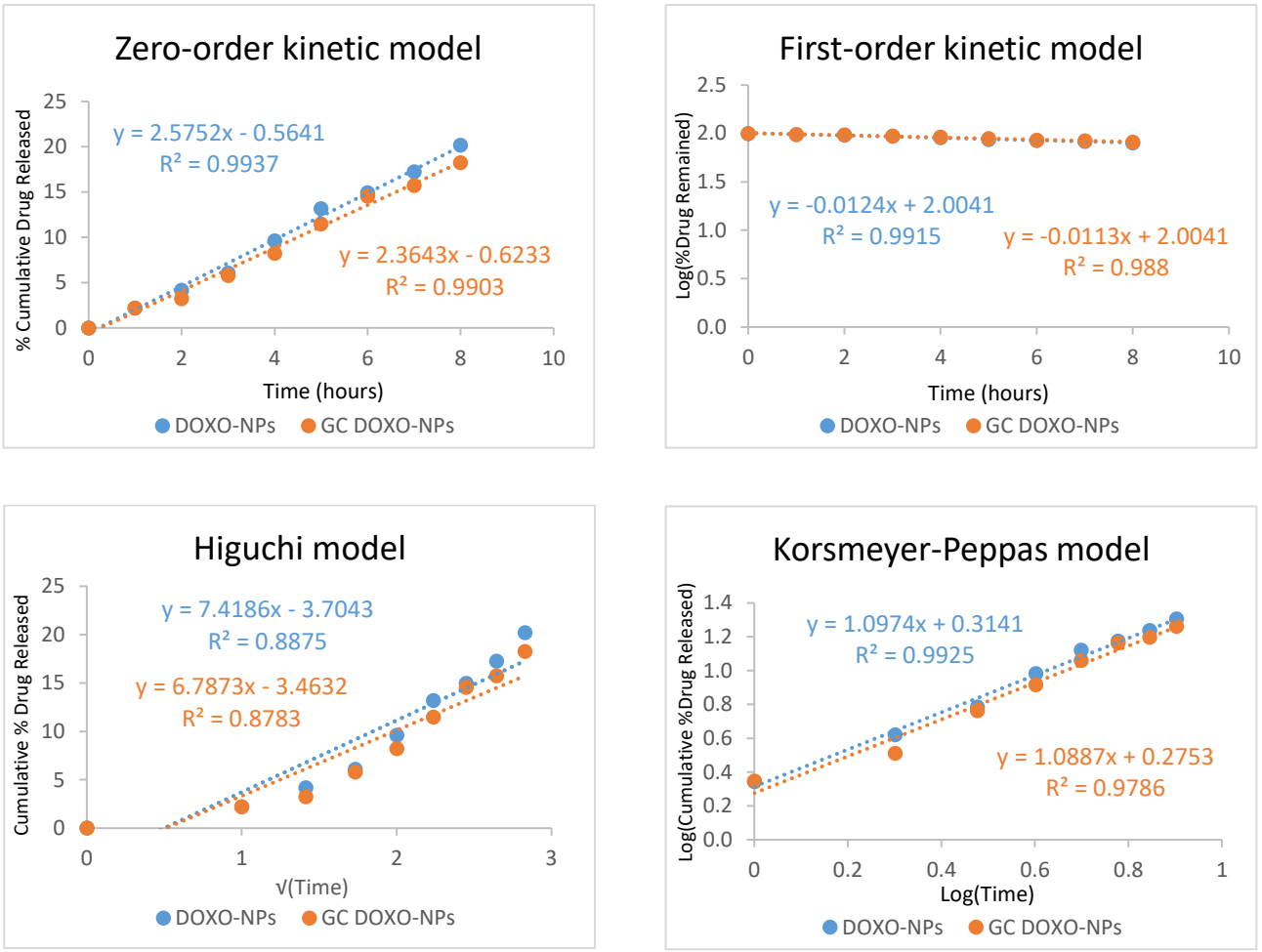

Kinetic models	DOXO-NPs	GC DOXO-NPs
	R^2	
Zero-order	0.9937	0.9903
First-order	0.9915	0.988
Higuchi	0.8875	0.8783
Korsmeyer-Peppas	0.9925	0.9786

Figure 5. Doxorubicin release from DOXO-NPs and GC DOXO-NPs (points, representing average values) fitted to kinetic models (lines). The cumulative release was fitted to each kinetic model: zero-order kinetic model by plotting cumulative % drug release vs time, first-order kinetic model by plotting log of % drug remaining vs time, simplified Higuchi model by plotting cumulative % drug release vs square root of time, and Korsmeyer-Peppas model by plotting log cumulative % drug release vs log time (graphs). For DOXO-NPs, the zero-order kinetic, the first-order kinetic and the Korsmeyer-Peppas models showed a high correlation with R^2>0.99. For GC DOXO-NPs, the zero-order kinetic showed R^2>0.99. The R^2 values are reported in the Table.

Albumin Doxorubicin-loaded nanoparticles impaired A2780res and EMT6/AR10 viability and proliferation

The cytotoxicity of DOXO solution, DOXO-NPs, GC DOXO-NPs, and their blank counterparts was *in vitro* evaluated on A2780res and EMT6/AR10 cell lines, with a Doxorubicin resistant profile. After 24 and 48 hours of incubation, DOXO-NPs and GC DOXO-NPs inhibited A2780res and EMT6/AR10 viability in a greater extent than free Doxorubicin (Figure 6). After 24 hours, A2780res presented 20% of cell viability where incubated with DOXO-NPs 10 µg/mL, while EMT6/AR10 cells just 50%. After 48 hours, the viability was even more inhibited. On the other hand, GC DOXO-NPs showed to be a little bit less effective, giving a cell viability of 40% after 24 hours and 65% after 48 hours for A2780res. Instead, in the EMT6/AR10 the cytotoxicity was around 50%. Besides, the DOXO solution presented cytotoxicity of less than 40% after 48 hours of incubation. Taken together these results, the nanoparticles resulted to be *in vitro* more effective than free DOXO solution because they acted as "trojan horses", thus reducing the contribution of the P-gp in pumping out the drug from the cells. The nanoparticles remain inside the cells, where they release for a prolonged time the drug. Moreover, IC_{50} values of free Doxorubicin, DOXO-NP, and GC DOXO-NP in A2780res were calculated (Table 2).

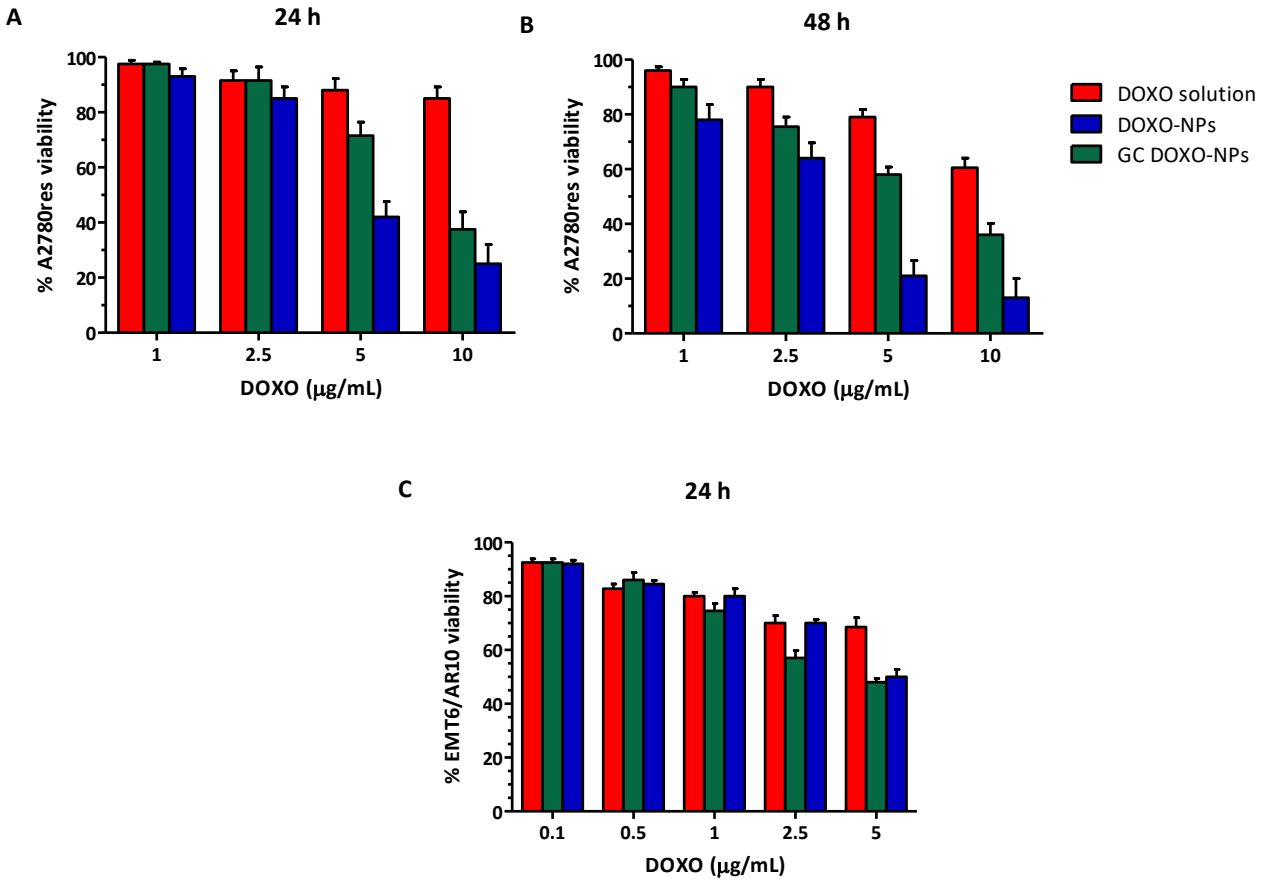

Figure 6. DOXO solution, DOXO-NPs, GC DOXO-NPs were incubated with A2780res and EMT6/AR10 cells for 24 hours (**A**, **C**) and 48 hours (**B**) and the cell viability was evaluated. Each bar represent the mean ± SD of five different experiments (n=3).

Table 2. Determination IC_{50} values of free Doxorubicin, DOXO-NPs and GC DOXO-NPs in A2780res cells after 24 and 48 hours of incubation. Results are mean ± SD for three different experiments. *p<0.05.

Cell line	Time of incubation	**DOXO IC_{50} (µM)**	**DOXO-NPs IC_{50} (µM)**	**GC DOXO-NPs IC_{50} (µM)**
A2780res	24 h	$1.2 \times 10^{-1} \pm 0.60$	$5.6 \times 10^{-3} \pm 0.50$	$8.2 \times 10^{-3} \pm 0.50$
	48 h	$2.7 \times 10^{-2} \pm 0.60$	$9.8 \times 10^{-5} \pm 1.60$	$3.7 \times 10^{-3} \pm 0.90$

The anti-proliferative effect of the albumin-based doxorubicin-loaded NPs was *in vitro* tested. The cells were incubated for 3 and 20 hours with the different formulations, and then cultured for additionally 10 days. After that time, the colony formed was evaluated. As shown in Figure 7, DOXO-NPs and GC DOXO-NPs significantly hampered the proliferation of A2780res cells after just 3 hours of incubation at a concentration of 1 µg/mL. After 20 hours of incubation, instead, the nanoformulations resulted to be effective starting from 0.5 µg/mL of the drug.

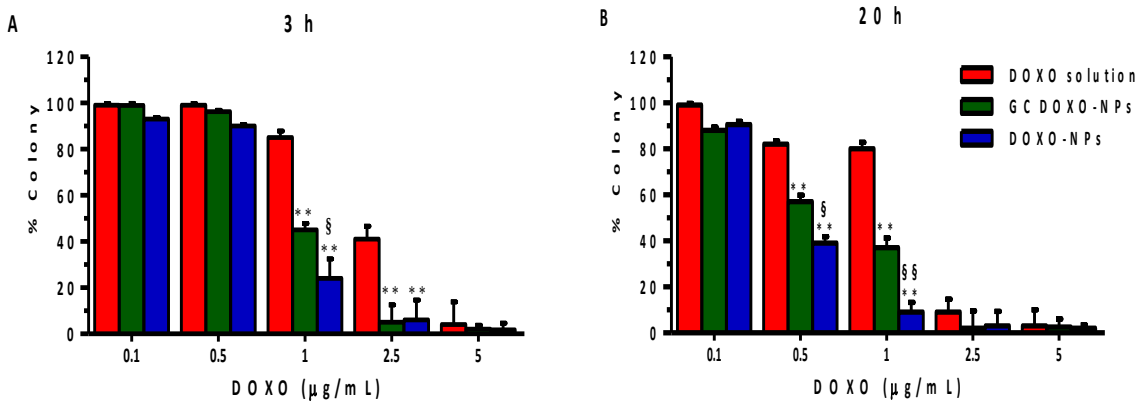

Figure 7. Doxorubicin-loaded nanoparticles impaired A2780res proliferation. Clonogenic assay was performed at 3 (**A**) and 20 hours (**B**) of incubation with increasing concentration of DOXO-NPs, GC DOXO-NPs and DOXO solution. **p<0.01 vs DOXO solution; §p <0.05, §§p<0.01 vs GC DOXO-NPs.

Albumin Doxorubicin-loaded nanoparticle internalization in A2780res cells

To study the ability of A2780res cells to internalize the albumin-based doxorubicin-loaded nanoparticles, confocal analysis was performed exploiting DOXO fluorescence. A2780res were incubated for 1 hour with DOXO-NPs, GC DOXO-NPs and DOXO solution and then fixed and stained with DAPI to visualize the nuclei. The images reported in Figure 8 showed that the nanoparticles were avidly and fast internalized by the cells (Figure 8A and B). Whereas, DOXO solution may appear at the edges of the cell membrane, probably at the efflux pump level (Figure 8C).

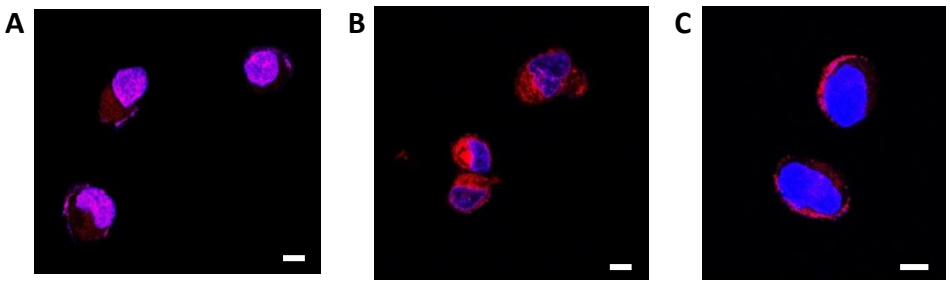

Figure 8. DOXO-NPs were internalized in A2780res and entered in cell nuclei. A2780res cells were incubated with DOXO-NP (**A**), GC DOXO-NP (**B**) and DOXO solution (**C**) for 1 hour. Laser scanning confocal microscope images at 63X. Scale bar, 4 µm.

Conclusions

It is worth noting that resistance to chemotherapy limits the effectiveness of anticancer drug treatment. Overcoming this limitation, the impact on the survival of cancer could change. In this project, a reproducible coacervation method to obtain albumin-nanoparticles with narrow size distribution was fine-tuned. Notably, glycol chitosan-coated and uncoated albumin-based Doxorubicin-loaded nanoparticles were prepared with a reproducible method. These nanoparticles significantly inhibited the *in vitro* viability and proliferation of cell lines resistant to DOXO, thus demonstrating the importance of the vehicle to counteract drug resistance. Taken together, these *in vitro* results showed that GC DOXO-NPs and DOXO-NPs may represent a novel platform to overcome the mechanism of drug resistance in cancer cell lines, thus improving the efficacy of the chemotherapy.

In vivo studies are ongoing to evaluate the pharmacokinetics and the biodistribution of the nanoformulations. Moreover, it could be a challenge to co-load a chemotherapeutic and chemosensitizers (i.e. siRNA or miRNA) to enhance the concentration of the drug in the tumor site inhibiting Doxorubicin mechanism of resistance.

References

[1] I. Genovese, A. Ilari, Y.G. Assaraf, F. Fazi, G. Colotti, Not only P-glycoprotein: Amplification of the ABCB1-containing chromosome region 7q21 confers multidrug resistance upon cancer cells by coordinated overexpression of an assortment of resistance-related proteins, Drug Resist. Updat. 32 (2017) 23–46. doi:10.1016/j.drup.2017.10.003.

[2] I.Y. Zhitnyak, I.N. Bychkov, I. V. Sukhorukova, A.M. Kovalskii, K.L. Firestein, D. Golberg, N.A. Gloushankova, D. V. Shtansky, Effect of BN Nanoparticles Loaded with Doxorubicin on Tumor Cells with Multiple Drug Resistance, ACS Appl. Mater. Interfaces. 9 (2017) 32498–32508. doi:10.1021/acsami.7b08713.

[3] I.D. Kyrochristos, D.E. Ziogas, D.H. Roukos, Drug resistance: origins, evolution and characterization of genomic clones and the tumor ecosystem to optimize precise individualized therapy, Drug Discov. Today. (2019). doi:10.1016/j.drudis.2019.04.008.

[4] R.A. El-Awady, F. Hersi, H. Al-Tunaiji, E.M. Saleh, A.H.A. Abdel-Wahab, A. Al Homssi, M. Suhail, A. El-Serafi, T. Al-Tel, Epigenetics and miRNA as predictive markers and targets for lung cancer chemotherapy, Cancer Biol. Ther. 16 (2015) 1056–1070. doi:10.1080/15384047.2015.1046023.

[5] K. Macet, Juli 2011, 21 (2011) 10430. doi:10.1097/FPC.0b013e32833ffb56.Doxorubicin.

[6] M. Baxter-Holland, C.R. Dass, Doxorubicin, mesenchymal stem cell toxicity and antitumour activity: implications for clinical use, J. Pharm. Pharmacol. 70 (2018) 320–327. doi:10.1111/jphp.12869.

[7] M. Mohajeri, A. Sahebkar, Protective effects of curcumin against doxorubicin-induced toxicity and resistance: A review, Crit. Rev. Oncol. Hematol. 122 (2018) 30–51. doi:10.1016/j.critrevonc.2017.12.005.

[8] C. Z., Z. Y., S. Y., C. Z., Overcoming tumor cell chemoresistance using nanoparticles: Lysosomes are beneficial for (stearoyl) gemcitabine-incorporated solid lipid nanoparticles, Int. J. Nanomedicine. 13 (2018) 319–336. doi:10.2147/IJN.S149196.

[9] S. Kulshrestha, A.U. Khan, Nanomedicine for anticancer and antimicrobial treatment: an overview, IET Nanobiotechnology. 12 (2018) 1009–1017. doi:10.1049/iet-nbt.2018.5112.

[10] C. Yang, Y. Qin, K. Tu, C. Xu, Z. Li, Z. Zhang, Star-shaped polymer of β-cyclodextrin-g-vitamin E TPGS for doxorubicin delivery and multidrug resistance inhibition, Colloids Surfaces B Biointerfaces. 169 (2018) 10–19. doi:10.1016/j.colsurfb.2018.05.001.

[11] M. Bar-Zeev, Y.D. Livney, Y.G. Assaraf, Targeted nanomedicine for cancer therapeutics: Towards precision medicine overcoming drug resistance, Drug Resist. Updat. 31 (2017) 15–30. doi:10.1016/j.drup.2017.05.002.

[12] F. Bai, Y. Yin, T. Chen, J. Chen, M. Ge, Y. Lu, F. Xie, J. Zhang, K. Wu, Y. Liu, Development of liposomal pemetrexed for enhanced therapy against multidrug resistance mediated by ABCC5 in breast cancer, Int. J. Nanomedicine. 13 (2018) 1327–1339. doi:10.2147/IJN.S150237.

[13] H. Batra, S. Pawar, D. Bahl, Curcumin in combination with anti-cancer drugs: A nanomedicine

review, Pharmacol. Res. 139 (2019) 91–105. doi:10.1016/j.phrs.2018.11.005.

[14] M. Lei, G. Ma, S. Sha, X. Wang, H. Feng, Y. Zhu, X. Du, Dual-functionalized liposome by co-delivery of paclitaxel with sorafenib for synergistic antitumor efficacy and reversion of multidrug resistance, Drug Deliv. 26 (2019) 262–272. doi:10.1080/10717544.2019.1580797.

[15] P.Y. Xu, R.K. Kankala, Y.J. Pan, H. Yuan, S. Bin Wang, A.Z. Chen, Overcoming multidrug resistance through inhalable siRNA nanoparticles-decorated porous microparticles based on supercritical fluid technology, Int. J. Nanomedicine. 13 (2018) 4685–4698. doi:10.2147/IJN.S169399.

[16] M. Zhang, C.T. Hagan, Y. Min, H. Foley, X. Tian, F. Yang, Y. Mi, K.M. Au, Y. Medik, K. Roche, K. Wagner, Z. Rodgers, A.Z. Wang, Nanoparticle co-delivery of wortmannin and cisplatin synergistically enhances chemoradiotherapy and reverses platinum resistance in ovarian cancer models, Biomaterials. 169 (2018) 1–10. doi:10.1016/j.biomaterials.2018.03.055.

[17] Y. Lin, Y. Wang, H.-W. An, B. Qi, J. Wang, L. Wang, J. Shi, L. Mei, H. Wang, Peptide-based Autophagic Gene and Cisplatin Co-delivery Systems Enable Improve Chemotherapy Resistance, Nano Lett. (2019) acs.nanolett.9b00083. doi:10.1021/acs.nanolett.9b00083.

[18] Y. Peng, J. Huang, H. Xiao, T. Wu, X. Shuai, Codelivery of temozolomide and siRNA with polymeric nanocarrier for effective glioma treatment, Int. J. Nanomedicine. 13 (2018) 3467–3480. doi:10.2147/IJN.S164611.

[19] S.A. Shahin, R. Wang, S.I. Simargi, A. Contreras, L. Parra Echavarria, L. Qu, W. Wen, T. Dellinger, J. Unternaehrer, F. Tamanoi, J.I. Zink, C.A. Glackin, Hyaluronic acid conjugated nanoparticle delivery of siRNA against TWIST reduces tumor burden and enhances sensitivity to cisplatin in ovarian cancer, Nanomedicine Nanotechnology, Biol. Med. 14 (2018) 1381–1394. doi:10.1016/j.nano.2018.04.008.

[20] N. Zhao, M. C Woodle, A.J. Mixson, Advances in Delivery Systems for Doxorubicin, J. Nanomed. Nanotechnol. 09 (2018). doi:10.4172/2157-7439.1000519.

[21] M. Gonçalves, S. Mignani, J. Rodrigues, H. Tomás, A glance over doxorubicin based-nanotherapeutics: From proof-of-concept studies to solutions in the market, J. Control. Release. 317 (2020) 347–374. doi:10.1016/j.jconrel.2019.11.016.

[22] Y. Barenholz, Doxil® - The first FDA-approved nano-drug: Lessons learned, J. Control. Release. 160 (2012) 117–134. doi:10.1016/j.jconrel.2012.03.020.

[23] S. Rivankar, An overview of doxorubicin formulations in cancer therapy, J. Cancer Res. Ther. 10 (2014) 853–858. doi:10.4103/0973-1482.139267.

[24] A.O. Elzoghby, W.M. Samy, N.A. Elgindy, Albumin-based nanoparticles as potential controlled release drug delivery systems, J. Control. Release. 157 (2012) 168–182. doi:10.1016/j.jconrel.2011.07.031.

[25] F.F. An, X.H. Zhang, Strategies for preparing albumin-based nanoparticles for multifunctional bioimaging and drug delivery, Theranostics. 7 (2017) 3667–3689. doi:10.7150/thno.19365.

[26] K. Kimura, K. Yamasaki, K. Nishi, K. Taguchi, M. Otagiri, Investigation of anti-tumor effect of doxorubicin-loaded human serum albumin nanoparticles prepared by a desolvation technique, Cancer Chemother. Pharmacol. (2019). doi:10.1007/s00280-019-03832-3.

[27] E.S. Lee, Y.S. Youn, Albumin-based potential drugs: focus on half-life extension and

nanoparticle preparation, J. Pharm. Investig. 46 (2016) 305–315. doi:10.1007/s40005-016-0250-3.

[28] B. Bhushan, V. Khanadeev, B. Khlebtsov, N. Khlebtsov, P. Gopinath, Impact of albumin based approaches in nanomedicine: Imaging, targeting and drug delivery, Adv. Colloid Interface Sci. 246 (2017) 13–39. doi:10.1016/j.cis.2017.06.012.

[29] H.K. and T.J. Das C, Lucia MS, 乳鼠心肌提取 HHS Public Access, Physiol. Behav. 176 (2017) 139–148. doi:10.1016/j.physbeh.2017.03.040.

Appendix

List of published Papers

Argenziano, M., Gigliotti, C. L., Clemente, N., Boggio, E., Ferrara, B., Trotta, F., Pizzimenti, S., Barrera, G., Boldorini, R., **Bessone, F.**, Dianzani, U., Cavalli, R., Dianzani, C.
Improvement in the Anti-Tumor Efficacy of Doxorubicin Nanosponges in In Vitro and in Mice Bearing Breast Tumor Models
Cancers, 2020, 12, p. 162

Matencio, A., Dhakar, N. K., **Bessone, F.**, Musso, G., Cavalli, R., Dianzani, C., García-Carmona, F., Trotta F.
Study of oxyresveratrol complexes with insoluble cyclodextrin based nanosponges: developing a novel way to obtain their complexation constants and application in an anticancer study
Carbohydrate Polymers, 2020, 231, 115763

Argenziano, M., **Bessone, F.**, Cavalli, R.
Nanobubbles: State of the Art, Features, and the Future
Handbook of Materials for Nanomedicine: Metal-Based and Other Nanomaterials, 2019
Jenny Stanford Publishing Pte. Ltd.

Dhakar, N. K., Caldera, F., **Bessone, F.,** Cecone, C., Pedrazzo, A. R., Cavalli, R., Dianzani, C. Trotta, F.
Evaluation of solubility enhancement, antioxidant activity, and cytotoxicity studies of kynurenic acid loaded cyclodextrin nanosponge
Carbohydrate Polymers, 2019, 224, 115168

Bessone, F., Argenziano, M., Grillo, G., Ferrara, B., Pizzimenti, S., Barrera, G., Cravotto, G., Guiot, C; Stura, I., Cavalli, R., Dianzani, C.
Low-dose curcuminoid-loaded in dextran nanobubbles can prevent metastatic spreading in prostate cancer cells
Nanotechnology, 2019, 30 (21), 214004

Khadjavi, A., Stura, I., Prato, M., Minero, V. G., Panariti, A., Rivolta, I., Gulino, G.R., **Bessone, F.**, Giribaldi, I., Quaglino, E., Cavalli, R., Cavallo, F., Guiot, C.
In Vitro, In Vivo and In Silico Investigation of the Anticancer Effectiveness of Oxygen- Loaded Chitosan-Shelled Nanodroplets as Potential Drug Vector
Pharmaceutical research, 2018, 35 (4), p. 75

Femminò, S., Penna, C., **Bessone, F.**, Caldera, F., Dhakar, N., Cau, D., Pagliaro, P., Cavalli, R., Trotta, F.
a-Cyclodextrin and a-Cyclodextrin Polymers as Oxygen Nanocarriers to Limit Hypoxia/Reoxygenation Injury: Implications from an In Vitro Model
Polymers, 2018, 10 (2), p. 211

List of Posters presented to scientific congresses

- "Albumin-based nanoparticles for enhancing the intracellular delivery of Doxorubicin in resistant cancer cell lines"

F. Bessone, B. Ferrara, C. Dianzani and R. Cavalli.
NanoDDS2019 - 17th International Nanomedicine and Drug Delivery Symposium
Boston (MA, US) 22-24 Sep 2019

- "Thermosensitive Hydrogels loaded with Hemoderivatives: promising platforms for sustained release of growth factors to favor tissue regeneration"

F. Bessone, M. Argenziano, C. Gentili, M. Miccichè, G. Turatti, M. Giordano, R. Cavalli
Poster contribution at MIPOL2019 - Milan Polymer Days
Milan (Italy) 11-13 Mar 2019

- "Albumin-based nanoparticles for improving intracellular delivery of Doxorubicin in resistant cancer cell lines"

F. Bessone, B. Ferrara, C. Dianzani and R. Cavalli.
CRS Italy Chapter Workshop, Advances in Drug Delivery and Biomaterials: facts and vision
Padova (Italy) 18-20 Oct 2018

- "Nanocarriers for adjuvant drug delivery during robotic surgery"

M. Argenziano, **F. Bessone**, G. Grillo, P. Rampa, M. Oderda, P. Diemunsch, C. Dianzani, G. Cravotto, R. Cavalli, C. Guiot
2018 E-MRS Spring Meeting and Exhibit
Strasbourg (France) 18-22 Jun 2018

- "Theranostic curcuminoid-loaded Nanobubble as new tool to prevent metastatic spreading in prostate cancer cells"

F. Bessone, G. Grillo, A. Binello, C. Dianzani, B. Ferrara, G. Cravotto, C. Guiot, and R. Cavalli
11th World Meeting on Pharmaceutics, Biopharmaceutics and Pharmaceutical Technology
Granada (Spain) 19-22 Mar 2018

- "Iron concentration in CSF as possible early biomarker for dementia: the need for accurate measurements in small samples"

Ruffinatti, S.Boschi, I. Rainero, **F. Bessone**, R. Cavalli, C. Guiot, F. Da- gata, O. Abollino
AAT-AD/PDTM Focus Meeting 2018
Torino (Italy) 15-18 Mar 2018

- "Polymer shelled nanobubbles: a novel multifunctional delivery tool"

R. Cavalli, **F. Bessone**, M. Argenziano
Seconde Giornate Italo-Francesi di Nanoscienze
Bardonecchia (Italy) 31 Jan-2 Feb 2018

- "Polymer-shelled Albumin-based nanoparticles for improving intracellular delivery of Doxorubicin in a resistant ovarian cancer cell line"

F. Bessone, B. Ferrara, A. Varese, C. Dianzani, R. Cavalli Poster contribution at MIPOL2018 - Milan Polymer Days
Milan (Italy) 14-16 Feb 2018

- "Novel albumin nanoparticles for treatment of resistant cancer cells"

F. Bessone, B. Ferrara, A. Varese, C. Dianzani, R. Cavalli
CRS Italy Chapter WORKSHOP, Macromolecules in Drug Delivery
Salerno (Italy) 26-28 Oct 2017

- "Oxygen Melatonin-loaded chitosan nanobubbles: a dual advanced tool to improve the wound healing process"

F.Bessone, M. Argenziano, A. Varese, F. Maione, E. Giraudo, C. Guiot, R. Cavalli
Poster contribution at Advanced School in Nanomedicine
Pula (Italy) 22-28 Sept 2017

- "Nanobubble technology-based HER2 immunotherapy through dendritic cells targeting"

R. Cavalli, S. Occhipinti, M. Argenziano, **F. Bessone**, C. Guiot, M. Giovarelli Controlled Release Society Annual Meeting Exposition (CRS2017)
Boston (MA), US 16-19 Jul 2017

- "New polymer nanobubbles for improving wound healing treatment"

F. Bessone, M. Argenziano, A. Varese, F. Maione, E. Giraudo, C. Guiot, R. Cavalli
Poster contribution at MIPOL2017 - Milan Polymer Days
Milan (Italy) 15-16 Feb 2017